“Molecular mechanisms and pharmacogenomics of constituents of *Salvia miltiorrhiza* for anticancer therapy”

Dissertation

zur Erlangung des Grades

“Doktor der Naturwissenschaften”

im Promotionsfach Pharmazie

am Fachbereich Chemie, Pharmazie und Geowissenschaften der

Johannes Gutenberg-Universität Mainz

vorgelegt von Ching-Fen Wu

Mainz, April 2016

Betreuer:

Gutachter der Arbeit:

Datum der mündlichen Prüfung: 21.04.2016

Prüfer:

Erklärung

Hiermit erkläre ich an Eides statt, dass ich diese Arbeit selbständig verfasst und keine anderen als die angegebenen Quellen und Hilfsmittel verwendet habe.

Mainz, 01.03.2016

----------	----------
Ort, Datum	Ching-Fen Wu

Acknowledgement

Abstract

Cancer is a worldwide public health problem. Owing to severe side effects and development of resistance, new anticancer agents are urgently required. Natural products provide novel options, because they are considered as being less toxic and more active by multifactorial mechanisms. *Salvia miltiorrhiza* Bunge (Lamiaceae), *Danshen* in Chinese, is a well-known traditional herb widely used in China. In addition to its activity against cardiovascular diseases, recent reports also focused on the anticancer effects this plant. In this thesis, I hypothesized that *S. miltiorrhiza* can bypass drug resistance. I investigated molecular mechanisms underlying cytotoxic effects of the extract and three main chemical compounds of *S. miltiorrhiza*. The root extract of *S. miltiorrhiza* exerted profound cytotoxicity towards various sensitive and multidrug-resistant, P-glycoprotein over-expressing CEM/ADR5000 leukemia cells, EGFR transfected U87.MGΔEGFR glioblastoma cells and HCT-116 p53-knockout colon cancer cells. The plant extract activated the intrinsic apoptotic pathway, which was experimentally determined by increased cleavage of caspase 3, 7, 9 and poly ADP-ribose polymerase (PARP). Further *in vitro* studies revealed that cryptotanshinone and miltirone as main constituents of *S. miltiorrhiza* induced the intrinsic apoptotic pathway, G2/M cell cycle arrest, DNA damage, as well as the generation of reactive oxygen species (ROS). Furthermore, signaling of the transcription factor NFκB and cellular movement has been inhibited. These effects have been unraveled by transcriptome-wide microarray-based mRNA expression. Bioinformatic analyses of microarray results also showed that unfolded protein response (UPR) and eIF-mediated translation initiation, which determine cancer cell fate and which are recognized as anticancer targets, were regulated by cryptotanshinone. Rosmarinic acid induced apoptosis and necrosis by pathways, which were ROS-, DNA damage and caspase-independent. Molecular docking and Western blotting provided supportive evidence suggesting that cryptotanshinone, miltirone and rosmarinic acid bound to IKK-κ and inhibited the translocation of p65 from the cytosol to the nucleus. In addition, the three compounds inhibit cellular movement as shown by a fibronectin-based cellular adhesion assay, indicating that this compound exerts anti-invasive features. In an additional project, rosmarinic acid and salvianolic acid B were determined to be the main phenolic compounds from *S. miltiorrhiza* stem and leaf of callus culture. Here too, the cytotoxic activities could be determined. In summary, my findings suggest the possibility to isolation bioactive constituents with anti-cancer properties from in vitro callus cultures of stem and leaf of S. miltiorrhiza. These results may serve as starting point for drug development from this plant.

Zusammenfassung

Krebs ist ein weltweites Problem. Aufgrund schwerer Nebenwirkungen und Resistenzentwicklungen werden neue Krebsmedikamente dringend benötigt. Naturstoffe bieten neue Optionen, weil sie als weniger toxisch und aktiver sind gegen Krebszellen durch multifaktorielle Mechanismen. *Salvia miltirrhiza* (Lamiaceae), *Danshen* auf Chinesisch, ist eine bekannte traditionelle Heilpflanze, welche in China viel verwendet wird. Zusätzlich zu ihrer Aktivität gegen kardiovaskuläre Krankheiten trat in letzter Zeit die Antikrebs-Aktivität dieser Pflanze in den Mittelpunkt des Interesses. In der vorliegenden Dissertation stellte ich die Hypothese auf, dass *S. miltiorrhiza* die Zytostatika-Resistenz umgehen kann. Ich untersuchte die molekularen Mechanismen der Zytotoxizität vom Extrakt und drei chemischen Hauptsubstanzen dieser Pflanze. Der Wurzelextrakt von *S. miltiorrhiza* zeigte eine starke Zytotoxizität gegenüber sensiblen und multidrug-resistenten (P-Glykoprotein-überexprimierenden) CEM/ADR5000 Leukämiezellen, EGFR-transfizierten U87.MGΔEGFR Glioblastomzellen sowie HCT-116 p53-*knockout* Darmkrebszellen. Der Pflanzenextrakt aktivierte den intrinsischen Apoptoseweg, was experimentell durch erhöhte Spaltung der Caspasen 3,7 und 9 sowie Poly-ADP-Ribose Polymerase (PARP) nachgewiesen wurde. Weitere *in vitro* Studien zeigten, dass Ctyptotanshinon und Miltirone als Hauptsubstanzen von *S. miltiorrhiza* den intrinsischen Apoptoseweg, G2/M Zellzyklus-Arretierung, DNA-Schädigung sowie die Generierung von ROS induzierten. Weiterhin wurden die Signalweiterleitung von NF-κB und der zellulären Beweglichkeit gehemmt. Diese Effekte wurden durch Transkriptom-weite Microarray-basierte mRNA Analysen herausgearbeitet. Bioinformatische Analysen der Microarray-Analysen zeigten auch, dass der *unfolded protein response* (UPR)-Weg und die eIF-vermittelte Hemmung der Translationsinitiation, welche als Schicksal von Krebszellen determinieren und als Zielstruktur für Krebsmedikamente bekannt sind, durch Cryptotanshinon reguliert wurden. Rosmarinsäure induzierte Apoptose und Nekrose mit Signalwegen, welche ROS-, DNA-schädigungs- und Caspase-unabhängig waren. Molekulare Docking und Westernblot-Analysen lieferten unterstützende Beweise, dass Cryptotanshinoin, Miltirone und Rosmarinsäure an IKK-κ banden und die Translokation von p65 vom Zytosol zum Kern hemmten. Zusätzlich hemmten alle drei Substanzen die zelluläre Bewegung, wie im Fibronectin-basierten zellulären Adhäsionstest gezeigt wurde. Dies weist darauf hin, dass diese Substanz anti-invasive Eigenschaften ausprägt. In einem zusätzlichen Projekt, wurde nachgewiesen, dass Rosmarinsäure und Salvianolsäure die hauptsächlichen phenolischen Komponenten von *S. miltiorrhiza* in Stamm- und Blatt-Calluskuluren waren. Hier konnte die zytotoxische Aktivität ebenfalls

nachgewiesen werden. Diese Ergebnisse können als Ausgangspunkt zur weiteren Entwicklung von Krebsmedikament aus dieser Pflanze dienen.

Table of contents

1 Introduction

1.1 General aspects of cancer

1.1.1 Prevalence and etiology

Cancer belongs to the one of the most important public health issues. According to the report of the World Health Organization (WHO) global burden of disease (GBD), it is estimated that 14.9 million new cancer cases are diagnosed and 8.2 million deaths are caused worldwide, and has been ranked as the second leading cause of death behind cardiovascular diseases in 2013 [1]. By 2030, the continuous growing aging population caused new cancer cases which are expected to exceed 20 million every year [2]. Environmental/acquired factors including carcinogen exposure (e.g. tobacco or alcohol consumption, chemicals, pollution), infection of virus and changes of life style (e.g. obesity and diabetes) are responsible for approximately 90-95% of the occurrence of all cancer cases, whereas only 5-10% attribute to internal factors such as inherited gene mutation, hormone and immune conditions [3]. Therefore, the occurrence of cancer is controllable and preventable, when people know to avoid exposing themselves in the circumstances of environmental risks which likely induce cancer.

1.1.2 Characteristics of cancer

Cancer refers to multistep process that genetic alterations lead to progressively transformation of healthy cells into malignant ones [4]. This feature makes cancer difficult to differentiate from normal cells, which results in failure of chemotherapy in early stages because of overlap in target of treatment between normal and cancer cells. Hanahan and Weinberg have described the acquired capabilities of cancer: evading cell death, self-sufficiency in growth signals, insensitivity to anti-growth signals, activating invasion and metastasis, limitless replicative potential, sustained angiogenesis, avoiding immune destruction and reprogramming of energy metabolism (Figure 1) [4]. These characteristics notify the underlying genomic instability and encompass the contribution of tumor microenvironment during tumorgenesis. For decades, abundant efforts were made based on the hallmarks for developing cancer treatment against cancer.

(A)

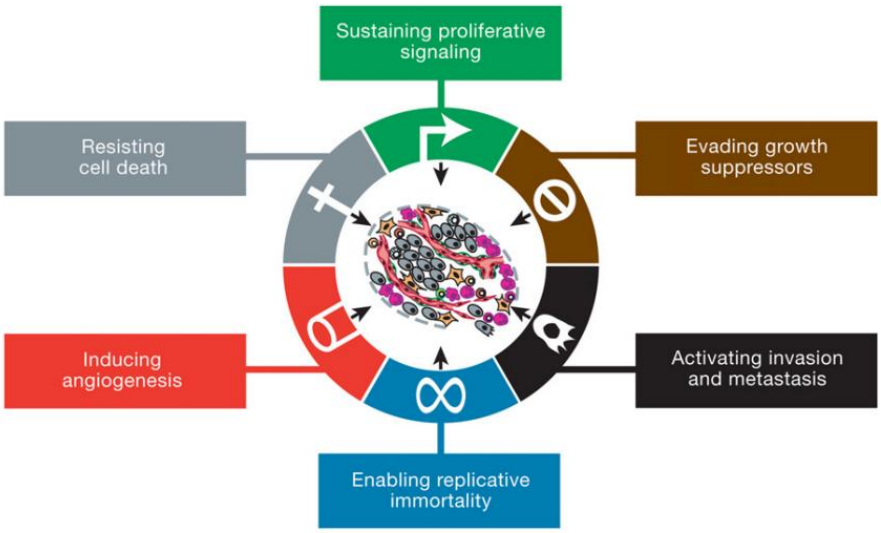

(B)

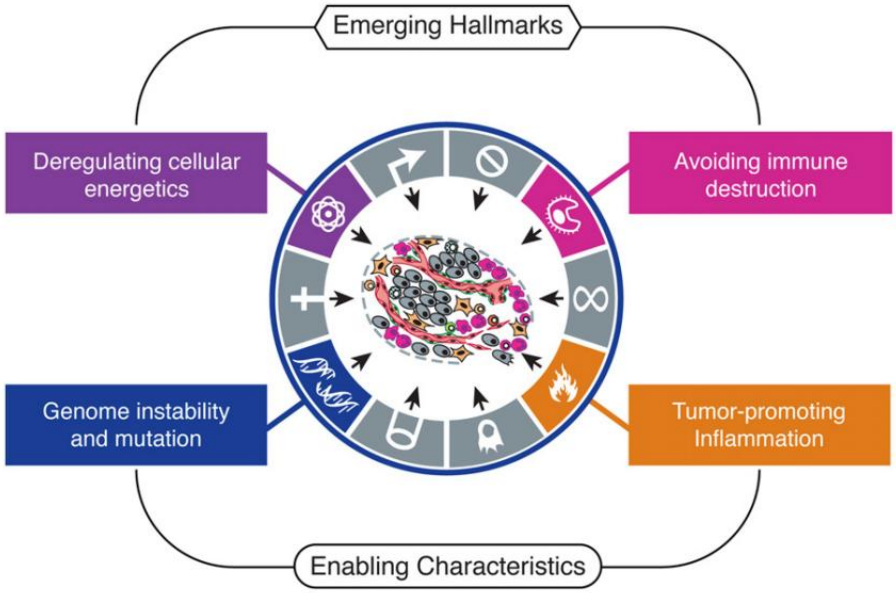

Figure 1. Hallmarks of cancer. (A) Six hallmark capabilities; (B) Two emerging hallmarks and enabling characteristics. Illustration is adapted from Hanahan and Weinberg, 2011[4].

1.1.3 Hematological malignancies: acute lymphoblastic leukemia (ALL)

Hematological malignancies are cancer forms that are initiated in the immune system or blood-generating sites (e.g. bone marrow), including various types of leukemia, lymphoma and myeloma [5]. Leukemia was firstly clarified in 1845 by John Hughes Bennett and Rudolph Virchow, who contributed to describe the principal feature of leukemia as accumulated leukocytes in the blood circulation [6].

Acute lymphoblastic leukemia (ALL), a progressive and malignant disorder accounting for nearly 80% of pediatric leukemia and 30% of the most common childhood cancers is characterized by uncontrolled proliferation of lymphoid progenitor cells. These abnormal blood progenitor cells are unable to differentiate into hematopoietic cells due to specific genomic mutations. The prevalence of ALL peaks between 2-5 years of age. Improved therapies raised cure rates of childhood ALL up to 85% during the past years [7-9]. Optimized combination chemotherapeutical regimens steadily improved outcome of patients. Despite high survival rates by current chemotherapy, many challenges still exist. First, unlike high cure rate in children, survival rates of only approximately 40% adults were reported for adults [10]. Second, relapsed ALL, which is responsible for low survival rates, occurs in around 20% of ALL patients [11].

1.1.4 Current cancer therapy

Cancer treatment mainly counts on surgery, radiation therapy, chemotherapy, targeted therapy, hormone therapy and immunotherapy. Depending on the type, location and grade of cancer as well as general health status of patients, combination of the treatments are adapted for clearance or shrinkage of primary tumor/cancer (radiation, surgery and chemotherapy) and prevention of metastasis (chemotherapy). Combined modality treatment with maximized therapeutical effects and minimized toxicity to normal tissues has become the standard clinical practice [12]. In the future, with the discovery of molecular mechanisms regarding cancer and completion of human genome sequencing in 2003, person's individual genetic profile can be tested in a routine laboratory test and provides comprehensive information for targeted therapy to combat cancer [13].

1.2 Drug resistance

A critical problem in cancer therapy is the occurrence of drug resistance. Cancers can develop drug resistance against chemotherapy via inherent cell heterogeneity, drug efflux, increased drug inactivation, drug target alteration, cell death inhibition, stimulated repair of DNA damage caused by chemotherapeutic agents, epigenetic alterations and epithelial-mesenchymal transition [14]. These mechanisms promote direct or indirect drug resistance independently or in combination through diverse molecular pathways.

1.2.1 ABC transporter

Multidrug resistance (MDR) represents acquired-resistance phenomenon of cancer cells to structurally diverse chemotherapeutic agents, which target different cellular molecules [15]. Cellular or genetic alterations acquired during development of drug resistance involve increased efflux of cytotoxic drugs mediated by overexpression of the ATP-binding cassette (ABC) transporter. Identified with 48 genes in human, ABC transporter family is combined with two transmembrane domains (TMDs) and two nucleotide-binding domains (NBDs) [16, 17].

P-glycoprotein (P-gp, *ABCB1/MDR1*) is the best studied mediator in this family [18]. P-gp is widely distributed in normal human tissues and functionally expressed in some specific organs for protection of susceptible tissues (e.g. blood brain barrier) and excretion of metabolites and xenobiotics (e.g. gastrointestinal tract, liver and kidney) [19]. P-gp has broad substrate specificity and can confer resistance to a wide range of different cytotoxic compounds [20]. Studies confirmed that overexpression of this transporter was responsible for drug efflux and resistance to several unrelated hydrophobic used in cancer chemotherapy e.g. anthracyclines, vinca alkaloids, taxanes, epipodophyllotoxines, and probably hundreds of other compounds [21].

The structure of P-gp is illustrated in figure 2A. P-gp is comprised of two bundles each consisting of six transmembrane helix. The two bundles with intracellular-facing conformation open to the cytoplasm and the inner leaflet of the lipid bilayer creates the cavity (substrate-binding pocket, SBP), in which amino acids interact with P-gp substrates. Triggered by the interaction between the substrate and residues in the SBP, adenosine triphosphate (ATP) binds to the nucleotide-binding domain (NBD) and results in dimerization of the NBDs. This conformational change of NBD occludes transport of the substrate into the cytoplasm or the inner leaflet of the bilayer. Therefore, the substrate is released into the outer leaflet or to the extracellular space, preventing transport of the substrate across the lipid bilayer [16, 22].

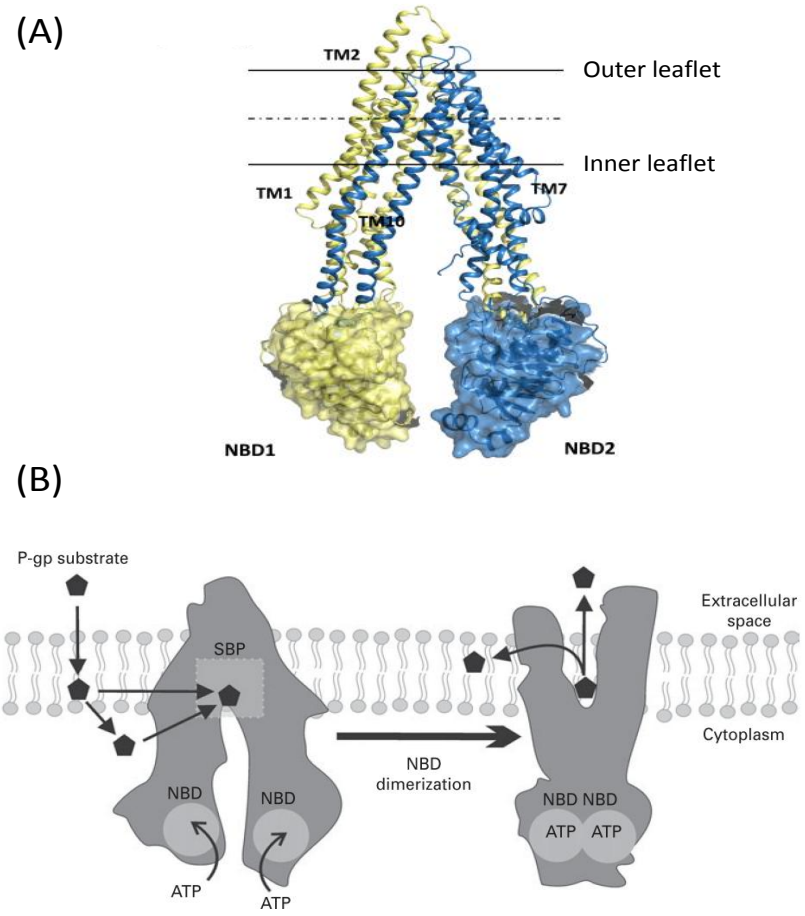

Figure 2. (A) 3D-structure of mouse P-gp in cartoon and colored in yellow and blue illustrating each moiety of the protein (photo adapted from Martinez and Falson [16]). (B) Mechanism of efflux by P-glycoprotein (P-gp). P-gp substrates bind to the P-gp substrate-binding pocket (SBP). Binding of adenosine triphosphate (ATP) to the nucleotide-binding domain (NBD) results in dimerization of the NBDs. This triggers a conformational change that extruds the substrate to the extracellular space. Photo adated from O'Brien et al. [22]

Efforts have been made to develop P-gp inhibitors after the discovery of P-gp-mediated MDR. Most preclinical trials aim to inhibit activity of P-gp, however, these compounds used in clinical trials which inhibit activity of P-gp had unfavorable properties involving limited efficiency, toxicity, unrelated pharmacological effects, pharmacokinetic interaction with other drugs and lack of potency for specific mechanisms of resistance [23,24]. To search for new generation of P-gp inhibitors, in addition to traditional pharmacological modulation, new alternative strategies are emerged: 1) engage: co-administration of P-gp inhibitors and cytotoxic agents; 2)

evade: the use of cytotoxic agents that bypass P-gp-mediated efflux; 3) exploit: approach takes advantage of the collateral sensitivity of MDR cells [24] (Figure 3).

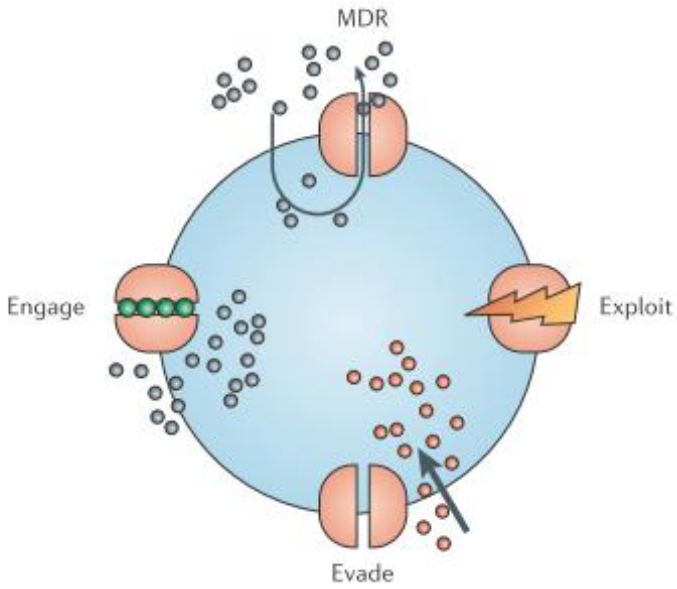

Figure 3. Scheme of targeting P-gp. Image adapted from Szakács et al. [24]

1.2.2 Epidermal growth factor receptor (EGFR)

In addition, other alterations including drug detoxification by phase I and II enzymes increased DNA repair, point mutations in drug targets as well as deregulated cell death signaling lead to drug resistance [25]. The epidermal growth factor receptor (EGFR), a well-characterized oncogene also referred to ErbB1 or HER1, is a 170 kDa transmembrane protein belonging to the erB family of tyrosine kinase receptors. The structure of EGFR is composed of an extracellular cysteine region, a single transmembrane region and an intracellular domain involving an ATP-binding site and tyrosine kinase activity [26-28]. Active EGFR dimers undergo autophosphorylation of tyrosine residues in the cytoplasmic tail of the receptor, subsequently activating multiple signal transduction pathways, including the MAPK signaling cascade, Src, STAT3/5, the phosphoinositide-3-kinase (PI3K) pathway, which recruits Akt/PKB to the plasma membrane, and the phospholipase Cγ pathway, which leads to protein kinase C (PKC) activation [28,29]. Activation of these downstream signaling pathways results in oncogenesis, angiogenesis, cell cycle progression and differentiation in a variety of cancers. The overexpression of EGFR is presumably caused by multiple epigenetic mechanisms, gene amplification, and oncogenic viruses [30].

1.2.3 Tumor suppressor p53

Tumor suppressor p53, encoded by *TP53* gene, plays an important role in maintaining genome stability and tumor prevention [31]. As a transcription factor, p53 mainly exerts its tumor suppressive function through transcriptional regulation of its target genes. Under normal condition, expression and activity of p53 is maintained at a low level by negative regulators (e.g. MDM2, Cop1 and Pirh2), which are E3 ubiquitin ligases for p53 degradation [32]. A variety of stress signals, including DNA damage, nutrient deprivation, hypoxia and oncogene activation which related in many ways to carcinogenesis, release p53 from negative regulators-mediated inhibition. This increases p53 protein levels and activity. Once activated, p53 regulates a group of genes targeting cell cycle arrest (e.g. p21, Gadd45, cdc25c and 14-3-3σ) [33], DNA repair (e.g. p48XPE) [34], apoptosis (e.g. Puma, Bax, Noxa) [35] or senescence (e.g. p21) [36]. In addition, recent reports indicates that p53 also enables cells to adjust its metabolism in response to mild normal physiological fluctuations, including those in glucose and other nutrient levels [31] (Figure 4).

Somatic p53 is frequently mutated in almost every type of human tumors [37]. In those tumors with low p53 mutation rates, p53 is often inactivated by alternative mechanisms [31]. Mutations in the *TP53* tumor suppressor gene silence the function of the encoded p53 protein, which promotes oncogenic transformation and drug resistance [38,39]. Thus, given these alterations, new strategies are urgently needed to treat drug-resistant malignancies [40,41].

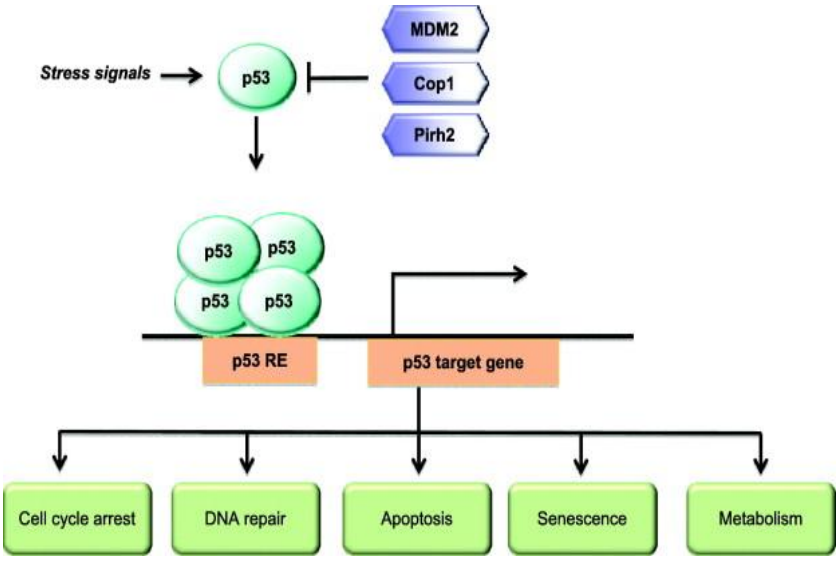

Figure 4. Simplified scheme of p53 pathway. Image adapted from Liu et al. [31]

1.3 Cancer treatment

1.3.1 Chemotherapy

The German chemist Paul Ehrlich is the first one who documented results of animal models for screening chemicals which exerted positive effects against diseases and defined the term "chemotherapy" as the use of chemicals to treat diseases in early 1900s [12]. In cancer chemotherapy, the chemicals refer to cytotoxic/cytostatic drugs. The general function of classic chemotherapeutic agents is to interrupt with cell division by targeting DNA, RNA, and protein synthesis [42,43]. Taken treatment of ALL for example, established drugs include vincristine (mitotic tubulin inhibitor), *L*-asparaginase, cytarabine (inhibition of DNA polymerase), dexamethasone (anti-inflammatory glucocorticoid), anthracyclines such as daunorubicin (DNA topoisomerase II inhibitor) and many others [44]. Traditional chemotherapeutical agents target fast-dividing cells, one of the main properties of cancer cells. Therefore, they also affect other fast-proliferating cells in normal tissues e.g. cells in mucosa, bone marrow and hair follicles. Major complications by side effects which many patients under treatments of chemotherapy may encounter involve hair loss, immunosuppression, anemia, gastrointestinal distress, infertility and organ damages (e.g. hepatoxicity and nephrotoxicity).

1.3.2 Natural products for cancer treatment

1.3.2.1 Natural products

Natural products are secondary metabolites which serve for survival of organisms. These small molecules display molecular structures, named "privileged scaffolds", which are constructed with high-affinity to bind multiple targets (e.g. proteins) [45]. In fact, natural products exert biological effects by binding to specific biological targets as chemical weapons.

Natural products have been historically considered as important resources for anticancer drug discovery and a variety of natural products have been identified as potent anticancer drugs. With development of the genetic identification, new technologies such as high-throughput screening, targeted therapies which count on small synthesized molecules or antibodies to target specific proteins in cancer growth were thought to be the future to combat cancer. Natural products, therefore, were once considered to be outdated by pharmaceutical companies in the 1990's [46]. Targeted therapies improve cure rate of some forms of cancers and life expectancy of patents. However, the cure rate is disappointing in man of solid tumors. Most of the cancers

are shown to deregulate multiple signaling pathways, and either primary resistance responding to targeted agents or acquired resistance to inhibition of cell signaling often occurs in few months after treatment. Combination of targeted agents has been proposed to combat resistance, nevertheless, unexpected side effects and toxicity might take place during treatment. In addition, enormous cost of target therapies has to be taken into consideration [47]. These drawbacks of targeted therapies revitalized the research interests of natural products. Instead of monospecific chemotherapeutical drugs which cancer cells frequently develop resistance to, natural products with multifactorial properties may be of advantage to overcome or bypass drug resistance [48]. In comparison with synthesized chemical drugs, natural products show a favorable profile with low toxicity.

The authors Swinney and Anthonyshowed that over a time frame between 1999 and 2008, 36% of the first-in-classs mall-molecules approved by U.S. Food and Drug Administration (FDA) were NPs or NPs derivatives [49]. From 1940s-2010, of the 175 anticancer drugs approved worldwide, 74.9% are naturally inspired agents, with 48.6% actually being either natural products or directly derived there from. [50]. To date, several natural products and derivatives thereof are in clinical use against cancer, such as anthracyclins, L-asparaginase, *Vinca* alkaloids, campthothecins, taxanes, epipodophyllotoxines, etc., demonstrating that natural products play a key role in cancer research.

1.3.2.2 Natural products derived from traditional Chinese medicine (TCM)

Traditional Chinese medicine (TCM) commands a unique position among all traditional medicines not only because of its 5000 years of history, but also its focus on holism and naturalism, combining Chinese medical experience with Chinese culture [51,52]. Combination of individual herbal ingredients (called formulas) based on patients' symptoms, which in accordance with the theory of "individual therapy", is the basic principle of TCM. It aims to multiple targets simultaneously against diseases, generating synergetic actions of each ingredient [53]. The ingredients of herbal remedies are extracted from natural resources: plants, animal parts, shells, insects and even stones and minerals. Each herb has its own properties. Recently, the development of modern cellular/molecular biology has contributed to the interpretation of the anticancer effects of TCM. It was illustrated that TCM plays important role in inhibiting cancer progress by inducing apoptosis, modulating the immune system, reducing multidrug resistance (MDR), etc. Targeting multiple mechanisms against cancer was the most described features among the herbal ingredients [52,54].

1.3.2.3 *Salvia miltiorrhiza*

In traditional Chinese medicine, cancer was described as the results of blood stasis or *qi* stagnation [55,56]. Herbal plants which are able to promoting circulation and removing blood stasis (a Chinese medicinal term named *huoxue huayu*) are traditionally used for patients with cancers [57]. *Salvia miltiorrhiza* Bunge (Lamiaceae, also named *danshen* in Chinese, figure 5) is a well-known Chinese medicinal herb and is classified as *huoxue huayu*. Therefore, besides the clinical use as hemorrheologic agent, *S. miltiorhriza* has also traditionally used in the treatment of cancer [58]. The root of the plant contains most of the bioactive ingredients, which mainly belong to two groups of compounds: hydrophilic phenolic acids (*e.g.* caffeic acid, rosmarinic acid, salvianolic acid, isoferulic acid, etc.) and hydrophobic tanshinones (*e.g.* tanshinone 1, tanshinone 2A, tanshinone 2B, cryptotanshinone, etc.) [59-61]. These bioactive compounds refer to as secondary metabolites and exert multiple therapeutic activities, such as anti-oxidative stress, anti-neurodegenerative, anti-inflammatory, anti-hypertensive effects etc [62-64]. In addition, lipophilic compounds, especially tanshinones such as tanshinone I, tanshinone IIA and cryptotanshinone showed significant anti-cancer activities [65-68].

1.3.2.4 Cryptotanshinone (CPT)

Cryptotanshinone (CPT), whose chemical name is 1,2,6,7,8,9-hexahydro-1,6,6-trimethyl-(R)- phenanthro(1,2-b)furan-10,11-dione with a molecular formula of $C_{19}H_{20}O_3$, is a main ingredient derived from the root extracts of *Salvia miltiorrhiza*. CPT has been considered to prevent cardiovascular diseases such as ischemia [69] and atherosclerosis [70,71], as well as to possess neuroprotective effects against Alzheimer disease [72,73]. Other potentially therapeutic properties include anti-bacterial [74], anti-inflammatory [75,76], anti-diabetic [77], anti-osteoporotic [78,79], and anti-cancer [80,81] activities.

1.3.2.5 Miltirone

Miltirone is a lipophilic compound from *S. miltiorrhiza*. It was first identified in the 1970s as a tanshinone [82]. Miltirone inhibits cytochrome P450 enzymes [83] and modulates the $GABA_A$-benzodiazepine receptor [84-86]. Additionally, miltirone exerts anti-plasmodial, anti-trypanosomal and anti-oxidant activities [87,88]. Several studies advocated that miltirone inhibits cancer cell growth [51,89,90]. A recent study revealed that miltirone inhibits P-gp on doxorubicin-resistant cancer cells [91].

1.3.2.6 Rosmarinic acid (RA)

Rosmarinic acid (RA) or 3,4-dihydroxyphenyllactic acid, classified as a polyphenolic

compound, is an ester derivative of caffeic acid and found in numerous medicinal and culinary plants, such as *S. miltiorrhiza*, sweet basil, oregano and many others [92]. RA modulates the immune system [93,94] and acts anti-microbial [95-100], antioxidant [101,102] anti-carcinogenic [103,104], anti-inflammatory [105,106] as well as neuroprotective [107,108]. Cytotoxic effects of RA against cancer cells have been studied [109]. This compound inhibited colon cancer cell proliferation by repressing 12-O-tetradecanoylphorbol-13-acetate (TPA)-induced binding of AP-1, c-Jun and c-Fos to cyclooxygenase-2 (COX-2) and reducing COX-2 activity [110,111]. Furthermore, RA induced cancer cell apoptosis and inhibited invasion by modulating phosphorylation of ERK [112,113]. Moreover, RA inhibited DNA methyltransferase activity, which in turn promoted transcriptional expression of tumor suppressor genes [114]. In addition, RA sensitized TNFα-induced apoptosis by down-regulating ROS regeneration and NFκB activation in U937 leukemia cells [115].

1.3.2.7 Salvianolic acid B (Sal B)

Salvianolic acid B (Sal B) is a phenolic acid ingredient of *S. miltiorrhiza*, and has also proven strong pharmacological activities. It has been used to treat cardiovascular diseases [116-118], ameliorate hepatic fibrosis [119,120], inhibit oxidative stress [121,122] and prevent cancer [123,124].

(A) (B)

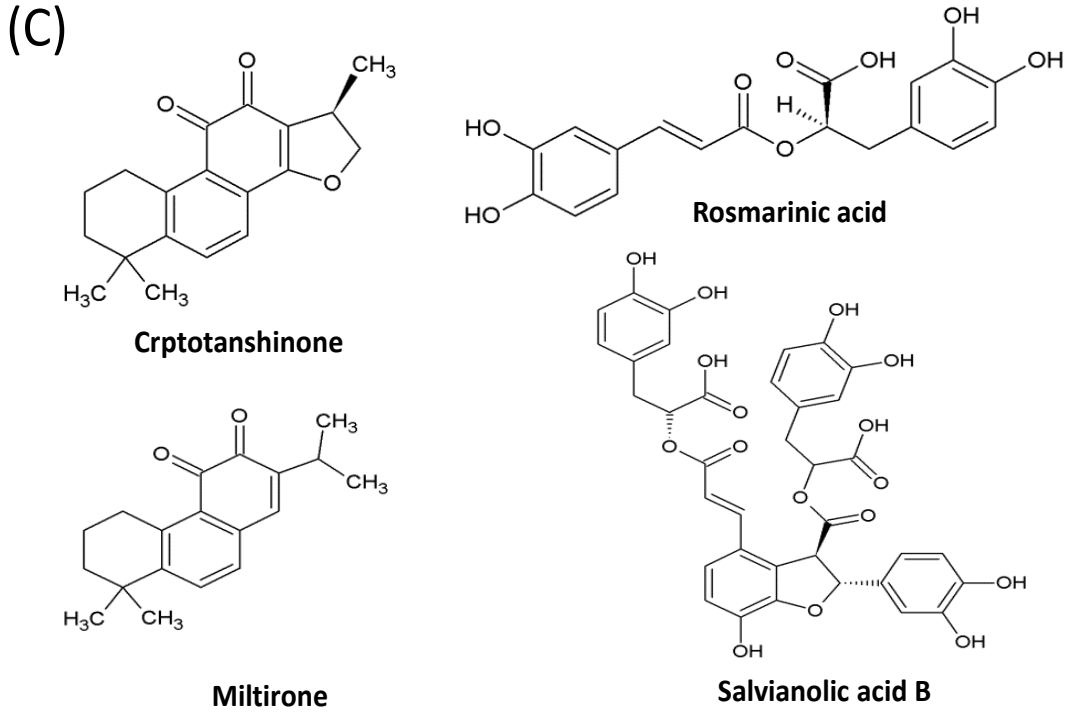

Figure 5. Pictures of plant *S. miltiorrhiza*. (A) Leaf and stem part of *S. miltiorrhiza.* (B) Root part of *S. miltiorrhiza.* (C) Chemical structure of compounds.

1.4 Drug targets for cancer therapy

1.4.1 Apoptosis

As mentioned in the chapter "General aspects of cancer", evading cell death, in particular apoptosis, is one of the main features in the cancer progress. Apoptosis is a gene-directed program has had profound implications that cell numbers can be regulated by factors that influence cell survival as well as those that control proliferation and differentiation. Moreover, the genetic basis for apoptosis implies that cell death can be disrupted by mutation [125].

Morphological hallmarks of apoptosis include cell shrinkage, blebbing of plasma membrane, maintenance of organelle integrity, condensation and fragmentation of DNA [126]. In addition, during early apoptosis, phosphatidylserine (PS) flipped out from the inner layers to outer layers of the cell membrane, allowing recognition and phagocytosis of macrophages without the release of pro-inflammatory cellular components. Apoptosis has been classified into two types of pathways: the death receptor-mediated (extrinsic) pathway and the mitochondria-mediated (intrinsic) pathway. The intrinsic pathway is mainly described in the following paragraph.

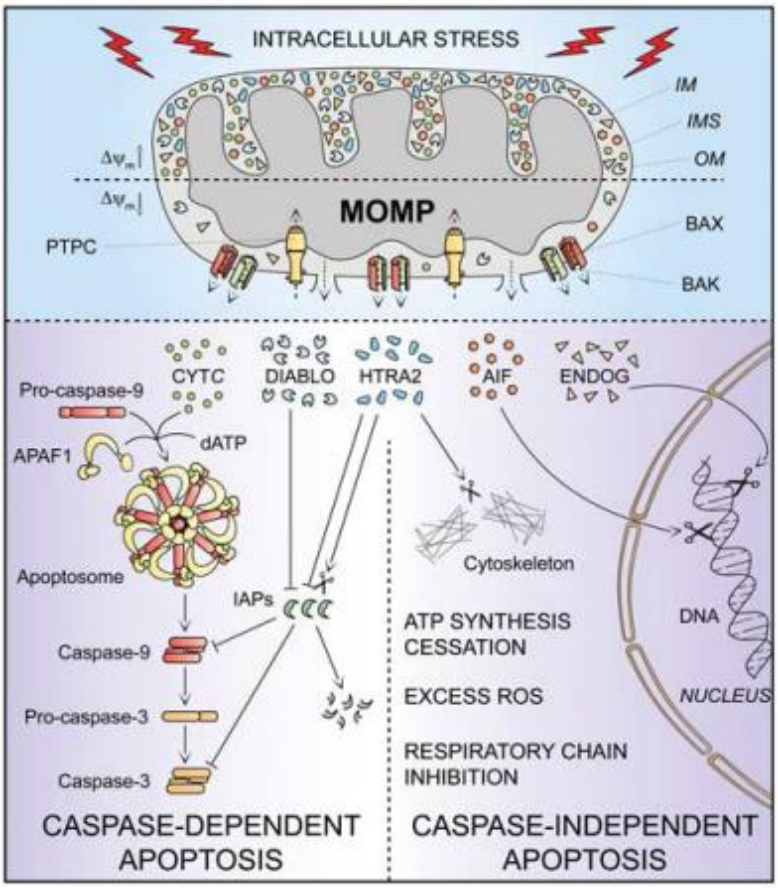

Figure 6. The intrinsic pathway of apoptosis. Image adapted from Galluzzi et al., 2012 [127].

As its name implies, the intrinsic pathway is initiated within the cell. The intrinsic mitochondrial-mediated pathway can be triggered in response to stimuli such as DNA damage, severe oxidative stress, overload of cytosolic Ca^{2+} and unfolded protein responses. In brief, this pathway is the result of increased mitochondrial permeability and the release of pro-apoptotic molecules such as cytochrome-c into the cytoplasm. This pathway is closely regulated by a group of proteins belonging to the Bcl-2 family, which contains pro-apoptotic proteins (e.g. Bax, Bak, Bad, Bcl-Xs, Bid, Bik, Bim and Hrk) and the anti-apoptotic proteins (e.g. Bcl-2, Bcl-X_L, Bcl-W, Bfl-1 and Mcl-1) [128]. When pro-death signals prevail, mitochondrial outer membrane permeabilization (MOMP) occurs and leads to mitochondrial transmembrane potential ($\Delta\psi_m$) depolarization, arrest of mitochondrial ATP synthesis and $\Delta\psi_m$-dependent transport activities [127]. Cytoplasmic release of cytochrome c activates caspase 3 via the formation of a complex known as apoptosome which is made up of cytochrome c, Apaf-1 and caspase 9 [129]. Smac/DIABLO or Omi/HtrA2 binding to inhibitor of apoptosis proteins (IAPs) leads to degradation of IAPs and promotes activation of caspase 3 and 9 [130]. Other apoptotic factors that are released from the

mitochondrial intermembrane space into the cytoplasm via caspase-independent pathway include apoptosis inducing factor (AIF) and endonuclease G (ENDOG), which translocate to the nucleus and mediate large-scale DNA fragmentation [127].

Molecular targets of apoptosis for cancer treatment include targeting Bcl-2 family, p53, IAPs and caspase activities [130].

1.4.2 Nuclear factor kappa B (NFκB) signaling

Organisms develop a system for inducible regulation of gene expression in response to environmental changes such as chemical and microbiological stresses. NFκB, as a model of transcriptional factors, controls DNA transcription and regulates primarily in immune response, as well as a variety of biological events, such as cell survival and differentiation [131,132]. In cancer cells, activation of NFκB favors with many carcinogenic processes, including activation of anti-apoptotic genes, proliferation, angiogenesis, metastasis as well as resistance in response to anti-cancer drug treatment [133,134].

There are five NFκB family members in mammals: RelA/p65, RelB, c-Rel, p50 (NFκB1), and p52 (NFκB2). NF-kB proteins bind to kB sites as dimers, either homodimers or heterodimers (e.g. p50/p65, p50/c-Rel, and p52/p65), and can exert both positive and negative effects on target gene transcription. NFκB activation is stimulated by a number of positive and negative regulatory elements [131,135]. NFκB is normally held inactive in the cytoplasm through its association with the inhibitory molecule IκB. Inducing stimuli trigger activation of the IκB kinase (IKK) complex, leading to phosphorylation, ubiquitination, and degradation of IκB proteins. This step allows release of NFκB dimmers, which in turn translocate to the nucleus, bind specific DNA sequences, and promote transcription of target genes (Figure 7). Binding sites for the transcriptional regulatory factor NFκB are present in the promoter regions of targeted mediators important associated with critical illness. The core elements of the NFκB pathway are the IKK complex, IκB proteins, and NFκB dimers. Research regarding the regulation of NFκB has concentrated on the activation of the IKK complex, the inhibition of NFκB by IκB proteins, and the capacity of NFκB family members to bind to and promote transcription from the promoters of selected target genes. These mechanisms serve as therapeutic targets for drug development [133].

Evidence reveals that compounds that block NFκB activation can serve to block

cancer cell growth. Curcumin has been shown to suppress NFκB activation and NFκB-dependent gene expression (e.g. cyclin D1, Bcl-2, and Bcl-xL) and exerted antitumor effects on cancer cell lines [136]. The IKK inhibitors (e.g. BAY 11-7082 and AS602868), the NFκB inhibitor (e.g. parthenolide) and proteasome inhibitors that blocks NFκB activation have shown efficacy in a variety to cancer models via increased apoptosis [133, 137-139]

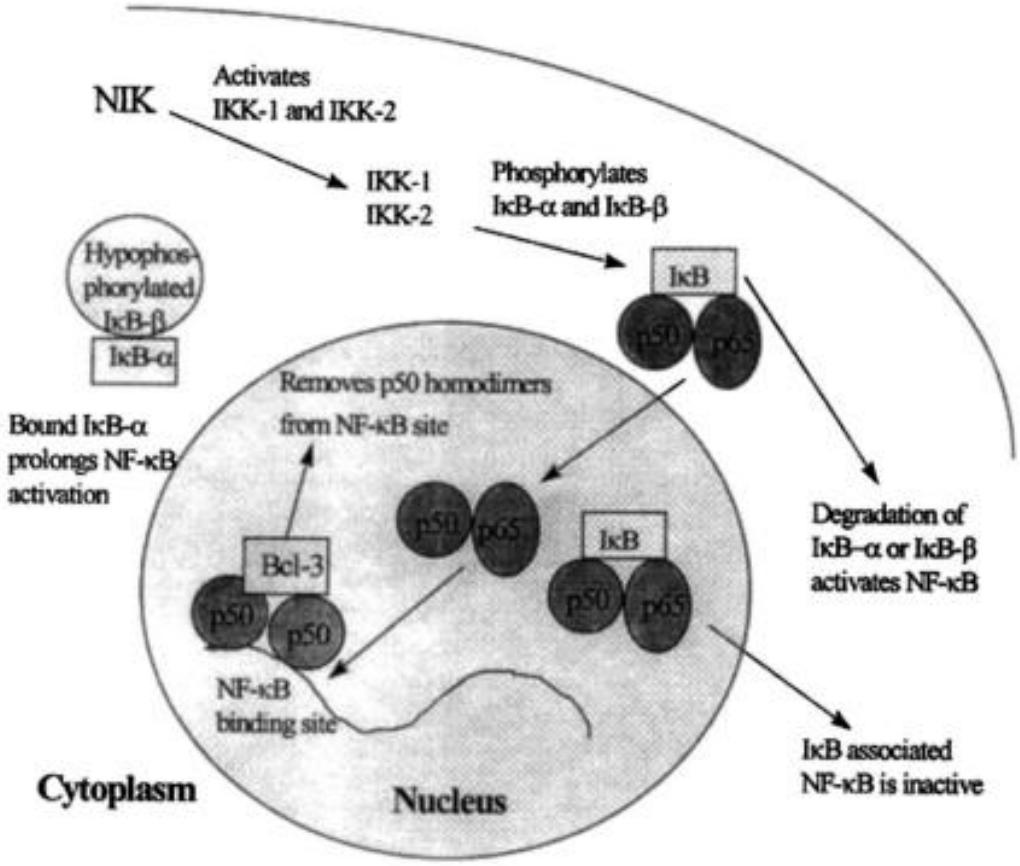

Figure 7. Pathways regulating nuclear factor kappa B (NFκB) activation and the ability of NFκB to act as a transcriptional enhancer. NIK, NFκB inducible kinase; IκB, inhibitor of κB. Image adapted from Sun and Andersson [135].

1.4.3 Unfolded protein response (UPR)

Proteins have to be folded into specific conformations to properly execute their cellular functions. Besides being a major site for calcium storage and lipid biosynthesis, the endoplasmic reticulum (ER) is an essential organelle for post-translational modifications, structure maturation and correct folding of transmembrane and secretory proteins. These processes require molecular chaperones and enzymes residing in the ER such as oxidoreductases [140]. Acting as quality

control system, the ER exports correctly-folded proteins to the sites of actions and eliminates misfolded proteins through the ER-associated degradation (ERAD) pathway, which disposes misfolded proteins from the ER to the cytosol for ubiquitin-mediated proteolytic degradation [141].

Accumulation of misfolded proteins, which is considered to be harmful to cells threatening their survival, results from numerous physiological or pathophysiological factors, such as hypoxia, nutrient deprivation, loss of calcium homeostasis, and elevated uncompleted folding forms of proteins due to mutations and a failure in degradation [140]. As shown in figure 8, in response to such a cellular condition referred to as ER stress, cells have evolved an adaptive mechanism, termed unfolded protein response (UPR) to maintain cellular homeostasis. UPR is triggered by three major ER-resident transducers: inositol-requiring enzyme-1 (IRE1), protein kinase RNA-like endoplasmic reticulum kinase (PERK), and activating transcription factor-6 (ATF6). IRE1 represents a strong homeostatic transcription factor, which multimerizes and trans-autophosphorylates upon stimulation, cleaves X-box protein 1 (*XBP1*) mRNA to a spliced mature form (*XBP1s*). *XBP1s* translocates to the nucleus and induces the transcription of ERAD component genes and genes related to ER chaperones and biogenesis [142]. Activated PERK phosphorylates eukaryotic initiation factor 2 (eIF2α) on Ser51 thereby blocking global protein synthesis by decreasing cap-dependent translation from most mRNAs. This in turn alleviates the heavy load of new peptides that require modification and folding in the ER compartment [143]. Nevertheless, mRNAs encoding *ATF4* paradoxically sustain translational efficiency, which induces transcription of target genes coding enzymes involved in amino acid metabolism, enzymes required for protein folding and degradation, GADD34 phosphatase, and the transcription factor C/EBP homologous protein (CHOP/*DDIT*) [144]. ATF6 translocates to the Golgi apparatus for cleavage by site-1 and site-2 proteases. Together with XBP1, activated ATF6 subsequently translocates into the nucleus and regulates transcription of target genes to restore ER function [145]. Taken together, UPR activation serves as adaptive system against ER stress and promotes cell survival. Nevertheless, if prolonged ER stress occurs and UPR fails to restore protein folding homeostasis, PERK and IRE1 stimulate pro-apoptotic signaling and increase CHOP expression. CHOP, a key molecule involved in ER-stress-driven apoptosis, is associated with repression of BCL-2, which in turn translocates BCL-2-associated protein X (BAX) to mitochondria, ultimately leading to release of cytochrome c. This suggests that ER stress modulates intrinsic apoptosis via disruption of mitochondrial membrane potential and a series of caspase activation [146,147]. CHOP strongly correlates with ER stress-driven apoptosis and

CHOP-deficient cell lines are resistant to ER stress-induced apoptosis [148]. In light of the previous facts, sustained UPR activation, which leads to programmed cell death, might be a potential strategy in cancer therapy.

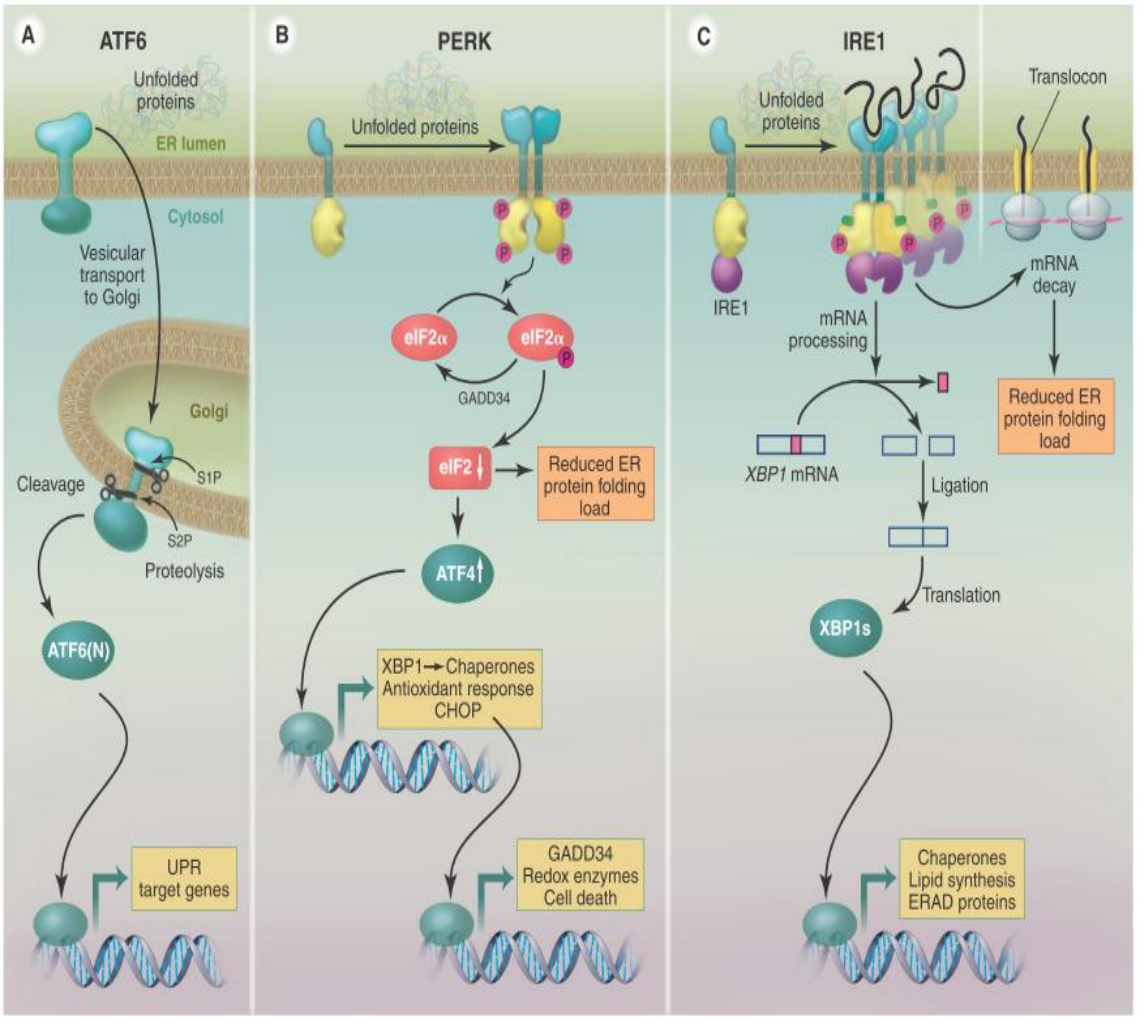

Figure 8. The three branches of the UPR. Each pathway uses a different mechanism of signal transduction: ATF6 by regulated proteolysis, PERK by translational control, and IRE1 by nonconventional mRNA splicing. Image adapted from Walter and Ron [149].

1.4.4 Translation regulation

Translation can be divided into four phases including initiation, elongation, termination and ribosome recycling. The most predominant regulatory mechanism occurs during the rate-limiting phase of initiation [150]. Basic steps of translation initiation includes: 1) Assemble cap-binding complex: During the first steps of cap-dependent translation initiation, messenger RNA (mRNA) associates at its 5′UTR with the eukaryotic initiation factor eIF4F, containing the cap-binding protein eIF4E,

the scaffold protein eIF4G, and the 5′UTR unwinding RNA helicase eIF4A that operates in conjunction with eIF4B. The circularization and activation of mRNAs takes place where poly-A binding proteins (PABP) bind to eIF4G at the 3′UTR end. 2) Recruit 43S complex to mRNA: The 43S pre-initiation complex [composed of the 40S ribosomal subunit, the eIF2 ternary complex (eIF2, GTP, and Met-tRNA), eIF3, eIF1, eIF1A, and eIF5] joins the activated RNA structure (via eIF4G and eIF3 interaction). 3) Scanning of 40S ribosomal subunits to AUG: 40S ribosomal subunits scan 5′UTR until AUG start codon recognition occurs, followed by the hydrolysis of eIF2-bound GTP and the release of eIF2-bound GDP, eIF5, eIF3, and eIF1. 4) 60S ribosomal subunits join: The subsequent association of the 60S ribosomal subunit with eIF5B-bound GTP leads to eIF5B-mediated GTP hydrolysis and the release of eIF5B-GDP and eIF1, thus allowing the assembly of the 80S complex, which is then ready for translation elongation [151,152].

Stimulation of eIF4F assembly is caused in part by the activation of the PI3K/Akt/mTOR pathway, which contributes to oncogenetic process. Under the circumstances that mitogens and growth factors exist, mTOR is activated via PI3K/AKT pathway, in turn resulting in phosphorylation of 4E-BPs (to dissociate 4E-BPs from eIF4E), eIF4G and eIF4B for formation of eIF4F complex. Stress or starvation promotes phosphorlation of eIF2α, which blocks eIF4F assembly and reduces global protein synthesis. Meanwhile, phosphorylation of eIF2α triggers unfolded protein response to assume cell survival (Figure 9) [151,153].

Regulation of gene expression at the level of protein synthesis is a unique mechanism, by which cells rapidly respond to extra- and intracellular stresses. In the case of cancer progression, synthesis of specific proteins required to initiate and maintain the transformed phenotype is hyperactivated by post-transcription via translation initiation. This process utilizes existing mRNA species to produce target proteins and skips transcription steps, favoring cancer cell development [151]. Therefore, the susceptibility of translation initiation to protein synthesis may be a determinant factor in cancer development. Currently, therapeutic approaches targeting deregulated translation in cancers include reduction of eukaryotic initiation factors (e.g. eIF3, eIF4E) [154,155], disruption of their RNA-binding ability or eIF4F complex formation (e.g. eIF4A) [156,157], as well as inhibition of PI3K/AKT/mTOR pathway [158].

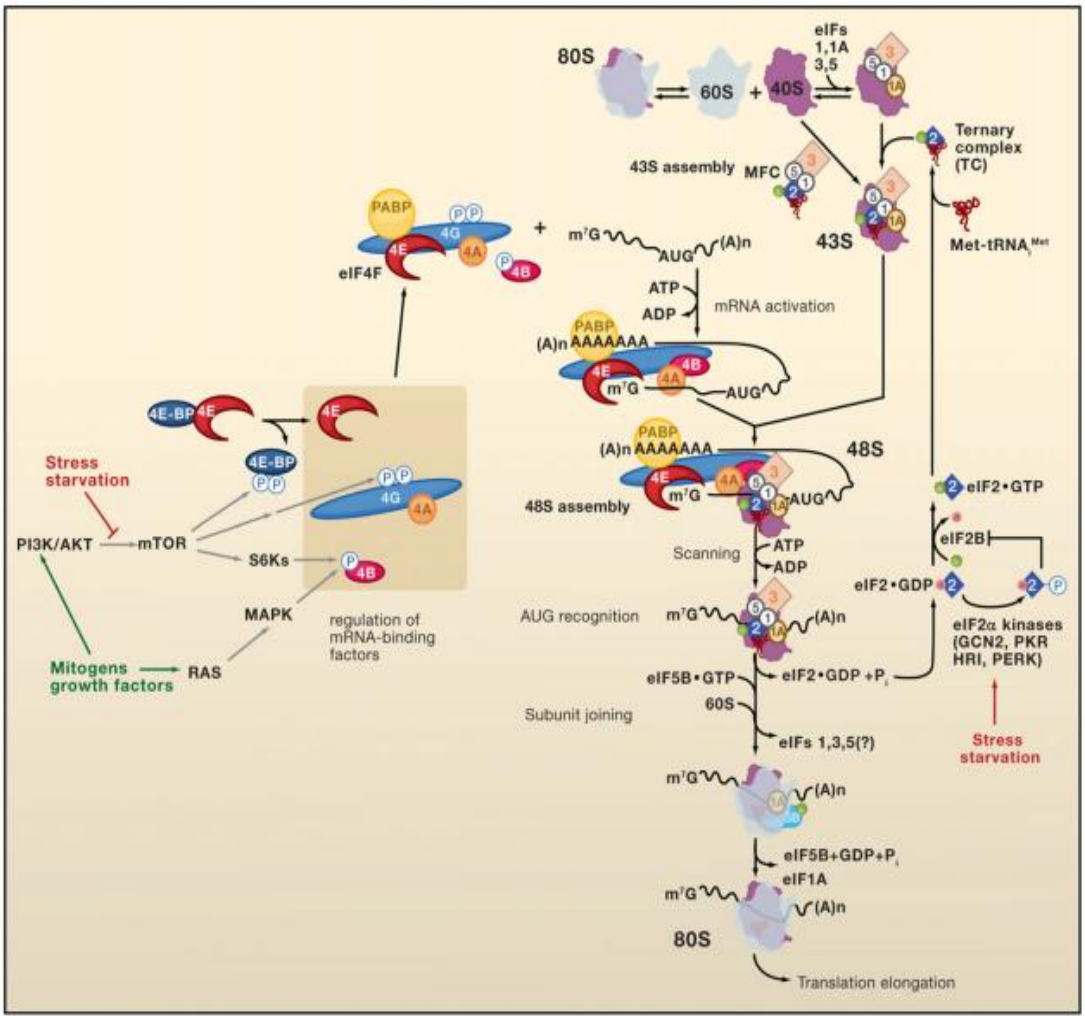

Figure 9. Eukaryotic cap-dependent translation initiation and its regulation by eIF2α kinases and other signaling pathways. Figure adapted from Sonenberg and Hinnebusch [153].

1.5 Callus culture

Accumulation of secondary metabolites in plants plays an important role for plants to survive. Secondary metabolites are synthesized in response to environmental stress, especially in defense against pathogens and herbivores [159]. Based on different biosynthetic origins and structural diversity, secondary metabolites include flavonoids, phenolic and polyphenolic compounds, terpenoids, alkaloids, etc. These bioactive compounds in plants represent valuable and unique resources as food additives, cosmetics, and pharmaceutical drugs [160].

Nowadays, the commercial supply of phytochemical for either therapeutic purposes or research uses mainly relies on extraction from field-cultivated plants. Quality and safety issues arouse from field-cultivated plants concerning the variation in contents

of bioactive constituents and contaminations with heavy metals, microbes and pesticide. Geographical and climate-related reasons also generate phenotypic variations of field-cultivation of herbal plants. In addition, the price of herbal products is rising due to increasing demand and production costs [161,162]. Therefore, there is a need to develop a controllable and sustainable system for efficient production of herbal plants. Plant tissue culture is the most useful technique for exploring various measures on biosynthesis of desired secondary metabolites [163]. Plant tissue cultures not only avoid the disadvantages mentioned above, which the field-cultivated plants may exert, but also shorten the growth cycle into weeks rather than years of growing plants in the field [164].

Numerous investigations have reported that production of useful compounds using callus culture [164]. Callus, a term originated from Latin word *callum*, refers to undifferentiated parenchymatous cell masses derived from plant tissues (explants). Callus cells are thought to be totipotent, being capable of developing to whole plant [165,166]. In plant biology, callus formation is often induced on the wounds of plant organs. With the supplement of essential growth hormones, differentiated cells from the wounded explants undergo the process of dedifferentiation, which lead to generation of callus. Callus has been widely used in both basic research and pharmaceutical industries [167]. The composition of culture medium including carbon source, nitrate and phosphoate and concentration of growth hormones determine the production of target compounds from callus [168].

2 Aims of the thesis

Fighting cancer is a long-term war. Failure of cancer therapy principally attributes to intrinsic or acquired resistance of cancer cells. With the properties of multi-target potential, natural products certainly have their place in the field of anticancer treatment, alongside with a comprehensive understanding of molecular mechanisms. In TCM, *S. miltiorrhiza* is recognized with high-valued clinical therapuetical effects and used for the treatment of patients with cardiovascular diseases. Until recently, it was reported that *S. miltiorrhiza* and major substances extracted thereof have significant anticancer activities. However, the molecular targets and the mode of action of *S. miltiorrhiza* in cancer cells are not fully understood.

Thus, the aims of the thesis are:

(1) to evaluate the cytotoxic effects of root extract of *S. miltiorrhiza* towards multidrug resistant cell lines and to identify the major compounds in *S. miltiorrhiza*

(2) to explore the molecular target and mode of actions of the three major compounds towards ALL cells

-- Analysis of the effects of miltirone on G2/M cell cycle arrest and apoptosis

--Analysis of the molecular mechanisms of cryptotanshinone-induced anticancer activities integrated with mRNA microarray and bioinformative techniques

-- Analysis of the antioxidant, rosmarinic acid, -induced cytotoxic effects

The stem and leaf parts of *S. miltiorrhiza*, which are thought to be without medical effects as waste, are collected for plant tissue culture (callus culture). It leads to the last project of the study:

(3) Identification and comparison of the main compounds of stem and leaf extracts from callus culture and plant, and evaluation of cytotoxic effects on cancer cells

---

The results presented in the following chapters were recently published as first author in the six peer-reviewed scientific journals (please see Appendix: Publication 2014-2016, Journal paper No. 3-8).

All text passages, tables and figures of the publication that are used in a modified form in this thesis were prepared or written by myself.

3 Materials and methods

3.1 Preparation of plant materials

3.1.1 Cultivation and harvest of *S. miltiorrhiza*

The seeds of *S. miltiorrhiza* were obtained from the Bavarian State Research Center for Agriculture (LfL, Freising, Germany), where a voucher specimen (No. BLBP01) was deposited. *S. miltiorrhiza* was cultivated and harvested in the botanical garden of the Johannes Gutenberg University (Mainz, Germany). Leaves, stems and roots were collected from field-grown *S. miltiorrhiza* plants and dried in the oven at 37℃ for 7 days. The dried materials were cut into small pieces and then powdered using a mechanical grinder.

3.1.2 Extraction of *S. miltiorrhiza* root

Dried and powdered root material (50 g) was immersed in a mixture of dichloromethane-methanol (1:1) for 48 h at room temperature. The extract was concentrated to obtain the crude extract. The dried extracts were stored at 4℃ until use.

3.1.3 Callus formation

The preparation of callus formation was performed by Doris Rohr. Leaves and stem explants from *S. miltiorrhiza* were cultured on the day, they were harvested. The stems and leaves were washed with tap water and then soaked in distilled water. Thereafter, leaves and stem explants were surface sterilized for 10 sec in 80% EtOH followed by rinsing two times with sterilized distilled water and for 10 sec with 20% sodium hypochlorite (NaClO) solution and then rinsed three times with sterilized distilled water under laminar flow. Sterilized stem explants were cut into 1 cm long pieces and cultured in AM1 medium, which was modified after Murashige and Skoog (MS) [169]. The medium contained 40 g/l sucrose as carbon source and 8 g/l agar for gelling, and growth regulators such as 2,4-dichlorophenoxyacetic acid (2,4-D, 1 mg/l) combined with kinetin (0.45 mg/l) and 1-naphtylacetic acid (0.01 mg/l). The leaves, on which wounds were made by bladecuts, were cultured in MS medium containing 0.022 mg/l of kinetin. For callus initiation, the culture medium was adjusted to pH 5.8. The culture plates were paraffined and maintained in the dark at 24℃. Medium was changed every four weeks. Callus induction was observed on the surface of the cut edges after 8 weeks. The calli collected from each plate were gently pressed on filter paper to remove excess water and the fresh weights were recorded. The dry weights were also recorded after the calli was freeze-dried.

3.1.4 Extraction procedure for callus and plant stem and leaf

The procedure was performed by Dr. Anastasia Karioti. All samples including calli and dry powdered plant stems and leaves were extracted with 60% EtOH, according to Dong et al [170]. Each stem callus sample was sonicated by Sonorex RK 100 H ultrasonic bath (Bandelin, Germany) with a medium operating frequence at 35 kHz for 25 min and was extracted with 50 ml 60% EtOH for 3 times (150 ml in total) and was filtered. Stem callus extracts were combined and concentrated under vacuum in a Rotavapor R200/205 (Büchi Italia s.r.l., Assago, Italy) and the volume was finally adjusted at 50 ml in a volumetric flask, while for leaf callus extracts a 20 ml volumetric flask was used. Before the HPLC analysis, each sample was filtered through a cartridge-type sample filtration unit with a polytetrafluoroethylene (PTFE) membrane (d=13 mm, porosity 0.45 μm, Lida manufacturing Corp.) and immediately injected.

3.2 Chromatography analysis

3.2.1 HPLC analysis for callus and plant stem and leaf

The analysis was performed by Dr. Anastasia Karioti.

Chemicals

All solvents used for HPLC analysis were HPLC grade. CH_3CN and MeOH for HPLC were purchased from Merck (Darmstadt, Germany). Formic acid (85% v/v) was provided by Carlo Erba (Milan, Italy). Water was purified by a Milli-Qplus system from Millipore (Milford, MA, USA). 0.45 mm PTFE membrane filter was purchased from Waters Co. (Milford, MA). For quantitative analysis, the following standards were used: rosmarinic acid (at 330 nm) and salvianolic acid B (at 290 nm). Rosmarinic acid (MW: 360.3; 97% purity) was purchased from Sigma-Aldrich (Munich, Germany). Salvianolic acid B (MW: 718.6; >98.5 purity) was kindly provided by the China's National Institute for the Control of Pharmaceutical and Biological Products (NICPBP).

HPLC–DAD analysis instrumentation

We used an HP 1100 L instrument coupled to a Diode Array Detector, managed by a HP 9000 workstation (Agilent Technologies, Palo Alto, CA, USA). The column was RP C18 Luna phenomenex ® (150 × 3mm), particle size 5 μm maintained at 27 °C. The eluents were H_2O at pH 3.2 by formic acid (A) and acetonitrile (B). 10μL of the sample solution were injected. The following multi-step linear gradient was applied: from 90% A to 85% A in 10 min, in 7 min to 22% B, with a plateau of 8 min; 2 min

to 25%; 13 min to 66% of B and then 5 min to 90% A. Total time of analysis was 45 min, equilibration time was 5 min, flow rate was 0.4 ml min−1. UV–Vis spectra were recorded in the range 220–600 nm, and chromatograms were acquired at 254, 290, 315, 330 and 350 nm.

HPLC–MS analysis instrumentation

The HPLC system described above was interfaced with a HP 1100 MSD API-electrospray (Agilent Technologies, Palo Alto, CA, USA). The same column, time period and flow rate were used during the HPLC–MS analyses. Mass spectrometry operating conditions were optimized, in order to achieve maximum sensitivity values. Negative and positive ionization modes with scan spectra from *m*/*z* 100 to 1000 were used with a gas temperature of 350 ºC, nitrogen flow rate of 10 l/min, nebulizer pressure of 30 psi, quadrupole temperature of 27ºC, and capillary voltage of 3500 V. The applied fragmentors used were 60, 120, and 180 V.

Identification of peaks and peak purity

Identification of all constituents was performed by HPLC–DAD/MS analysis by comparing the retention time, the UV, MS spectra of the peaks in the samples with those of authentic reference samples. The purity of peaks was monitored by a diode array detector coupled to the HPLC system, comparing the UV spectra of each peak with those of authentic reference samples and/or by examination of the MS spectra.

Quantitative determination of constituents

The method of external standard was applied to quantify each compound. Quantification of individual constituents was performed using a five point regression curve. Measurements were performed at 290 nm for Sal B and at 330 nm for RA.

Method validation of quantitative analysis: Linearity, limits of detection (LOD), limit of quantification (LOQ) and precision

The linearity range of responses of the standard Sal B and RA in plasma was determined on five concentration levels with three injections for each level. Calibration graphs for HPLC were recorded with sample amounts ranging from 6.6×10^{-3} to 2 μg (SalB) and from 5.2×10^{-3} to 3.3 μg (RA). Stock solutions of the standards to evaluate LOD and LOQ were prepared at different concentrations ranging from 3.3×10^{-3} to 0.33 mg/ml (Sal B) and from 2.8×10^{-3} to 0.286 mg/ml (RA) and injected into HPLC (injection volumes varying from 2 to 10 μl). The limit of detection (LOD) and quantification (LOQ) under the chromatographic conditions were determined by injecting a series of the standard solutions until the

signal-to-noise (S/N) ratio for each compound was 3 for LOD and 10 for LOQ. For the intra-day variability test, freshly prepared standard samples in the range of the calibration curve were analysed in six replicates within 1 day. For the interday variability test, the standard solutions were examined in triplicates for three consecutive days. The contents of SalB and RA in each sample were evaluated by HPLC-DAD to calculate the relative standard deviation (%RSD).

3.2.2 HPLC analysis for plant root

The work was cooperated with lab Prof. Eckhard Thines (IBWF, Mainz). Methanol was used as a solvent for *S. miltiorrhiza* root extract. DMSO was used as a solvent for standard compounds. *S. miltiorrhiza* root extract and standard compounds were analyzed by HPLC (Agilent 1100 Series) equipped with a LiChrospher RP 18 (3×125 mm; 5 μm, Merck KGaA, Darmstadt, Germany). The column was used at 40 ℃ and a flow rate of 1 mL min^{-1} with an elution gradient composed of H_2O and acetonitrile. The compounds were detected via a diode array detector.

HPLC-MS

The molecular weight of selected peaks was determined using an HPLC-MS (Agilent 1260 Series LC and 6130 Series Quadrupole MS System). The mass spectra were recorded using atmospheric pressure chemical ionization (APCI) with positive and negative polarization. A Superspher RP 18 (125×2 mm; 4 μm, Merck KGaA, Darmstadt, Germany) column was used at 40 ℃. For every run 1 μl of a sample at a concentration of 1-10 mg mL^{-1} was injected. The elution was performed with a gradient of H_2O and acetonitrile and a flow rate of 0.45 mL min^{-1}. The 3D-tool of the program Chemstation (Agilent, Santa Clara, CA, US) was used to create 3D graphics.

3.3 Substances

Epirubicin and doxorubicin were provided by the University Medical Center of the Johannes Gutenberg University Mainz (Mainz, Germany). CPT and G418 (geneticin) were purchased from Sigma-Aldrich (Munich, Germany). Miltirone was purchased from Chemfaces (Wuhan, People's Republic of China). RA and necrostatin-1 were purchased from Enzo Life Science GmbH (Lörrach, Germany). Sal B was kindly provided by the China's National Institute for the Control of Pharmaceutical and Biological Products (NICPBP). TNFα was purchased from Sino Biological Inc (Beijing, People's Republic of China) and MG-132 was obtained from Invivogen (San Diego, USA). 4',6-Diamidino-2-phenylindole (DAPI) was purchased from Sigma-Aldrich (Munich, Germany).

3.4 Cell culture

3.4.1 Cancer cell lines

CCRF-CEM and CEM/ADR5000 cells were kindly provided by Dr. Axel Sauerbrey (University of Jena, Department of Pediatrics, Jena, Germany). The cells were cultured in RPMI medium (Invitrogen, Germany) containing 10% fetal bovine serum (Invitrogen) and 1% penicillin/streptomycin (Invitrogen), and incubated in a 5% CO_2 atmosphere at 37 ℃. Human glioblastoma U87.MG wild-type cells and a subline transfected with the epidermal growth factor receptor (*EGFR*) gene with deletion of exon 2-7 (U87.MGΔEGFR) were kindly provided by Dr. Webster K. Cavenee (Ludwig Institute for Cancer Research, San Diego, USA). Human wild-type HCT116 ($p53^{+/+}$) and p53-knockout HCT116 ($p53^{-/-}$) colon cancer cell lines were obtained from Dr. Bert Vogelstein (Howard Hughes Medical Institute, Baltimore, USA). The four cell lines were cultured in complete DMEM culture medium with GlutaMAX (Invitrogen) supplemented with 10% fetal bovine serum and 1% penicillin and streptomycin. U87.MGΔEGFR and HCT116 ($p53^{-/-}$) cells were maintained in the culture medium containing 400 μg/ml of G418 (geneticin). MCF-7 breast cancer cell line, a kind gift from Prof. Shu-ling Fu (National Yang-ming University, Taipei, Taiwan), was cultured in complete DMEM medium containing L-glutamine (Life Technologies). Medium was supplemented with 10% fetal bovine serum (Invitrogen) and 1% penicillin and streptomycin.

3.4.2 Normal lymphocyte isolation

Fresh blood was collected in EDTA-coated tubes, layered onto Histopaque-1077 (Sigma Aldrich) and centrifuged at 400×g for 30 min at room temperature. Opaque interface was carefully transferred to a clean conical centrifuge tube. The cells were washed by PBS and centrifuged at 250×g for 10 min. After three wash-centrifuge steps, the cells were cultured in Panserin 413 medium (PAN-biotech GmbH, Aidenbach, Germany) containing cytokines and 2% v/v phytohemagglutimin (PHA) (Life technologies, CA, USA) and were used for cytotoxicity assay.

3.5 Cell based assay

3.5.1 Cytotoxicity assay

Resazurin assay was performed to measure cytotoxicity of test compounds or extracts. The indicator dye, resazurin, is reduced from blue to the red fluorescent resorufin in living cells. In brief, 5000 cells per well were seeded in 96-well-plates in 100 μl. Test compounds or extracts were added in additional 100 μl culture medium. After 72 h, 20 μl resazurin (Sigma-Aldrich) solution was subjected to each well and the plates

were placed in the incubator for 4 h. Fluorescence was measured using Infinite M2000 Proplate reader (Tecan, Germany) with 544 nm (excitation) and 590 nm (emission).

Cytotoxicity of MCF-7 cells was determined by MTT assay. MTT (Methylthiazolyldiphenyl-tetrazolium bromide**,** Sigma-Aldrich) was converted to blue, water-insoluble formazan by mitochondrial dehydrogenases of living cells. Formazan was solubilized by DMSO and the intensity was detected at 570 nm.

3.5.2 Evaluation of drug combination

The Loewe additivity model was used to confirm the drug interaction between RA and Sal B in cytotoxicity [171,172]. In the study, the combination index (CI) was calculated with the equation: $CI = C1_{50\%}/D1_{50\%} + C2_{50\%}/D2_{50\%}$, where $D1_{50\%}$ and $D2_{50\%}$ were the doses of single drug1 and drug 2 that produced 50% inhibition of cell growth, C1 and C2 were the doses of drug 1 and drug 2 in combination, which inhibited 50% of cell growth. The value of CI less than 1 represents synergetic effects, whereas more than 1 means antagonistic ones.

3.5.3 Caspases-Glo 3/7 and caspase-Glo 9 assay

The activity of caspases 3/7 and 9 was measured using Caspase-Glo 3/7 and Caspase-Glo 9 Assay kits (Promega, Germany). Cells were seeded in 96-well plates and treated with test compounds/extracts or DMSO. After 24 h incubation, caspase 3/7 and 9 luminescence was determined by Infinite M2000 Proplate reader.

3.5.4 Comet assay

Cells (2×10^5/well) were treated with test compounds/extracts or DMSO for 24 h. After harvesting and washing of cells with PBS, comet assay analysis was performed by using Oxiselect Comet Assay® kit (Cell Biolabs) according to the manufacturer's instruction. Briefly, collected cells were counted and mixed with low melting point agarose at a ratio of 1:10 (v/v), and then pipetted onto CometSlide™. After incubating the slides at 4℃ for 15 min, cells were incubated in lysis solution for 90 min before treatment with alkaline solution for 30 min to unwind DNA. The slides were then electrophoresed for 20 min at 25 V and 300 mA by adjusting the volume of the alkaline solution. The slides were fixed with ethanol for 5 min and stained by Vista Green DNA Dye. The images were visualized under fluorescent microscope using a band pass FITC filter (excitation 490 nm, emission >520 nm). Twenty-five cells were randomly selected and captured per sample using 40× magnification and were analyzed by using CASP comet assay software (http://casplab.com/). Tail length, percentage of DNA in the tail and head, tail movement and Olive moment were used

as parameters for DNA damage. Statistical significance was determined by one way ANOVA with Dunnett and Tucky *post hoc* test.

3.5.5 Fibronectin adhesion assay

We modified an assay described elsewhere [173]. 24-well plates were coated for 1 h at 37 ℃ with 20 µg/ml fibronectin (Sigma-Aldrich) and were air-dried for 45 min. Cells (3×10^5 cells/well in serum-free medium) were incubated with test compounds or extracts in 150 µl, and 150 µl cell suspensions were added into fibronectin-coated wells to obtain a total volume of 300 µl/well. Cells were allowed to adhere for 2 h at 37 ℃ and then wells were washed three times with PBS containing 5% FBS. Twenty microliters of resazurin solution was added to each well and the plates were placed in the incubator for 4 h. Fluorescence was determined by Infinite M2000 Proplate reader using 544 nm (excitation) and 590 nm (emission). Photographs of adherent cells were taken using a EVOS fluorescence microscope (AMG Advanced Microscopy Group, WA, USA).

3.6 Flow cytometry

3.6.1 Cell cycle assay

CCRF-CEM cells (3×10^6, 1.5×10^6, $0{,}75\times10^6$ and 0.375×10^6) were added to 6-well plates and treated with test compounds or extracts for 24 , 48, and/or 96 h. Cells were washed in PBS (Invitrogen) and fixed in ice-cold 95% ethanol. Then, cells were incubated with 50 µg/ml propidium iodide (PI) for 30 min in the dark. Cells were analyzed by LSR-Fortessa FACS analyzer (Becton-Dickinson, Germany) with 488 nm excitation and detected using a 610/20 nm band pass filter. The results were analyzed using FlowJo software (Celeza, Switzerland).

3.6.2 Detection of reactive oxygen species (ROS)

Briefly, 2×10^6 CCRF-CEM cells were resuspended in PBS and incubated with 10 µM H_2DCFH-DA for 30 min in the incubator. Cells were washed with PBS and suspended in RPMI 1640 medium containing test compounds/extracts or DMSO. After 1 h incubation, cells were washed and suspended in PBS. Subsequently, cells were measured in a LSR-Fortessa FACS analyzer. For each sample, 3×10^4 cells were counted. Fluorescence was measured at 488 nm (25 mW) excitation and detected using a 530/30 nm band pass filter. Histograms were analyzed using FlowJo software.

3.6.3 Measurement of mitochondrial membrane potential (MMP)

CCRF-CEM cells were treated with test compounds/extracts or DMSO for 24 or 48 h. Cells were collected and stained by JC-1 (Biomol, Germany) for 15 min. JC-1 signals were determined in an LSR-Fortessa FACS analyzer by counting 2×10^4 cells. The fluorescence of JC-1 J-aggregated form was detected at 561 nm (excitation) and 586/15 nm (emission). The fluorescence of JC-1 monomers was detected at 488 nm (excitation) and 530/30 nm (emission). Results were analyzed by using FlowJo software.

3.6.4 Annexin V-FITC apoptosis/necrosis detection

Phosphatidylserine (PS) is translocated from inner cell membrane sides to the surface during apoptosis. The annexin V (AV)-FITC apoptosis detection kit (Biovision, USA) was used to detect PS by staining with fluorescent-conjugated AV, which has high affinity to PS. Cells were treated with test compounds or extracts for 48 h and stained by AV and PI for 5 min at room temperature in the dark. AV-FITC binding was detected by LSR-Fortessa FACS analyzer at 488 nm (excitation) and 530 nm (emission). Cytographs were performed by using FlowJo software.

3.7 Computational approaches

3.7.1 Molecular docking

Preparation of docking files was carried out with AutodockTools-1.5.6rc3 and molecular docking was performed by Autodock4 using lamarckian algorithm [174]. The three-dimensional structures of compounds were prepared in protein data bank (PDB) format from PubChem website. The X-ray crystallography-based structures of target proteins were obtained from the PDB website (http://www.rcsb.org/pdb/home/home.do). We defined the docking space within a grid box placed at the pharmacophore of each protein. Docking parameters were set to 250 runs and 2,500,000 for energy evaluations. Docking sites and residues were visualized by using AutodockTools-1.5.6rc3 and Visual Molecular Dynamics (VMD) software (http://autodock.scripps.edu/; http://www.ks.uiuc.edu/Research/vmd/). Docking log (dlg) files provided information regarding the lowest binding energy, the number of clusters and predicted inhibition constant (pKi).

3.7.2 Analysis of gene promoter binding motifs

Motif analysis was performed by Cistrome analysis software [175]. Briefly, a BED format of deregulated genes was retrieved (http://genome.ucsc.edu/cgi-bin/hgTables). SeqPos motif analysis was used to screen for enriched motifs in given DNA regions

(http://cistrome.org). SeqPos scan all the motifs not only in Transfac, JASPAR, UniPROBE (pbm), hPDI database, but also try to find *de novo* motifs using MDscan algorithm. The output of genes was ranked by –log10 (p-value).

3.8 Microarray gene profiling

Total RNA was isolated by InviTrap Spin Universal RNA Mini kit (Stratec molecular, Berlin) according to the manufacturer's instruction. RNA was eluted with nuclease-free water and stored at -80℃ until analysis. The procedure of microarray including quality check of total RNA, probe labeling, hybridization, scanning and data analysis was performed by the Genomics and Proteomics Core Facility at the German Cancer Research Center (DKFZ) in Heidelberg, Germany [176,177].

Quality check of total RNA

The quality of total RNA was checked by gel analysis using the total RNA Nano chip assay on an Agilent 2100 Bioanalyzer (Agilent Technologies GmbH, Berlin, Germany). Only samples with RNA index values greater than 8.5 were selected for expression profiling. RNA concentrations were determined using the NanoDrop spectrophotometer (NanoDrop Technologies, Wilmington, DE).

Probe labeling

Biotin-labeled cRNA samples for hybridization on Illumina Human/Mouse/Rat Sentrix-6/8/12 BeadChip arrays (Illumina, Inc.) were prepared according to Illumina's recommended sample labeling procedure based on the modified Eberwine protocol (Eberwine *et al.*, 1992). In brief, 250–500 ng total RNA was used for complementary DNA (cDNA) synthesis, followed by an amplification/labeling step (*in vitro* transcription) to synthesize biotin-labeled cRNA according to the MessageAmp II aRNA Amplification kit (Ambion, Inc., Austin, TX). Biotin-16-UTP was purchased from Roche Applied Science, Penzberg, Germany. The cRNA was column purified according to TotalPrep RNA Amplification Kit, and eluted in 60-80 µl of water. Quality of cRNA was controlled using the RNA Nano Chip Assay on an Agilent 2100 Bioanalyzer and spectrophotometrically quantified (NanoDrop).

Hybridization

Hybridization is performed at 58℃, in GEX-HCB buffer (Illumina Inc.) at a concentration of 100 ng cRNA/µl, unsealed in a wet chamber for 20 h. Spike-in controls for low, medium and highly abundant RNAs were added, as well as mismatch control and biotinylation control oligonucleotides. Microarrays were washed once in High Temp Wash buffer (Illumina Inc.) at 55℃ and then twice in

E1BC buffer (Illumina Inc.) at room temperature for 5 minutes (in between washed with ethanol at room temperature). After blocking for 5 min in 4 ml of 1% (wt/vol) Blocker Casein in phosphate buffered saline Hammarsten grade (Pierce Biotechnology, Inc., Rockford, IL), array signals are developed by a 10-min incubation in 2 ml of 1 µg/ml Cy3-streptavidin (Amersham Biosciences, Buckinghamshire, UK) solution and 1% blocking solution. After a final wash in E1BC, the arrays are dried and scanned.

Scanning

Microarray scanning was done using a Beadstation array scanner, setting adjusted to a scaling factor of 1 and PMT settings at 430. Data extraction was done for all beads individually, and outliers are removed when > 2.5 MAD (median absolute deviation). All remaining data points are used for the calculation of the mean average signal for a given probe, and standard deviation for each probe was calculated.

Data analysis

Data analysis was done by normalization of the signals using the quantile normalization algorithm without background subtraction, and differentially regulated genes are defined by calculating the standard deviation differences of a given probe in a one-by-one comparison of samples or groups.

Bioinformatic evaluation

The set of genes analyzed by microarray were filtered using Chipster software (http://chipster.csc.fi/) with a *p* value lower than 0.05. These filtered genes with differential fold changes more than 1-fold were selected and subjected to the Ingenuity Pathway Analysis Software (http://www.ingenuity.com/).

3.9 Quantitative real-time polymerase chain reaction (qPCR)

Total RNA was extracted by InviTrap Spin Universal RNA Mini kit (Stratec Molecular, Berlin) according to the manufacturer's protocol. Three micrograms RNA were reverse-transcribed to cDNA by using RevertAid H Minus First Strand cDNA Synthesis Kit (Thermo Scientific). The mRNA levels were analyzed in triplicates with the use of 5× Hot Start Tag EvaGreen® qPCR Mix (Axon Labortechnik, Germany) by CFX384™ Real-Time PCR Detection System (Bio-Rad, CA, USA) and normalized to *RPS13* mRNA expression. The running protocol of qPCR was set as follows: 50℃ for 2 min, 95℃ for 10 min, 40 cycles including denaturation at 95℃ for 15 s, annealing at 58.1℃ (*AKR1C3* and *DDIT3*), 59℃ (*CCNB1*, *CDC2*, *TP53* and *CDKN1A*) or 59.4℃ (*DUSP6*, *TXNIP*, *IGLL1*, *VPREB1* and *BIK*) for 1 min and

extension at 72℃ for 1 min following 95℃ for 1 min. Primer sequences were designed using NCBI and GenScript Real Time PCR Primer Design (https://www.genscript.com/ssl-bin/app/primer) websites and synthesized by Eurofins MWG Operon (Ebersberg, Germany). Primer specificities were checked by NCBI Primer-Blast (http://www.ncbi.nlm.nih.gov/tools/primer-blast). Properties of primers were scanned by Eurofins genomics (https://www.eurofinsgenomics.eu/en/dna-rna-oligonucleotides/oligo-design-more/oligo-property-scan.aspx).The sequences of the primers used for qPCR were listed in the table [178, 266].

Table 1. **Primer sequence**

Gene	Forward (5' – 3')	Reverse (5' – 3')
AKR1C3	CAGTTGTGGTGCCCAATAAA	TCTGCTTCAGCTTGAAATGG
BIK	AACCCCGAGATAGTGCTGGA	GGTGACAATTGCAGAGCCAT
CCNB1	AGGCGAAGATCAACATGGCA	AGCTGTTCTTGGCCTCAGTC
CDC2	AATCTATGATCCAGCCAAACGAA	TTCTTAATCTGATTGTCCAAATCATTAAA
CDKN1A	TGGAGACTCTCAGGGTCGAAA	GGCGTTTGGAGTGGTAGAAATC
DDIT3	GGAAACGGAAACAGAGTGGT	TGTTCTTTCTCCTTCATGCG
DUSP6	GGCATAGTAGGGCAAGGTTC	ACGGTACAGTCGGTCCATTC
IGLL1	GGACCCAGCTCACCGTTTTA	CACCGTCAAGATTCCCGGAT
OPTN	TGAAAGAGCAGCGAGAGAGA	GGCAGGAATGAATCGGAATA
RPS13	GGTTGAAGTTGACATCTGACGA	CTTGTGCAACACATGTGAAT
TP53	TTCCTGAAAACAACGTTCTGTCC	TCTGGACCTGGGTCTTCAGTGAA
TXNIP	GAGCAGCCTACAGGTGAGAA	CCCAGTAGTCTACGCAACCA
VPREB1	TTGGAACCACAATCCGCCTC	CGCTGTACACACCGATGTCA

3.10 Western blotting

The nuclear protein fraction of cells was extracted by NE-PER nuclear extraction reagent (Thermo Scientific, MS, USA). Twenty-five microgram of nuclear protein was subjected to SDS–PAGE with 10% resolving gel. The gel with separated proteins was then transferred onto Immobilon-PVDF membrane (Millipore, Bedford, MA, USA). The antibodies used were NFκB/p65 (Thermo Scientific) and Histon h3 (Cell Signaling Technology, MA, USA). Blots were developed using Luminata^{TM} Classico western HRP substrate (Millipore). The density of protein band was quantified and normalized to Histon h3.

The total cellular protein fraction was extracted by using M-PER® Mammalian Protein Extraction Reagent (Thermo Scientific) and complete Mini Protease Inhibitor Cocktail Tablets (Roche Diagnostics, Germany). The procaspase antibody sampler kit (Cell Signaling) was used detect PARP, caspase 3, 7, and 9. The evaluation of loading control was determined by expression of β-actin.

3.11 Compare analysis

COMPARE analysis has been previously described in detail [179]. COMPARE analysis is based on the transcriptome-wide correlation of mRNA expression of 60 cell lines in the NCI database (USA, http://dtp.nci.nih.gov) with response ($\log_{10} IC_{50}$ values) to a selected compound. Correlation coefficients (*R*-values) were generated by a Pearson correlation test-based algorithum to produce COMPARE rankings. In the present investigation, we used CPT as test compound with cutoffs for positive correlations (*R*-value >0.5) and negative correlations (*R*-value <-0.5). Informations about the respective gene function was obtained from the GeneCard database (Weizman Institute of Science, Israel, http://www.genecards.org/) and OMIM database (NCI, USA, http://www.ncbi.nlm.nih.gov/omim).

Hierarchical cluster analysis was performed obtained from COMPARE analysis with the mRNA expression profiles for 60 NCI cell lines using the WinSTAT program (Kalmia Inc., Cambridge, MA, USA). The χ^2 test was applied to test whether the separation of cell lines according to their gene expression profiles predicted sensitivity or resistance to CPT. This test defines dependencies of bivariate normal distribution for pairs [180].

3.12 Statistics

Results were shown as mean ± standard deviation. Results were obtained from three independent experiments. Statistical analysis was determined by using Student's t-test. $p < 0.05$ was considered as statistically significant.

4. Results

4.1 Cytotoxicity of *Salvia miltiorrhiza* root extract against multidrug -resistant cancer cells

Natural products are frequently considered to be less toxic than synthetic compounds. In addition, the multifactorial activity of many natural products leave less possibilities open for cancer cells to develop drug resistance, since resistance to one mode of action may not affect other therapy-relevant cellular targets [181]. Thus, natural products might be of advantage to overcome resistance to establish anticancer drugs and to provide novel strategies for chemotherapy. For this reason, we hypothesized that *S. miltiorrhiza* may be capable to bypass drug resistance. In this study, cytotoxic effects of *S. miltiorrhiza* root extracts towards several sensitive and drug-resistant cell lines as well as correlations to apoptotic cell death have been investigated.

4.1.1 Cytotoxicity on sensitive and resistant cancer cell lines

All cancer cells were treated with varying concentrations of *S. miltiorrhiza* root extract for 72 h and cell viability was detected by the resazurin assay. *S. miltiorrhiza* root extract was cytotoxic towards CCRF-CEM and CEM/ADR5000 cell lines with IC_{50} values of 1.9 ± 0.23 μg/ml and 3.2 ± 0.83 μg/ml, respectively (Figure 10A). CPT and RA, the main compounds of *S. miltiorrhiza* root extract, showed cytotoxicity towards CCRF-CEM and CEM/ADR5000 cell lines with IC_{50} values (CPT: 4.85 ± 0.54 μM vs. 5.34 ± 0.46 μM; RA: 7.52 ± 2.69 μM vs. 35.68 ± 1.55 μM). CPT exerted more profound cytotoxicity than RA. Furthermore, the IC_{50} values were 5.5 ± 0.83 μg/ml and 4.3 ± 0.47 μg/ml for *S. miltiorrhiza* root extract against HCT116 ($p53^{+/+}$) and HCT116 ($p53^{-/-}$) cells (Figure 10B). The *S. miltiorrhiza* root extract was also active against U87.MG and U87.MGΔEGFR cells with IC_{50} values of 13.8 ± 0.7 μg/ml and 6.3 ± 2.48 μg/ml, respectively (Figure 10C). It is remarkable that *S. miltiorrhiza* root extract was slightly more cytotoxic towards HCT116 ($p53^{-/-}$) and significantly towards U87.MGΔEGFR cells than their parental wild-type cells, as indicated by degrees of resistance below 1.0. This kind of hypersensitivity is termed collateral sensitivity. In the following experiments, CCRF-CEM cells were used for further investigation.

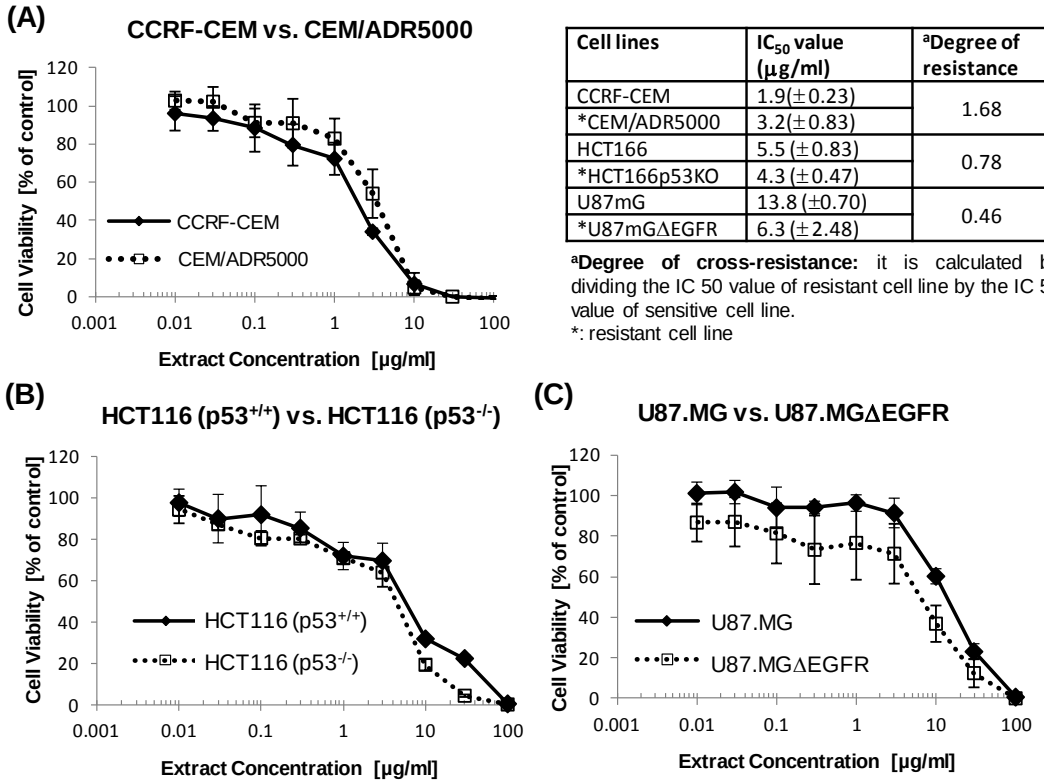

Cell lines	IC_{50} value (µg/ml)	[a]Degree of resistance
CCRF-CEM	1.9(±0.23)	1.68
*CEM/ADR5000	3.2(±0.83)	
HCT166	5.5 (±0.83)	0.78
*HCT166p53KO	4.3 (±0.47)	
U87mG	13.8 (±0.70)	0.46
*U87mGΔEGFR	6.3 (±2.48)	

[a]**Degree of cross-resistance:** it is calculated by dividing the IC 50 value of resistant cell line by the IC 50 value of sensitive cell line.
*: resistant cell line

Figure 10. Cell viability of resistant cells and their according parental cells with treatment of *S. miltiorrhiza* root extract. (A) CCRF-CEM cells and CEM/ADR5000 cells, (B) HCT116 ($p53^{+/+}$) cells and HCT116 ($p53^{-/-}$) cells and (C) U87.MG and U87.MGΔEGFR cells were treated with varying concentration of *S. miltiorrhiza* root extract. After 72 h of incubation, resazurin assays were performed. At least three independent experiments with each 6 parallel measurements were performed. IC50 values for different sensitive and resistant cancer cell lines after 72 h treatment were shown in the table.

4.1.2 Induction of cell cycle arrest and apoptosis

As leukemia cells are easier to process by flow cytometry than solid cancer cells, we continued our experiments with CCRF-CEM cells. We further explored the effect of *S. miltiorrhiza* root extracts on the cell cycle distribution of CCRF-CEM cells. As shown in Figure 11A and B, sub-G1 and S phases were induced upon treatment starting from a concentration of 10 µg/ml, implying that cellular DNA damage led to cell cycle arrest and apoptosis. DAPI staining revealed the appearance of apoptotic bodies and nuclear condensation upon treatment with *S. miltiorrhiza* root extract (Figure 11C).

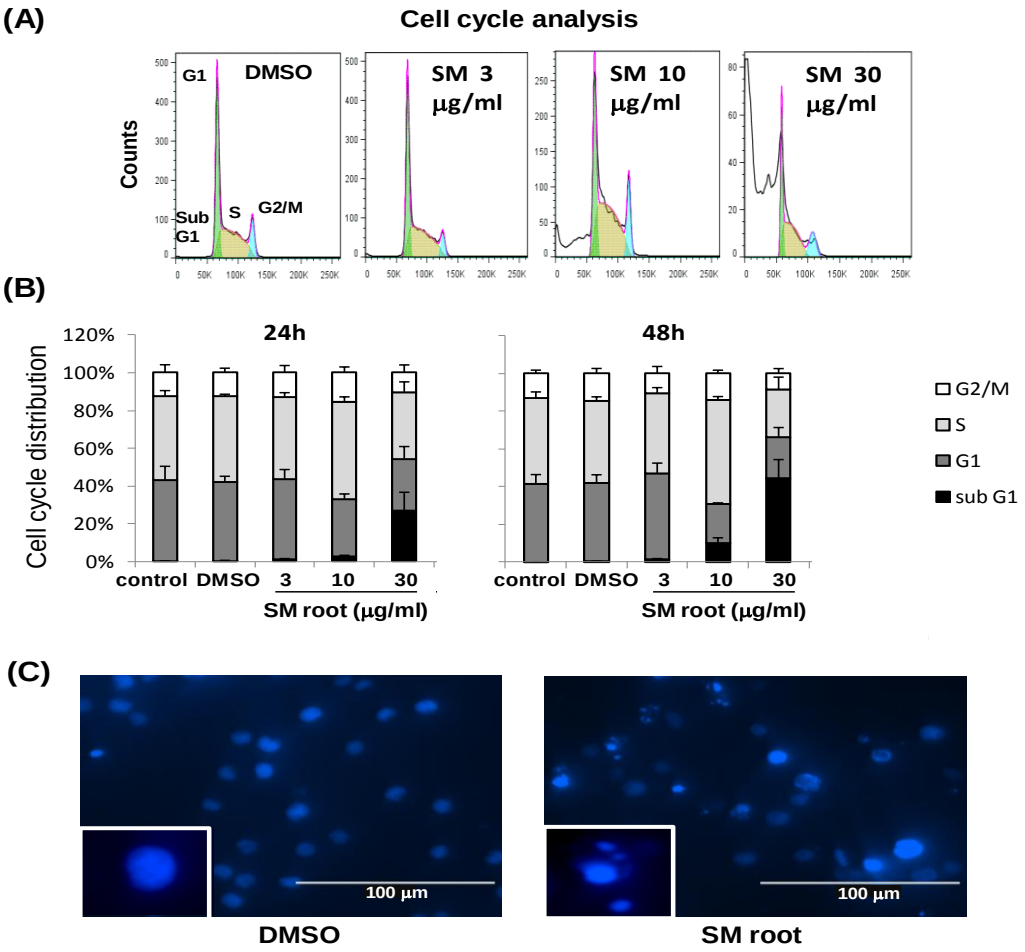

Figure 11. Effect of *S. miltiorrhiza* root extract on cell cycle distribution and apoptosis induction in CCRF-CEM cells. (A) Representative DNA content histograms of CCRF-CEM treated with indicated concentrations for 48 h. (B) Results upon treatment for 24 or 48 h presented as mean ± SD of three independent experiments. (C) CCRF-CEM cells were treated with DMSO or *S. miltiorrhiza* root extract. Nuclei were stained by DAPI and the fluorescent images were captured by fluorescent microscope.

4.1.3 Induction of ROS

Cell cycle arrest mediated by *S. miltiorrhiza* root extract implies cellular damage, which might be a consequence of oxidative stress [182]. Therefore, intracellular ROS levels were further investigated in CCRF-CEM cells upon treatment of *S. miltiorrhiza* root extracts. Indeed, *S. miltiorrhiza* root extracts as well as H_2O_2 induced ROS production as detected by flow cytometric H_2DCFH-DA staining (Figure 12A and B). Statistically significant increased ROS levels were observed after treatment with 3, 10 or 30 µg/ml (Figure 12C).

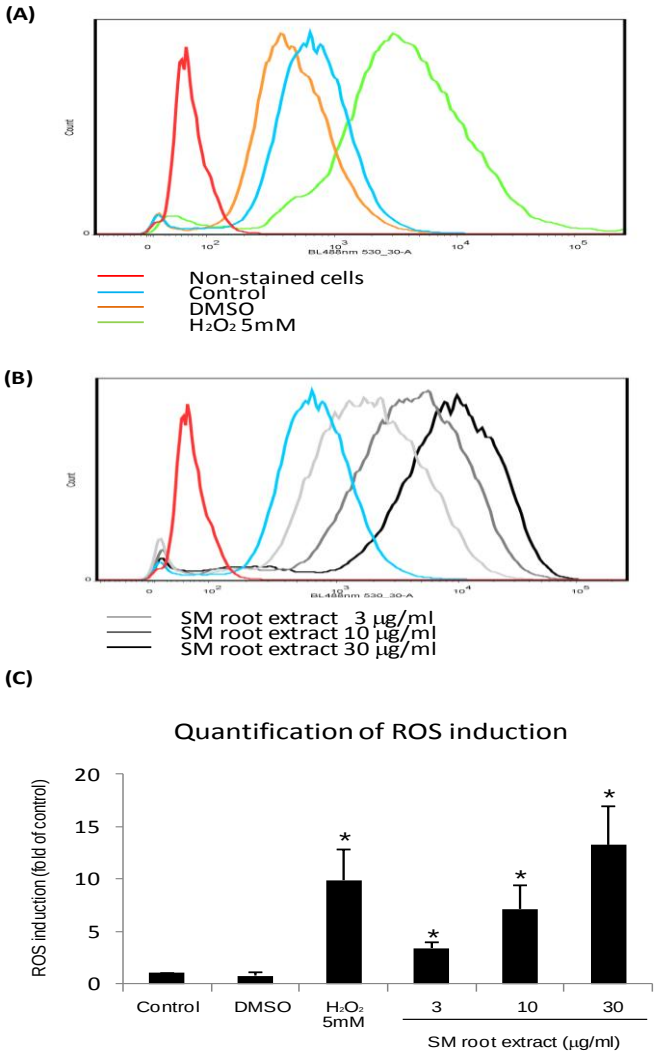

Figure 12. Effect of *S. miltiorrhiza* root extract on ROS generation. ROS production was measured by flow cytometry after treatment of CCRF-CEM cells with (A) 5 mM H_2O_2 for 15 min and (B) varying concentration of *S. miltiorrhiza* extract for 1 h. (C) Quantitative results of ROS production. *: $P<0.05$ compared with DMSO.

4.1.4 Cleavage of caspases and PARP

When cells undergo apoptosis, PARP, the nuclear enzyme, which binds to single-strand DNA, breaks assisting repair process, is cleaved and inactivated [183]. Thus, we investigated, whether PARP may be involved in *S. miltiorrhiza* root extract-induced apoptosis on CCRF-CEM cells. As indicated in Figure 13, Western blotting showed that full-length PARP (116 kDa) was cleaved into an 89 kDa fragment, suggesting involvement of PARP inactivation in apoptosis due to *S. miltiorrhiza* root extract application. Cleavage of PARP was predominately

mediated by caspase 3 [184]. Other caspases such as caspase 7 are also responsible for cleavage [185,186]. Our results demonstrated that caspase 3 and 7 were both activated upon application of *S. miltiorrhiza* root extracts by showing cleaved segments at 17 and 20 kDa, respectively (Figure 13A, B). Caspase 9, the initiator of the intrinsic mitochondrial apoptotic pathway, cleaving of effector caspases 3 and 7, was also cleaved and activated [187]. Taken together, *S. miltiorrhiza* root extract appeared to induce apoptosis through caspases and a PARP-dependent pathway.

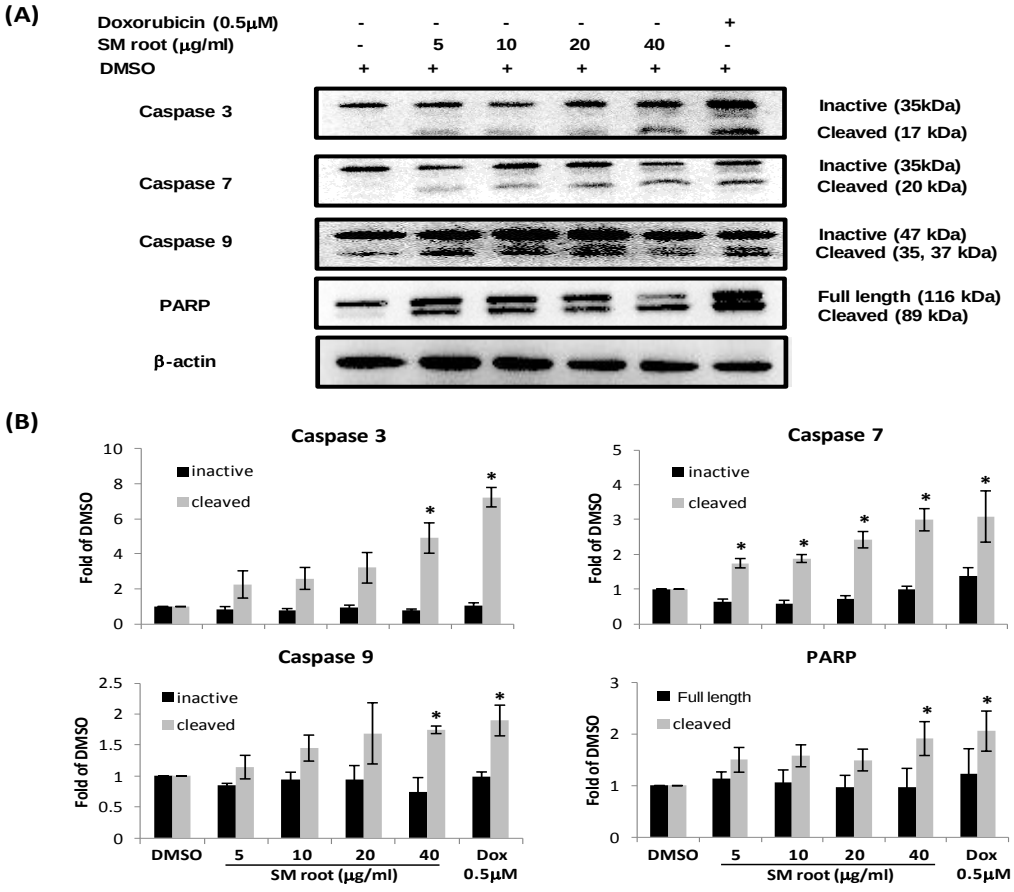

Figure 13. Effect of *S. miltiorrhiza* root extract on cleavage of caspases and PARP. (A) Western blot was performed to detect *S. miltiorrhiza* root extract-induced cleavage of caspases 3, 7, and 9 and PARP. β-actin was used as internal control. (B) Cleavage of caspases 3, 7, and 9 and PARP was quantified and normalized by expression of β-actin. *: $p<0.05$ compared with DMSO.

4.1.5 HPLC analysis

The ingredients in root extracts of *S. miltiorrhiza* were determined by HPLC analysis. The presence of miltirone, CPT and RA in *S. miltiorrhiza* root extracts was confirmed

by HPLC-MS. The other minor chemical compounds have not been further considered.

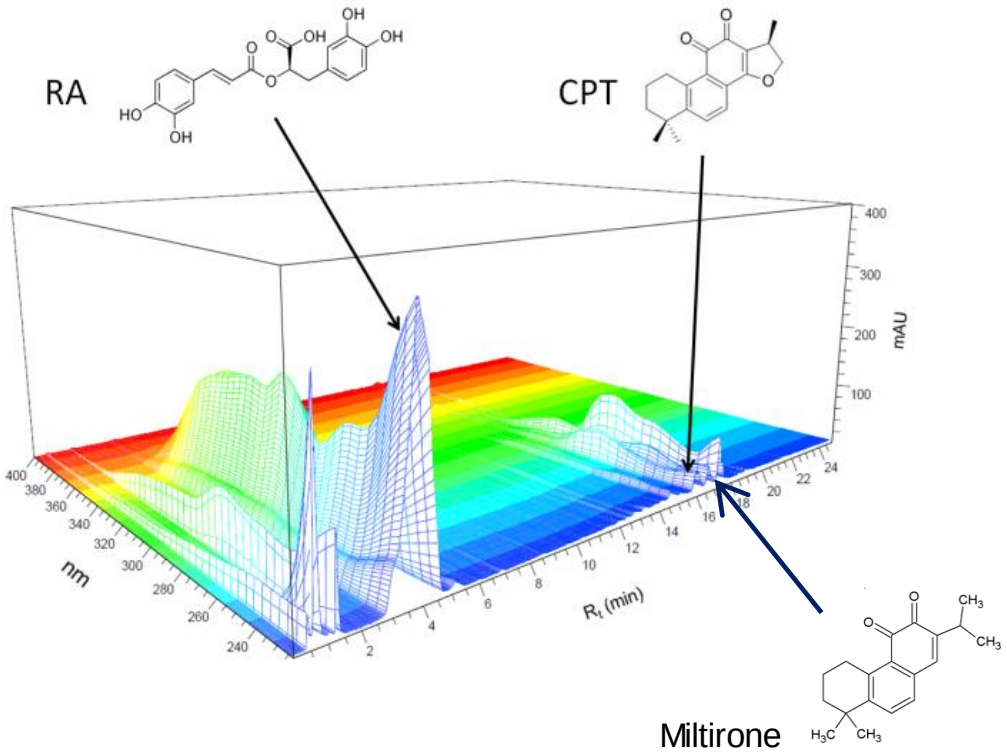

Figure 14. HPLC analysis for *S. miltiorrhiza* root extract. Chromatograms of *S. miltiorrhiza* root extract at an absorption of 250 nm.

4.1.6 Summary: Cytotoxicity of *S. miltiorrhiza* root extract against multidrug -resistant cancer cells

The results indicated that *S. miltiorrhiza* root extract has a strong cytotoxic effect on a wide variety of sensitive and resistant cancer cell lines. *S. miltiorrhiza* root extracts induced ROS-mediated apoptotic cancer cell death. Cell cycle arrest and PARP cleavage implied that *S. miltiorrhiza* root extracts are potentially inducing DNA damage. Furthermore, activation of caspase 9 suggested mitochondrial dysfunction. Cleavage of the effector caspases 3 and 7 ensured the activation of caspase-dependent apoptosis. Thereby, the investigation suggested that *S. miltiorrhiza* root extracts induced cytotoxicity through the mitochondria-mediated intrinsic apoptotic pathway. Guided by HPLC analysis which revealed *S. miltiorrhiza* root extract contains three major ingredients including CPT, miltirone and RA, the mechanisms of the three compounds towards leukemia cells were individually explored in detail in the following chapters.

4.2 Anticancer activity of cryptotanshinone (CPT) on acute lymphoblastic leukemia cells

In this study, we aim to investigate molecular modes of action of CPT in acute lymphoblastic leukemia (ALL) cells. Guided by transcriptomic microarray profiles, we validated CPT-regulated gene functions and pathways in drug-sensitive and multidrug-resistant ALL cell lines.

4.2.1 CPT induced cytotoxicity on sensitive and resistant leukemia cell lines

CCRF-CEM and CEM/ADR5000 cells were treated with varying concentrations of CPT for 72 h and cell viability was detected by the resazurin assay. CPT induced cytotoxicity towards both cell lines with IC_{50} values of 4.8 ± 0.66 µM and 6.0 ± 0.81 µM, respectively (Figure 15B). Doxorubicin is a substrate of P-gp and was used as control drug. It revealed IC_{50} values of 0.005 ± 0.0004 µM in sensitive and 16.6 ± 3.48 µM in resistant cells (Figure 15C). As indicated by the degrees of cross-resistance, doxorubicin was remarkably more active on sensitive cells than on resistant ones, while CPT showed equal sensitive to both resistant and sensitive cells with the degree of resistance value at 1.04. Thus, the results implied that CPT can bypass P-gp and can be used to treat P-gp overexpressing multidrug-resistant cancer cells with the same efficacy as sensitive ones.

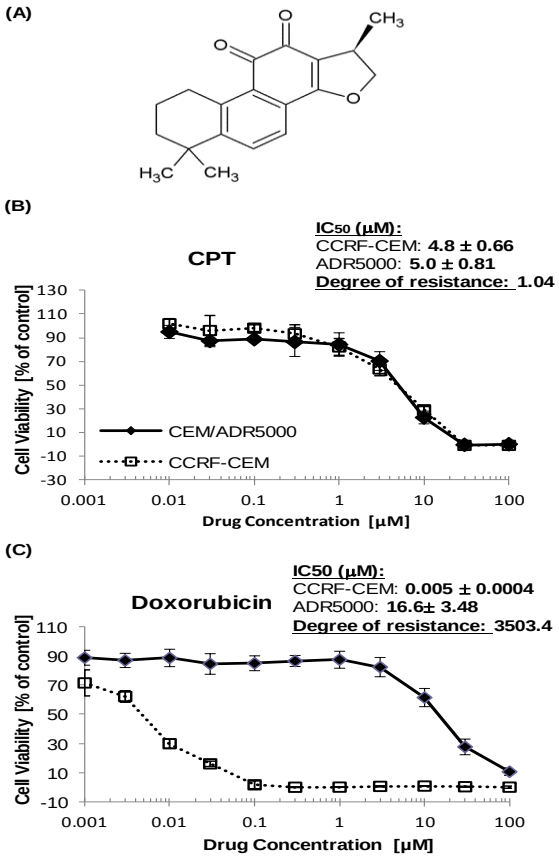

Figure 15. Cell viability of CCRF-CEM and CEM/ADR5000 cells with treatment of CPT. (A) Chemical structure of CPT. (B) Cells were treated with varying concentration of CPT and doxorubicin (C) following seeding. After 72 h of incubation, resazurin assays were performed.

4.2.2 Microarray gene profile of CPT on CCRF-CEM cells

Global gene expression of CCRF-CEM cells in response to CPT treatment was determined by microarray-based transcriptome-wide mRNA hybridization. CCRF-CEM cells were treated with 10 μM CPT or DMSO for 24 h. A total of 660 genes were significantly deregulated upon CPT treatment in comparison to DMSO treatment as analyzed by Chipster software ($p < 0.05$). Significance was assessed using empirical Bayes t-test ($P < 0.05$) with Benjamini-Hochberg correction. The dataset of deregulated genes from microarray hybridization was subjected to ingenuity Pathway Analysis (IPA) to identify possible signaling pathways and modes of action. The most remarkable biological functions identified by IPA were cellular growth and proliferation, cell death and survival, cell cycle, lipid metabolism, free radical scavenger, DNA replication and repair, cellular movement and energy production (Figure 16A). The most pronounced canonical pathways correlating with the deregulated genes included unfolded protein response (UPR), EIF2 signaling, Antioxidant action, TNFR2 signaling, and JAK/STAT signaling. Considering the top deregulated pathways, it can be implied that a 24 h treatment with 10 μM CPT affected UPR signaling, which in turn regulated general protein translation via eIF2 signaling (Figure 16B).

(A)

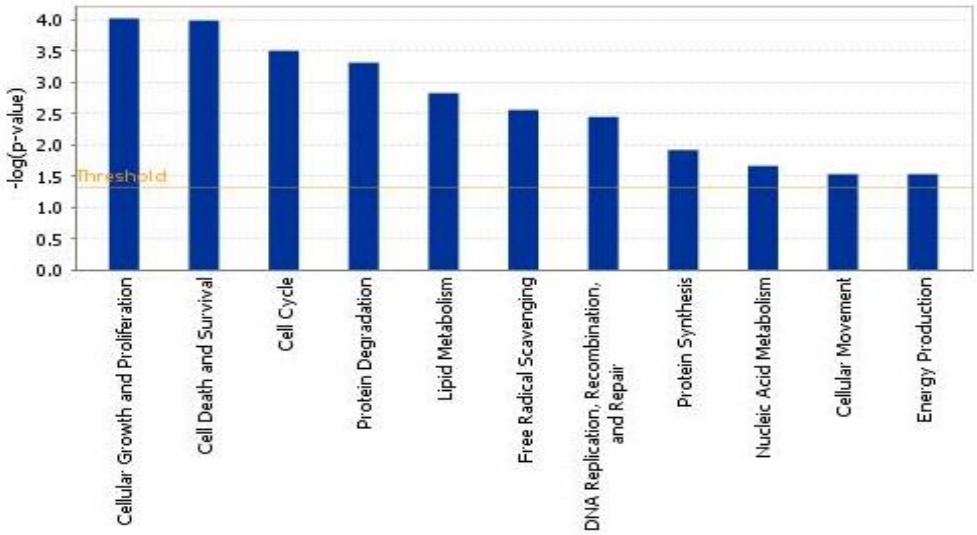

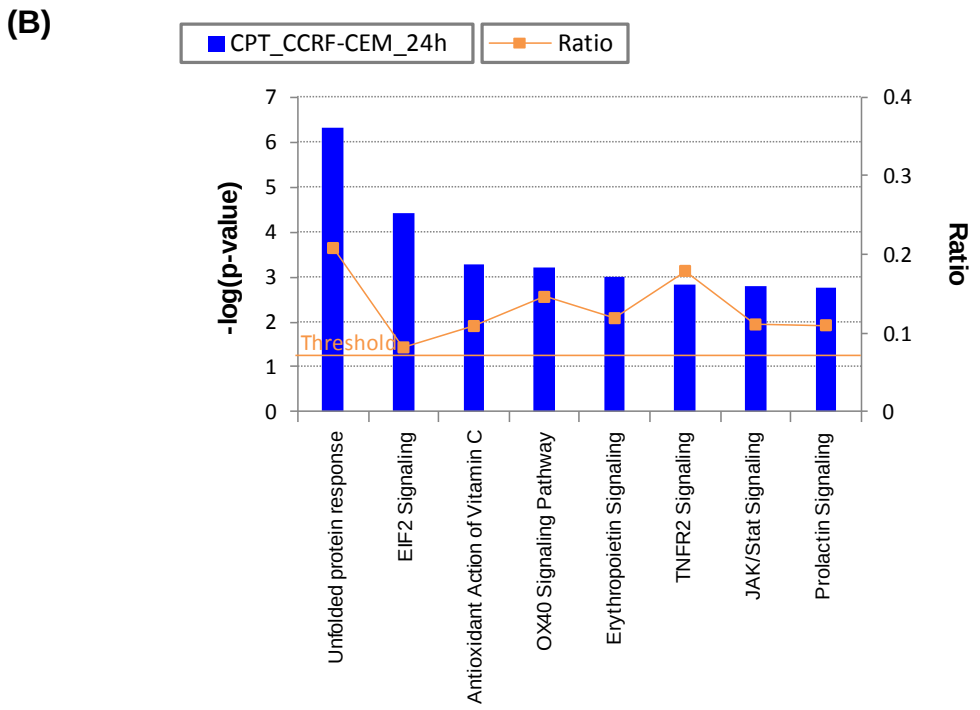

Figure 16. Microarray-based mRNA expression profiling of CCRF-CEM cells treated with CPT. Functional groups of genes were identified using the Ingenuity Pathway Analysis software. (A) Top biological function. (B) Canonical pathway. P-values were calculated using right-tailed Fisher's exact test. Ratio indicates the percentage of genes which are deregulated in a given pathway.

4.2.3 Validation of microarray gene expression

We performed quantitative real-time polymerase chain reaction (qPCR) in selected examples to validate the gene expression of microarray results by another independent technique. Seven up-or down-regulated genes were selected and the fold-change ratios of glue expressions in treated and non-treated cells were calculated. The fold-change values obtained from microarray hybridizations and qPCR reactions were subjected to linear regression. The correlation coefficient was R=0.9794, indicating high accordance between microarray and qPCR results (Table 2).

Table 2. Validation of microarray gene expression profiling for selected genes by quantitative real-time RT-PCR.

Gene name	Microarray data (FC)	qPCR data (FC)[b]
AKR1C3	1.765	1.5555 ± 0.12
DUSP6	2.181	3.164 ± 0.13
TXNIP	1.357	1.63 ± 0.47
IGLL1	-1.84	-1.755 ± 0.31
BIK	-1.879	-1.2835 ± 0.13
VPREB1	-1.542	-1.268 ± 0.11

[a]R value= 0.9794

[a]Correlation coefficient (R value) of mRNA expression values between microarray hybridization and RT-PCR as determined by Pearson Correlation Test.

[b] FC: Fold change

4.2.4 CPT induced oxidative stress, DNA damage and MMP disruption

The microarray-based gene expression profiling showed that CPT treatment was associated with free radical scavenger and DNA repair pathways, implying that ROS production and DNA damage may occur by CPT treatment. Therefore, we studied cellular ROS levels and induction of DNA damage upon CPT treatment. Indeed, one hour of CPT treatment induced ROS in a dose-dependent manner as detected by flow cytometric H_2DCFH-DA staining. Statistically significant increased ROS levels were observed after treatment with 1, 3, 10 or 30 μM. ROS induction by CPT was lower than by 5 mM H_2O_2 (Figure 17A, B).

Followed by the results that CPT induced excess ROS production, we further investigate whether DNA damage is induced by CPT. Increasing CPT concentration damaged DNA upon 24 h treatment as investigated by single cell gel electrophoresis (Comet assay). The percentage of tail DNA (= damaged DNA) increased and the percentages of head DNA (= intact DNA) simultaneously decreased. DNA migration was monitored by tail and Olive tail movements (Figure 17C, D). The *in vitro* results of DNA damage and ROS production corroborated the microarray results and implied that CPT-induced ROS production might lead to DNA damage.Since we found that CPT stimulated ROS and DNA damage, we further examined MMP upon CPT treatment. CCRF-CEM cells stained with JC-1 shifted from red to green fluorescence after CPT treatment for 24 or 48 h (Figure 17E, F), indicating a breakdown of MMP. The result that CPT induced mitochondrial dysfunction is consistent with the deregulated gene expression regulating energy production (Figure 16).

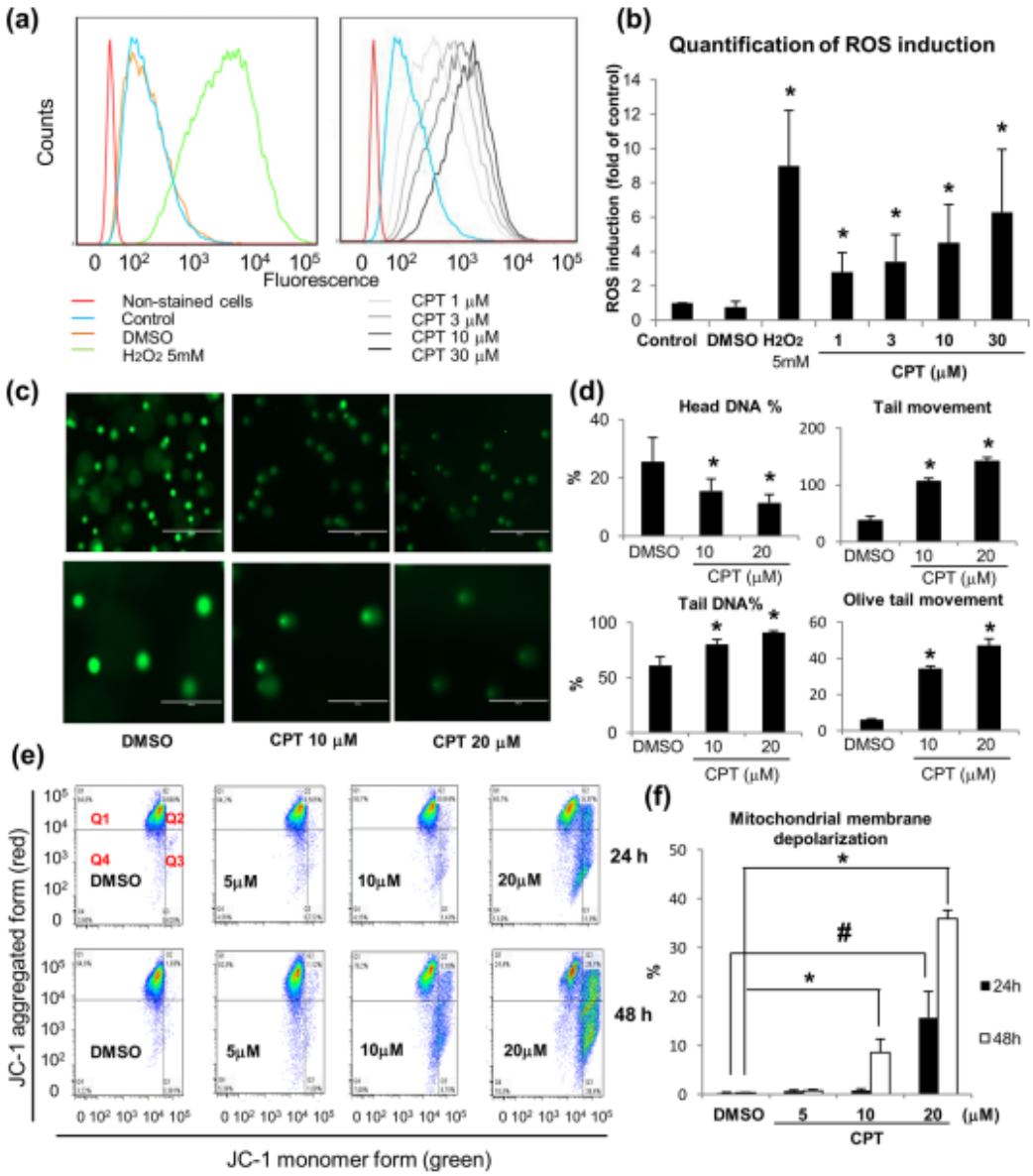

Figure 17. The effects of CPT on MMP, ROS and DNA damage. (A) ROS production was measured by flow cytometry after treatment of CCRF-CEM cells with varying concentrations of CPT for 1 h, DMSO or 5mM H_2O_2. (B) Statistical quantification of ROS levels as mean fold-change values ± SD (C) Cells were incubated with different concentration of CPT for 24 h. DNA damage was evaluated by the comet assay. (D) Representative pictures of comet assay magnification (upper panel: 100×; lower panel: 400×). Four parameters including % of head DNA, tail DNA, tail movement and Olive tail movement were measured. Tail movement and Olive tail movement were presented in arbitrary units. Results were presented as mean ± SD of 25 cells. *: P<0.05 compared with DMSO. (E) Cells were treated with CPT for 24 or 48 h, and stained by JC-1. Healthy cells mainly appeared in J-aggregared form with red fluorescence (Q1) and apoptotic cells formed JC-1 monomers with green fluorescence (Q3). (F) Statistical results of CPT on cell population in Q3, which was defined as disruption of mitochondrial membrane potential. #: P<0.05 compared with DMSO for 24 h; *: P<0.05 compared with DMSO for 48 h.

4.2.5 CPT initiated intrinsic mitochondrial apoptotic pathway

Since we have shown that CPT induced cytotoxicity, DNA damage and MMP disruption, we further hypothesized that CPT induced the intrinsic, mitochondrial apoptotic pathway on CCRF-CEM cells. Firstly, CPT induced apoptosis was validated by DAPI stain and cell cycle analysis. Apoptotic bodies and nucleus condensation were observed with DAPI staining after 24 h of CPT treatment (Figure 18A). Cell cycle analysis revealed that G2/M arrest was increased dose-dependently accompanied with slight S phase arrest after 24 h of CPT incubation. Expression of sub-G1 peak can be seen at high CPT doses (Figure 18B, C).

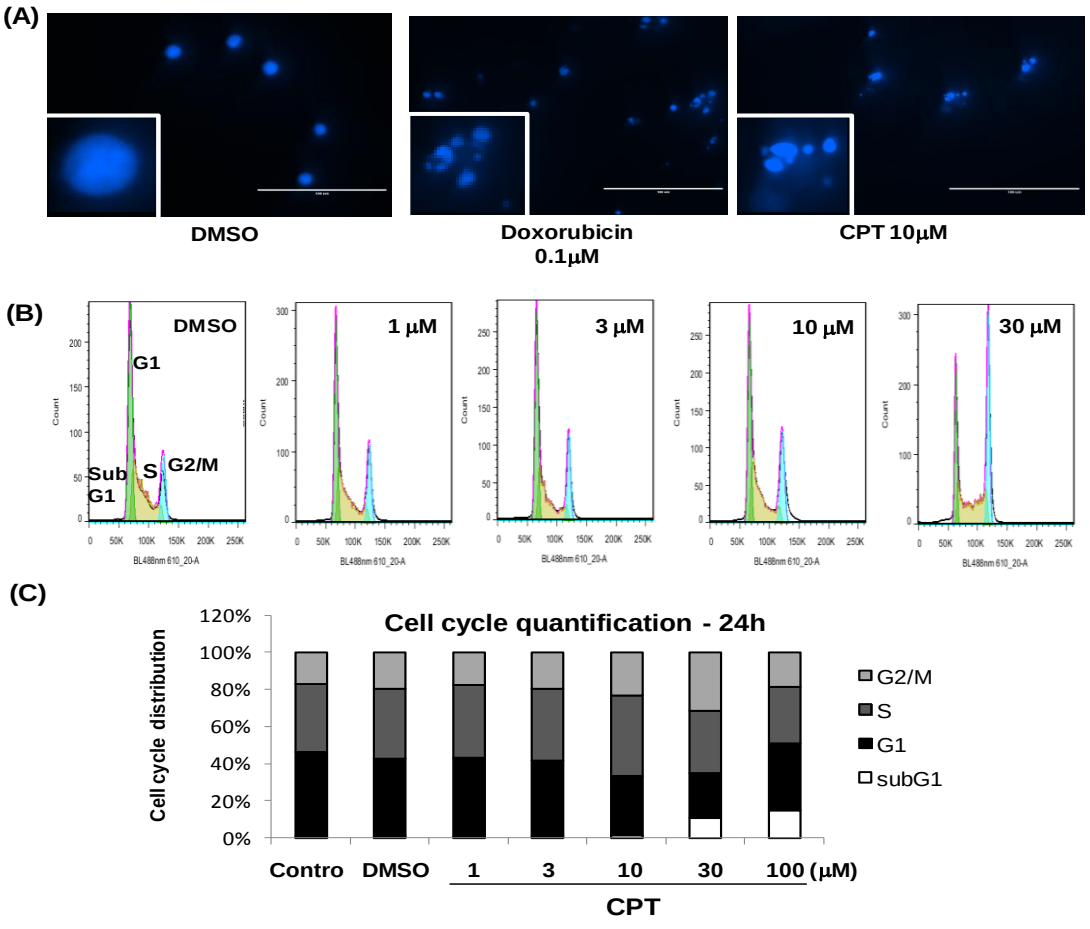

Figure 18. CPT induces apoptosis in CCRF-CEM cells. (A) DAPI-stained CCRF-CEM cells. The white arrow shows apoptotic bodies. Doxorubicin was used as control drug. (B) DNA content histograms of CCRF-CEM treated with indicated concentrations for 24 h. Cell cycle distribution of CCRF-CEM cells was statistically calculated after treatment with varying concentrations for 24 h. (C) These results were presented as mean value of three independent experiments.

After incubating with 5, 10 or 20 µM CPT for 48 h, early apoptosis was measured by flow cytometry and annexin V (AV)-FITC propidium iodide (PI) staining. The cell population of AV^+PI^- and AV^+PI^- fractions, which represent early apoptosis and late stage of apoptosis, respectively, increased in contrast to DMSO group (Figure 19A, B).

Upon MMP breakdown and initiation of the intrinsic mitochondrial apoptotic pathway initiator caspase 9 is activated, which in turn causes the cleavage of effector caspases including caspases 3 and 7 and finally leads to apoptosis. Therefore, we investigated the activity of caspases 3/7 and 9 in CPT-treated CCRF-CEM cells. The results of luminescence assays revealed that all caspases were cleaved and activated in a dose-dependent manner upon CPT treatment (Figure 19C).

PARP is a nuclear enzyme, whose expression is triggered by DNA damage. If cells undergo apoptosis, PARP is cleaved by caspase 3 to inactivate the ability of PARP to respond to DNA damage. As caspase 3 was activated by CPT, we also explored PARP cleavage by CPT. Western blotting showed that CPT dose-dependently induced PARP cleavage (Figure 19D). Taken together, these data showed that CPT leads to ROS generation, MMP disruption and caspase-dependent apoptosis.

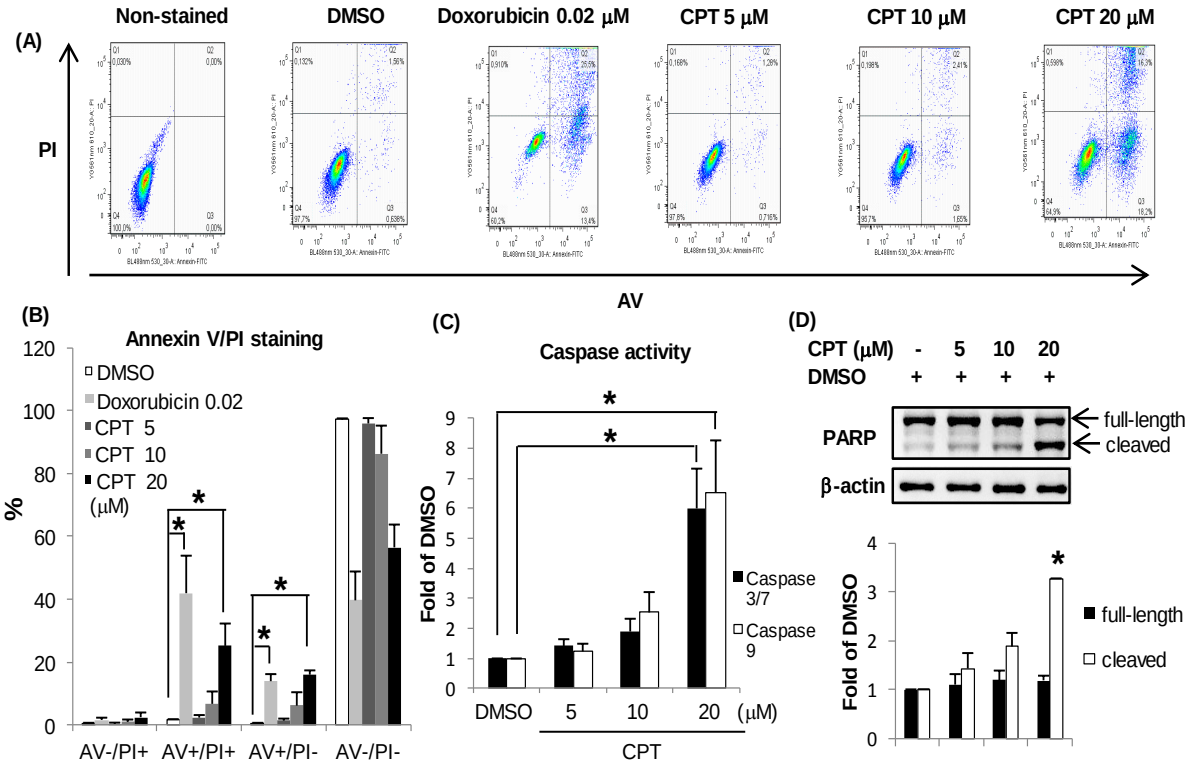

Figure 19. CPT stimulated caspase-dependent apoptosis. (A) Cells were treated with the compounds for 48 h. Doxorubicin was used as a positive control. The signals of AV-FITC binding and PI staining were detected by flow cytometry. (B) Quantification of AV-FITC and PI binding. (C) Induction of caspase 3/7 and caspase 9 after treatment of CCRF-CEM cells with CPT. Cells were treated with the compounds for 24 h. (D) Western blot was performed to detect CPT-induced PARPcleavage. The lower panel shows the quantification of inactive and cleaved PARP. β-actin was used as an internal control. *: $P<0.05$ compared with DMSO.

4.2.6 CPT binds IKK-β and inhibits nuclear p65 expression

We hypothesized that NFκB may be an important transcription factor regulating CPT-induced cellular responses. Deregulated genes of the most pronounced signaling networks identified by microarray data involving cell death and survival, cellular growth and proliferation, and cell cycle were selected for motif analysis. This is a computational approach aiming at the identification of binding sites for transcription factors in the DNA sequence of gene promoters. This technique has been applied for genes identified by microarray analysis and belonging to the most prevalent pathways. As shown in Table 3, diverse NFκB elements (NFκB1, NFκB2, RelA, RelB and c-Rel) were found among the top ranked transcription factors that may potentially bind to these gene promoters. This emphasizes that motifs of NFκB complex were predominant for deregulated genes and that NFκB may be a key regulator for the activity of CPT in ALL cells.

As CPT induced DNA damage and apoptosis, we further speculated that CPT may interact with NFκB signaling. IKK-β phosphorylates NFκB inhibitor protein IκB, leading to degradation of IκB and activation of NFκB, which in turn stimulates downstream transcriptional genes in the nucleus. Thus, we studied the binding of CPT to inhibitor κB kinase-β (IKK-β) by another computational approach. The most frequent hydrophobic binding residues of IKK-β are Leu21, Gly22, Gly24, Val29, Ala42, Tyr98, Gly102, Lys147 and Ile165. Additionally, IKK-β inhibitors are also supposed to interact with the hinge motif, which is composed of Glu97 and Cys99 [188]. As shown in molecular docking analysis, CPT was situated to the same ATP binding region as MG132, a reference compound for NFκB inhibition, with binding to the same ATP hydrophobic residues including Val29, Glu97, Tyr98, Cys99, Glu100 and Gly102. Meanwhile, CPT also formed a hydrogen bond at binding residue Glu100, as did MG132 (Figure. 20A, B). Notably, CPT showed better binding energy and lower predicted Ki values (-8.34 kcal/mol; 0.77 μM) than the known NFκB inhibitor, MG132 (-7.59 kcal/mol; 7.33 μM) (Table 4). This CPT revealed higher affinity to IKK-β than MG132, suggesting that CPT may interact with IKK-β.

Table 3. Motifs depending on Cistrome analysis for deregulated genes upon CPT treatment

	Motif	Z score	-log10(p-val)		Motif	Z score	-log10(p-val)
1	SREBF1	-6.311	226.97	33	cebpe	-3.953	101.607
2	CBF1	-6.097	213.37	34	Hmx3	-3.944	101.23
3	TFEB	-6.036	209.568	35	USF1	-3.94	101.084
4	CEBPA|Cebpb	-5.59	182.93	36	PTEN	-3.937	100.975
5	MAX	-5.574	182.036	37	Arnt	-3.878	98.501
6	***RELB|NFKB2**	**-5.414**	**172.927**	38	Yap6	-3.853	97.489
7	RAP1	-5.295	166.353	39	CST6	-3.851	97.394
8	CREB|CREB1	-5.229	162.789	40	DEAF1	-3.844	97.138
9	MECP2	-4.942	147.649	41	ZNF326	-3.838	96.891
10	TAF-1	-4.882	144.619	42	NR4A1	-3.831	96.603
11	MAF|Maf	-4.88	144.496	43	USF2	-3.756	93.587
12	EREG|ESR1	-4.818	141.39	44	AGP1	-3.724	92.285
13	PHO4	-4.751	138.022	45	YY1	-3.685	90.746
14	ATF2|Atf2	-4.736	137.271	46	TFAP4	-3.682	90.635
15	HEB|TCF12	-4.66	133.596	47	Mycn	-3.673	90.273
16	RXRA	-4.62	131.663	48	RUNX2	-3.67	90.166
17	STAT1	-4.524	127.065	49	BDP1	-3.647	89.288
18	HAC1	-4.5	125.915	50	PPARG	-3.643	89.118
19	p53|TP53	-4.493	125.593	51	E2F1	-3.633	88.725
20	NERF1a|ELF2	-4.463	124.199	52	Myc	-3.631	88.637
21	TCF4|Tcf4	-4.452	123.673	53	PIF1	-3.613	87.961
22	Ebox	-4.449	123.537	**54**	***REL**	**-3.612**	**87.936**
23	TGA1b	-4.344	118.68	55	Stra13	-3.59	87.094
24	MYF	-4.257	114.78	56	ZFP36L1	-3.56	85.937
25	SPF1	-4.206	112.52	57	CG1	-3.549	85.491
26	ATF3	-4.18	111.35	58	RITA-1	-3.513	84.155
27	***P50:RELA-P65**	**-4.177**	**111.218**	59	ZHX3	-3.512	84.1
28	Atf1	-4.126	109.017	60	TGIF2	-3.455	81.964
29	LEF1	-4.115	108.518	61	Tye7	-3.452	81.875
30	Hand1|Tcfe2a	-4.111	108.347	62	FOXP3	-3.439	81.372
31	PCF5	-4.078	106.944	**63**	***NFKB1**	**-3.4**	**79.961**
32	***c-Rel|REL**	**-4.047**	**105.613**	64	RUNX1	-3.376	79.075

*: belongs to NFκB complex

Table 4. Molecular docking of cryptotanshinone to IKK-β. The frame performed the lowest binding energy and name of hydrogen bond.

Compound	Lowest binding energy (kcal/mol)	Mean binding energy (kcal/mol)	Residues of hydrogen bond	Numbers of residues involved in hydrophobic interaction	PKi value[a] (μM)
MG132 (IKKβ inhibitor)	-7.59	-6.49	Cys99, Glu100, Gly102, Asp103	16	7.33
CPT	-8.34	-8.34	Glu100	10	0.77

[a]**pKi** (predicted Ki): Ki is the inhibition constant for a drug. The pKi value is used to evaluate affinity of drug to a target structure.

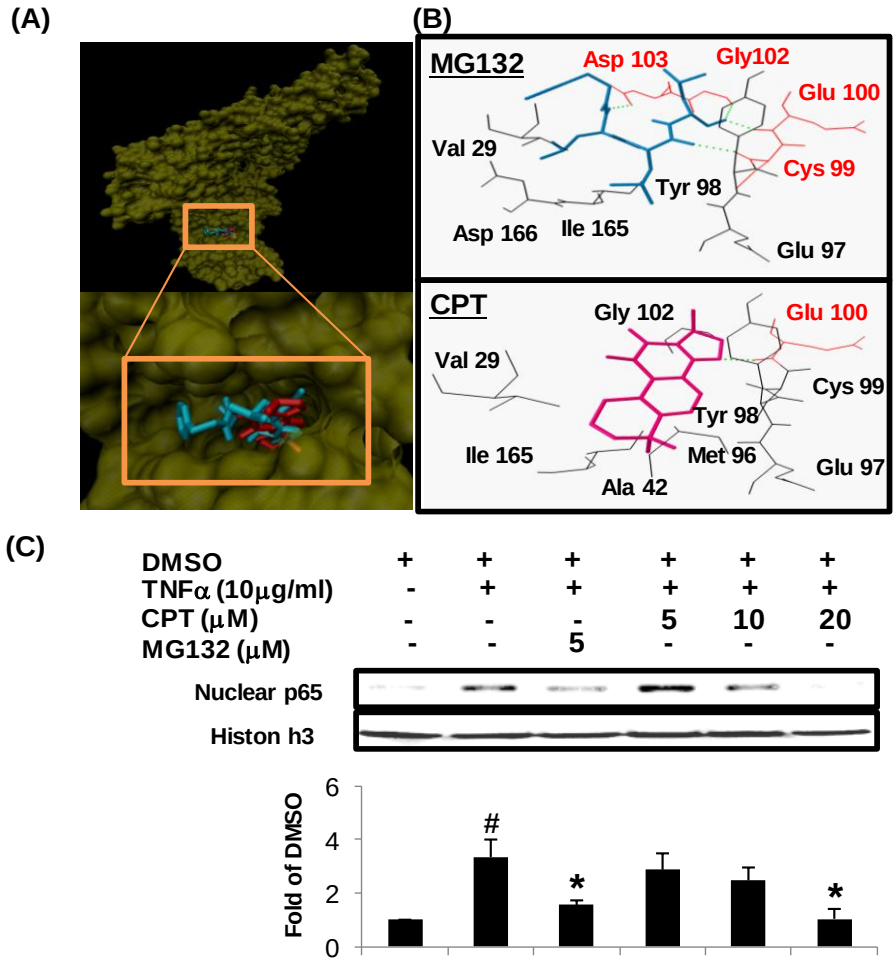

Figure 20. CPT interacts with NFκB signaling. (A) Molecular docking studies of CPT to IKK-β. Docking of MG132, a well-known IKK-β inhibitor was subjected as control drug. VMD files presented the binding site of CPT (red) in comparison with MG132 (blue). (B) The residues involved in the formation of hydrogen bonds are labeled in red, and hydrogen bonds are shown as green dots. (C) Cells were treated with CPT for 24 h and MG132 for 2 h prior to 1 h induction by TNFα. Cell lysates were collected and the nuclear protein fraction was extracted. Western blot analysis was used to detect nuclear p65 expression. Histon h3 was used as internal control. #: $P<0.05$ compared with DMSO; *: $P<0.05$ compared with TNFα.

We assumed that CPT might bind to IKK-β and influence downstream effects of transcription. Hence, we investigated whether CPT decreases nuclear p65 translocation. The expression of nuclear p65 protein was detected by western blotting. TNF-α was used as a strong inducer of NFκB activity. As shown in Figure 20C, TNFα-induced translocation of p65 from the cytoplasm to the nucleus was inhibited by CPT. In sum, CPT inhibited NFκB signaling, which may contribute to cell apoptosis.

4.2.7 CPT inhibited cell adhesion

Infiltration of tissues (e.g. central nerve system) by migrated leukemia cells are observed in ALL patients with poor prognosis. Invasion of leukemia cells into tissues results from cell adherence to endothelial cells [189]. The role of NFκB in the activation of adhesion molecules has been abundantly explored [190]. Activation of NFκB was reported to regulate the expression of adhesion molecules on human promyelocytic leukemia HL-60 cells [191]. Analysis of the adhesion molecules, such as VCAM-1, ICAM-1 and E-selectin, has revealed that these genes contain binding motifs for the NFκB transcription factor [192]. Inhibition of adherent molecules on leukemia cells and endothelial cells by blocking NFκB transcription or overexpression of IκBα lead to inhibition of cell adhesion [190,193,194]. These reports suggested that the relationship between NFκB transcription and cell adhesion plays an important role in development of ALL. We have shown that CPT inhibited NFκB signaling, therefore, we further investigate whether CPT influenced cell adhesion. After 2 h incubation, CPT dose-dependently down-regulated cell adhesion, reaching statistical significance and nearly 50% of inhibition at a concentration of 20 μM (Figure 21). Of note, the reduction of cell adhesion by CPT was not due to cytotoxicity and high doses of CPT did not change cell morphology. This result is consistent with the microarray gene expression profile showing the deregulation of genes involved in cellular movement, implying that CPT may have the potential to inhibit invasion of leukemia cells.

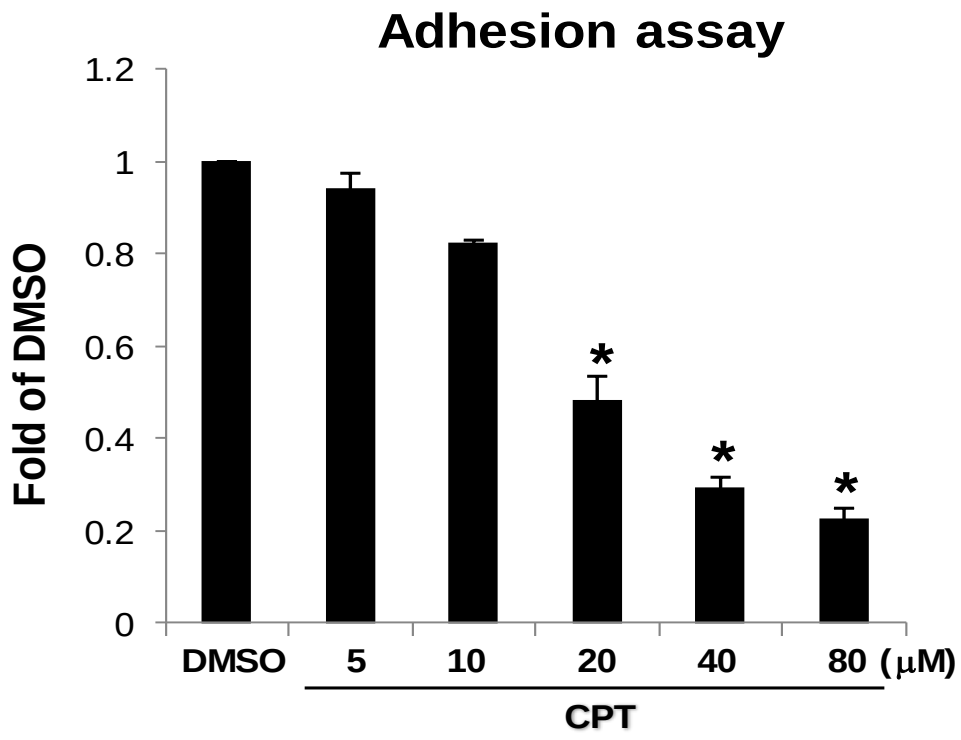

Figure 21. CPT inhibits cell adhesion. Cells were incubated with different doses of CPT in fibronectin-coated wells and were allowed to adhere for 2 h at 37°C. Attached cells were determined by resazurin assay. Representative results were shown in bar chart. *: $P<0.05$ compared with DMSO.

4.2.8 Cluster analysis of microarray-based transcriptome-wide mRNA expression

The genetic determinants of sensitivity and resistance to CPT were investigated at a transcriptome-wide level. Firstly, the $\log_{10} IC_{50}$ values of CPT for 60 tumor cell lines revealed that cell lines from different tumor types reacted in a different manner to CPT. Brain cancer and melanoma were most sensitive toward CPT, while renal and breast cancer cell lines were the most resistant ones. The other cell lines including leukemia were of intermediate sensitivity (Figure 22).

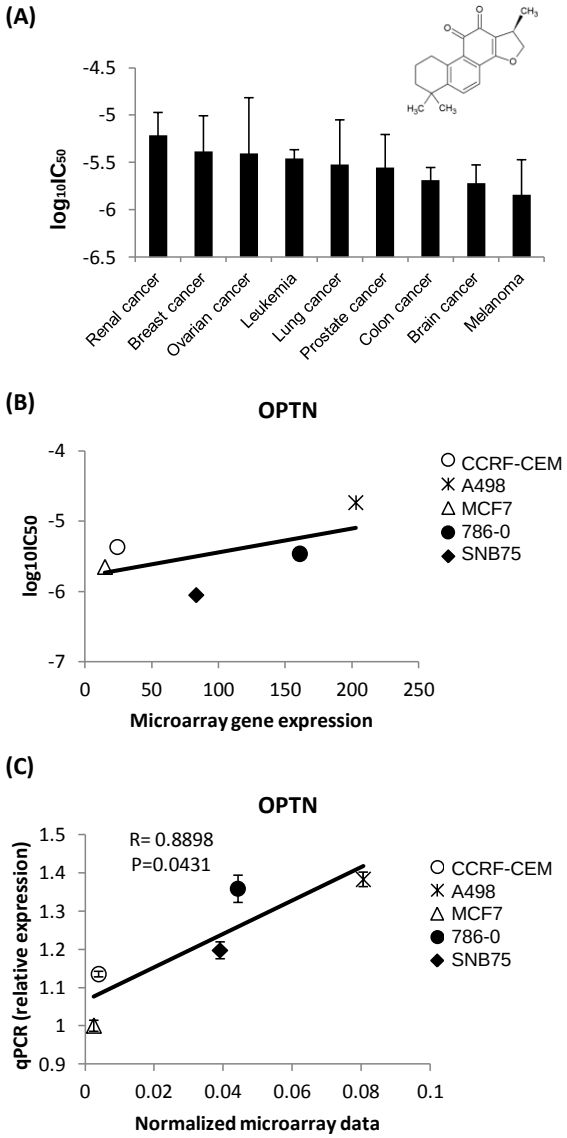

Figure 22. Structure of CPT and Mean $log_{10}IC_{50}$ value of 60 NCI cell lines for CPT. (A) Mean values were calculated according to type of cancer cell lines. The data was presented as mean ± SD. (B) Correlation of microarray *OPTN* mRNA expression sorted from the five cell lines with respective values of $log_{10}IC_{50}$ (C) Validation of microarray data by qPCR. The relative expression levels of *OPTN* measured by qPCR were calculated as levels relative to the housekeeping genes *RPS13* in five of the 60 NCI cell lines.

To identify the genes, which determined cellular responsiveness to CPT, we correlated the transcriptome-wide mRNA expression of the 60 cell lines to their log_{10} IC_{50} values to CPT by means of COMPARE analysis. The ranking of genes, whose mRNA expression directly (R>0.5) or inversely (R<-0.5) correlated to log_{10} IC_{50} values of CPT are listed in Table 5.

Table 5. Correlation of mRNA expression of genes obtained by COMPARE analysis with $\log_{10}$ IC_{50} values for CPT.

COMPARE coefficient	Pattern ID	Genbank Accession	Gene symbol	Name	Function
-0.528	GC63104	AI338045	*MRPL44*	mitochondrial ribosomal protein L44	component of the 39S subunit of mitochondrial ribosome
-0.527	GC184784	NM_006571	*DCTN6*	dynactin 6	mitochondrial biogenesis
-0.522	GC44082	AA425325	*FAM161A*	family with sequence similarity 161, member A	involved in ciliogenesis
-0.52	GC31816	AF010236	*SGCD*	sarcoglycan, delta (35kDa dystrophin-associated glycoprotein)	component of the sarcoglycan complex
-0.518	GC173303	BE539792	*ZCCHC9*	zinc finger, CCHC domain containing 9	transcriptional factor
-0.511	GC13135	H52516	*CLCN5*	chloride channel 5	proton-coupled chloride transporter
-0.505	GC60904	AI217950	*PLK1S1*	polo-like kinase 1 substrate 1	centrosomal protein required for establishing robust mitotic centrosome architecture
0.578	GC57560	AI038061	*PARD3*	par-3 partitioning defective 3 homologue (*C. elegans)*	adapter protein involved in cell division and cell polarization processes
0.547	GC32097	AF043325	*NMT2*	N-myristoyltransferase 2	catalyzation of N-terminal myristoylation of signaling proteins, including apoptosis
0.546	GC60060	AI184988	*FBN3*	fibrillin 3	structural components of extracellular calcium-binding microfibrils
0.534	GC10492	AA057701	*GNAS*	GNAS complex locus	tumor suppressor
0.529	GC55552	AF033382	*KCNF1*	potassium voltage-gated channel, subfamily F, member 1	voltage-gated potassium channel
0.527	GC32186	AF070533	*OPTN*	optineurin	polyubiquitin (polyUb)-binding protein regulating cell signaling
0.521	GC168333	AW085172	*PRKD1*	protein kinase D1	serine/threonine kinase that regulates a variety of cellular functions, including protection from oxidative stress at the mitochondria, gene transcription, and regulation of cell shape, motility, and adhesion

0.519	GC151375	AB037750	*SORCS2*	sortilin-related VPS10 domain containing receptor 2	neuropeptide receptor activity
0.518	GC153439	AF161345	*ZEB2*	zinc finger E-box binding homeobox 2	transcriptional inhibitor that binds to the DNA sequence 5'-CACCT-3' in different promoters.
0.516	GC150338	AA868332	*ZMIZ2*	zinc finger, MIZ-type containing 2	increases ligand-dependent transcriptional activity of nuclear hormone receptors
0.515	GC11822	T74107	*DMGDH*	dimethylglycine dehydrogenase	involved in the catabolism of choline, catalyzing the oxidative demethylation of dimethylglycine
0.513	GC72311	AI739142	*HAPLN3*	hyaluronan and proteoglycan link protein 3	function in hyaluronic acid binding and cell adhesion
0.508	GC179119	M59217	*COL13A1*	collagen, type XIII, a 1	involved in cell-matrix and cell-cell adhesion interactions in normal development
0.507	GC169960	AW440492	*ATP1A2*	ATPase, Na^+/K^+ transporting, a2 polypeptide	catalyzes the hydrolysis of ATP coupled with the exchange of sodium and potassium ions across the plasma membrane.
0.506	GC32392	U31628	*IL15RA*	interleukin 15 receptor, a	high-affinity receptor for interleukin-15
0.504	GC64188	AI377021	*C3orf55*	chromosome 3 open reading frame 55	unknown
0.503	GC13832	N58350	*LOC440173*	hypothetical LOC440173	unknown
0.501	GC166009	AL545500	*LOC440900*	hypothetical LOC440900	unknown
0.501	GC189362	NM_024311	*MFSD11*	major facilitator superfamily domain containing 11	unknown

To validate the microarray data, we selected one of the genes with positive correlation in Table 2 (*OPTN*) and analyzed its baseline expression in five cell lines (leukemia: CCRF-CEM; CNS cancer: SNB75; breast cancer: MCF7; renal cancer: 786-0 and A498). *RPS13* was selected as housekeeping gene to obtain a normalized gene expression. We confirmed the microarray data of the positive correlation between microarray OPTN mRNA expression and $\log_{10}IC_{50}$ value in the five selected cell lines (Figure 22B). As shown in Figure 22C, the mRNA expression of *OPTN* obtained from qPCR correlated to the value from microarray data with a significant level of $p < 0.05$. The correlation coefficient R is 0.8898, meaning a strong positive correlation between qPCR and microarray data. The mRNA expressions of these genes were then subjected to hierarchical cluster analysis to obtain a dendrogram (Figure 23), which represented the relatedness of these cell lines toward CPT responsiveness. In order to find out, whether these gene expression profiles can predict sensitivity or resistance to CPT, the median $\log_{10}IC_{50}$ value (-5.5945 M) was used to separate these cell lines as resistant or sensitive. The distribution of sensitive or resistant cell lines was significantly different ($p=3.12\times10^{-5}$; χ^2-test, Table 6). This means that the expression of these genes indeed determined and predicted the response of cancer cells towards CPT.

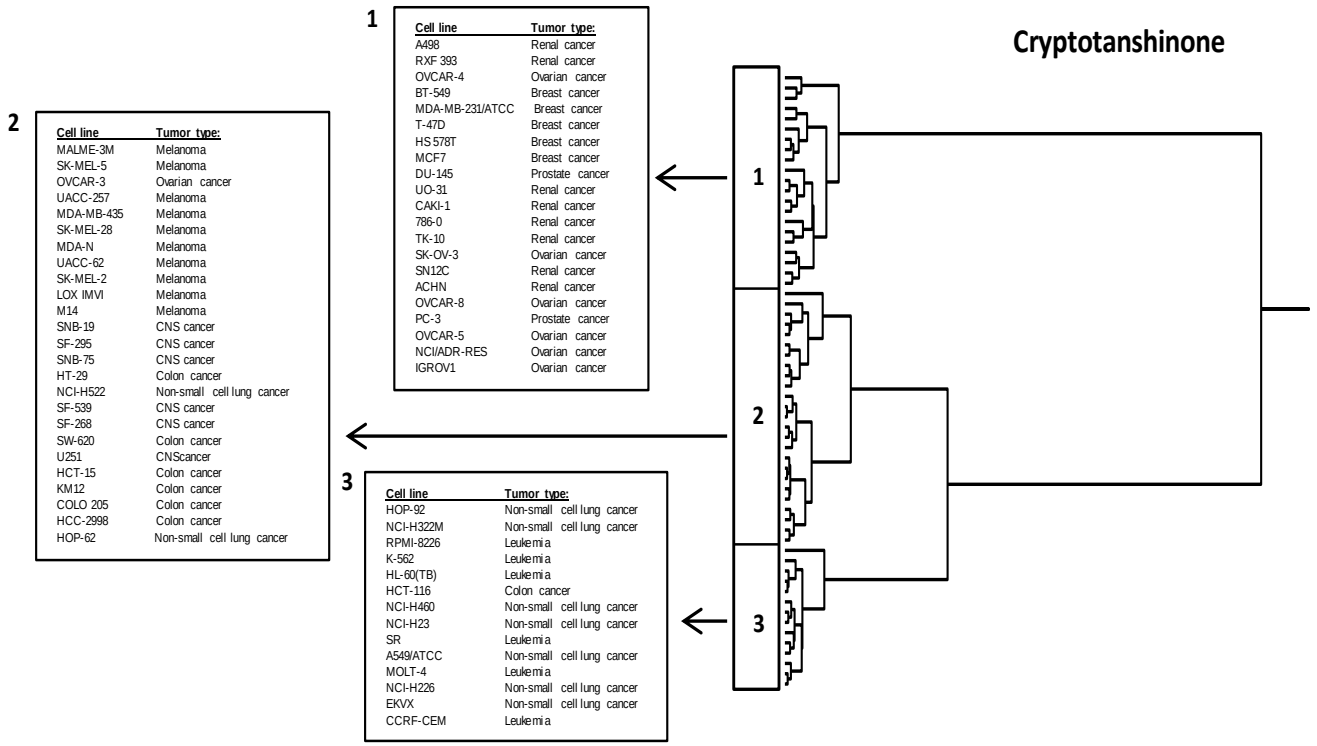

Figure 23. Hierarchical cluster analysis of microarray-based mRNA gene expression as determined by COMPARE analysis. The dendrogram presented three main clusters, which indicated concordances of resistance and sensitivity of the NCI cell line panel towards CPT.

Table 6. Clusters of NCI tumor cell line processed by hierarchical cluster analysis

	Partition	Cluster 1	Cluster 2	Cluster 3
Sensitive	< -5.5945 M	4	21	5
Resistant	> -5.5945 M	17	4	9

χ^2- test: $p=3.12 \times 10^{-5}$

Partition: The median $\log_{10}IC_{50}$value (-5.5945 M) was used as cutoff to categorize NCI tumor cell lines as being "sensitive" or "resistant".

4.2.9 Gene expression and Analysis of transcription factor binding motifs which account for initiation of UPR upon CPT treatment

According to our microarray and computational results, it is implied that 24 h of CPT treatment induced ER stress towards ALL cells mainly through deregulation of IRE1-XBP1 and ATF4-CHOP pathways. The detailed gene expression regarding UPR signaling is listed in Table 7. Upregulation of *CEBPB*, *CEBPG*, *SREBP-1*and *INSIG1* genes implied that ER stress-mediated lipid synthesis was activated. Expression of *XBP1* and *EDEM1* suggested induction of ERAD pathway, which in turn stimulates ER chaperones. Interestingly, expression of *HSPA4* and *HSPA14*, which encodes ER chaperone HSP70, was down-regulated, though a co-chaperone of HSP70 encoded by *DNAJB9,* which was upregulated.

Table 7. Genes involved in unfolded protein response (UPR) deregulated upon treatment with 10 µM CPT

Gene	Description	Fold change
Unfolded protein response (UPR)		
CEBPB	CCAAT/Enhancer binding protein (C/EBP), beta	1.537
CEBPG	CCAAT/Enhancer binding protein (C/EBP), gamma	1.439
DDIT3	DNA-damage-inducible transcript 3	1.905
DNAJB9	DnaJ (Hsp40) homologue, subfamily B, member 9	1.385
EDEM1	ER degradation enhancer, mannosidase alpha-like 1	1.510
HSPA4	Heat shock 70kDa protein 4	-1.542
HSPA14	Heat shock 70kDa protein 14	-1.361
INSIG1	Insulin induced gene 1	1.429
PPP1R15A	Protein phosphatase 1, regulatory subunit 15A	1.784
SREBP1	Sterol regulatory element binding transcription factor 1	1.380
XBP1	X-Box binding protein 1	1.790

This computational technique aims to identify binding sites for transcription factors in the DNA promoter regions. We applied this method to investigate the DNA promoter sequences of genes found to be deregulated in microarray experiments. In total, 166 genes with a fold-change threshold over 1 sorted from top CPT-deregulated cellular functions were subjected to Cistrome analysis for SeqPos motif search. These included genes involved in cell death and survival, cell cycle and cellular growth and proliferation. The most pronounced motifs for each deregulated gene list are depicted in Table 8. ATF4, a crucial transcription factor, which is induced by PERK-mediation of phosphorylation of eIF2α and activates pro-apoptotic factor CHOP and GADD34 [144], was found among the list of transcription factors that potentially bind to these gene promoters. ATF2 was also shown to regulate expression of CHOP [195]. XBP1 and SREBP1 motifs emphasized the participation of the activation of XBP1-ERAD pathway and lipid biogenesis potentially in CPT-induced ER stress. Taken together, occurrence of these motifs further supports a role of UPR in response to CPT treatment.

The CHOP/*DDIT3* gene was upregulated upon CPT treatment. This result was validated by qPCR and the microarray analysis (Table 7 and Figure 24). This and the upregulation of PPP1R15A/*GADD34*, a growth arrest and DNA-damage inducible factor [196] suggested that misfolded protein-stimulated PERK-eIF2α-ATF4 pathway was activated, which is stimulated by protein misfolding and that ER stress-mediated apoptosis was triggered. This global view of gene expression elucidated the possible mechanism, by which CPT may regulate the cellular response to ER stress.

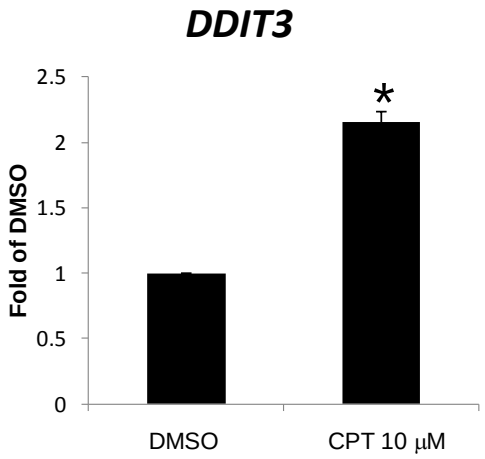

Figure 24. mRNA expression of *DDIT3* upon CPT treatment for 24 h. *: $p<0.05$ when compared with DMSO.

Table 8. Cistrome analysis of transcription factor binding motifs in DNA promoter sequences of genes deregulated upon CPT treatment (10 µM).

Upstream 2 kb				Upstream 3 kb			
	Motif	Z score	-log10(p-value)		Motif	Z score	-log10(p-value)
1	**CEBPA**	**-7.082**	**279.7**	1	ZBTB33	-6.312	227.0
2	Rhox11	-6.859	263.8	2	NR4A1	-5.466	175.8
3	Arid5a	-6.771	257.7	3	CDP|CUX1	-5.351	169.4
4	PBX1	-6.636	248.5	4	ETS1	-5.258	164.3
5	SNAPC5	-6.487	238.5	5	TFEB	-5.17	159.5
6	LARP1	-6.25	223.0	**6**	**XBP1**	**-5.034**	**152.4**
7	RARA	-6.245	222.7	7	NR2E3	-5.009	151.1
8	GATA-1	-6.036	209.6	**8**	**SREBP1**	**-4.999**	**150.5**
9	Nhp6b	-5.868	199.3	9	PU.1|SPI1	-4.943	147.6
10	FOXO3	-5.757	193.2	10	C-MAF	-4.897	145.3
11	DMRT3	-5.693	192.6	**11**	**ATF2**	**-4.892**	**145.1**
12	NKX2-5	-5.54	188.9	12	Zfp187	-4.878	144.4
13	TGA1a	-5.539	180.0	13	EFNA2	-4.849	142.9
14	POU2F3	-5.44	179.9	14	ELK1	-4.8	140.4
15	TBP	-5.436	174.3	15	POU6F1	-4.742	137.5
16	C1	-5.376	174.1	16	SPIB	-4.739	137.4
17	RGT1	-5.322	170.8	17	PEA3|ETV4	-4.695	135.2
18	FOXD1	-5.258	167.8	18	E2F1	-4.502	126.0
19	HOXA13	-5.244	164.3	19	FACB	-4.492	125.5
20	MATα2	-5.114	163.5	**20**	**CREB1**	**-4.475**	**124.7**
21	NFKB1	-5.013	156.6	21	SRY	-4.452	123.6
22	Pbx-1b	-4.988	151.3	22	C/EBPalpha|CEBPA	-4.342	118.6
23	TCF3	-4.98	150.0	23	HOXC9	-4.319	117.5
24	ZAP1	-4.775	149.6	24	aMEF-2	-4.294	116.4
25	**ATF4**	**-4.762**	**139.2**	25	PITX2|Nr2f2	-4.294	116.4
26	HNF1B	-4.756	138.5	26	NR3C1|PGR	-4.288	116.1
27	GZF3	-4.749	138.2	27	ERG	-4.252	114.5
28	FOXP3	-4.749	137.9	28	TATA	-4.239	113.9
29	TRAP4	-4.685	137.9	29	TBP	-4.239	113.9
30	STAT5A	-4.626	134.7	30	HLF	-4.21	112.6

*Items marked in bold: possible transcriptional motif related to UPR.

4.2.10 Expression of genes involved in eIF2 signaling upon CPT treatment

The eIF2 pathway was the second significant pathway deregulated after CPT treatment. Therefore, we further analyzed this pathway, which responds to UPR and regulates protein synthesis via initiation of PERK-eIF2α phosphorylation. A global inhibition of genes regulating eukaryotic initiation factors and ribosomal proteins has been observed (Table 9), implying that the overall protein synthesis was hampered due to sustained CPT-triggered UPR.

Table 9. Genes involved in eIF2 signaling deregulated upon treatment with 10 µM CPT.

Gene	Description	Fold change
eIF2 signaling		
EIF1AX	Eukaryotic translation initiation factor 1A, X-Linked	-1.343
EIF2B3	Eukaryotic translation initiation factor 2B, subunit 3 gamma, 58kDa	-1.361
EIF3B	Eukaryotic translation initiation factor 3, subunit B	-1.385
EIF4G1	Eukaryotic translation initiation factor 4 gamma, 1	-1.306
MAP2K1	Mitogen-activated protein kinase inase 1	1.306
PPP1R15A	Protein phosphatase 1, regulatory subunit 15A	1.784
RPL7L1	Ribosomal protein L7-like 1	-1.283
RPL14	Ribosomal protein L14	-1.297
RPL36	Ribosomal protein L36	-1.424
RPL36A	Ribosomal protein L36a	-1.400
RPS2	Ribosomal protein S2	-1.376
RPS7	Ribosomal protein S7	-1.619
RPS15	Ribosomal protein S15	-1.641

4.2.11 CPT interfered protein translation

During ER stress, protein synthesis is regulated not only by UPR through the control of eIF2α phosphorylation, but also by the PI3K/mTOR pathway. The latter represents a major hyperactivated signaling pathway in cancer development and hence, an important target in cancer therapy [151]. In our study, we observed a global reduction of genes related to protein synthesis (Table 9). Therefore, using a computational approach, we attempted to investigate, whether CPT potentially targets the PI3K/mTOR signaling pathway. Due to the high homology between mTOR and PI3Kc within the ATP binding site, the binding of the kinase domain of PI3Kγ could

provide insights into how drugs bind to the mTOR active site [197]. The region known as the affinity pocket within the ATP binding site contains hydrophobic interactions with Asp841 and Tyr867, and a hydrogen bond with Val882 (known as hinge residue) [198]. Other interacting residues include Met804, Trp812, Lys833, Asp836, Asp964 and Phe965. These interacting residues are conserved between mTOR and PI3Kγ [197]. PI-103 [199] and GSK2126458 [200] were selected as positive control in our study. CPT bound to the same binding site as the two control drugs. CPT formed a hydrogen bond with Val882 and hydrophobic interaction with Tyr867 implying that it bound to the affinity pocket (Table 10 and Figure 25, performed by Dr. Ean-Jeong Seo).

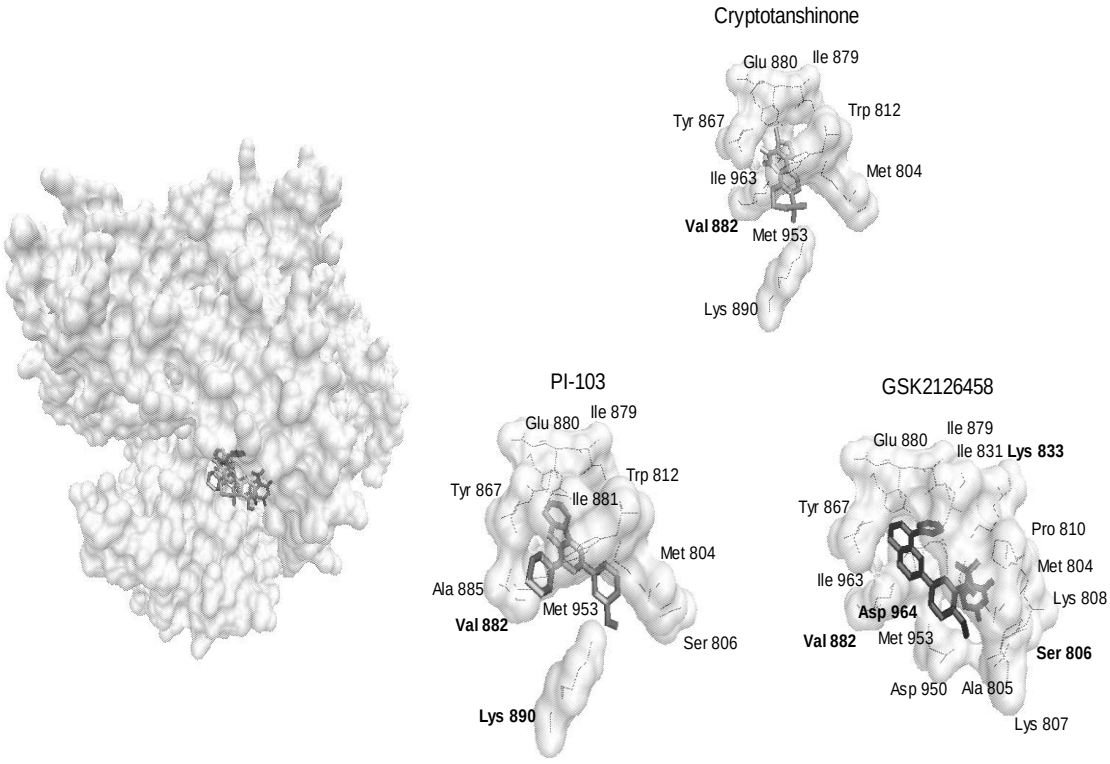

Figure 25. Molecular docking of CPT, PI-103 and GSK2126458 on PI3K (PDB ID: 1E8Y, white surface representation). PI-103 and GSK2126458 are specific PI3K inhibitors and were selected as reference compounds, in order to compare their docking sites of with those of CPT.

In general, cellular stress caused for example by DNA-damaging agents suppressed cap-dependent translation, mostly by inhibition of eIF4F and eIF2 ternary complex [201]. The PI3K/mTOR signaling pathway controls the assembly of eIF4F, which of eIF4A is a specific component with helicase activity in regulating protein translation [202]. eIF4A is considered as an oncogene, which is involved in T-cell ALL (T-ALL) development [203]. Targeting eIF4A is a novel anticancer strategy that has shown preclinical efficacy [202]. Thus, we studied the binding of CPT to eIF4A using molecular docking Our analysis showed that CPT bound to the same ATP binding region as pateamine A, a novel inhibitor for eIF4A, interacting with the same hydrophobic residues, including Phe200, Asn204, Phe227 and Arg229 (Figure 26, performed by Dr. Ean-Jeong Seo). Since, CPT showed lower binding affinity with higher binding energy and predicted Ki values (-8.03 kcal/mol; 1.31 μM) than pateamine A (-11.27 kcal/mol; 0.004 μM) (Table 10), the docking indeed suggests a possible interaction of CPT with eIF4A.

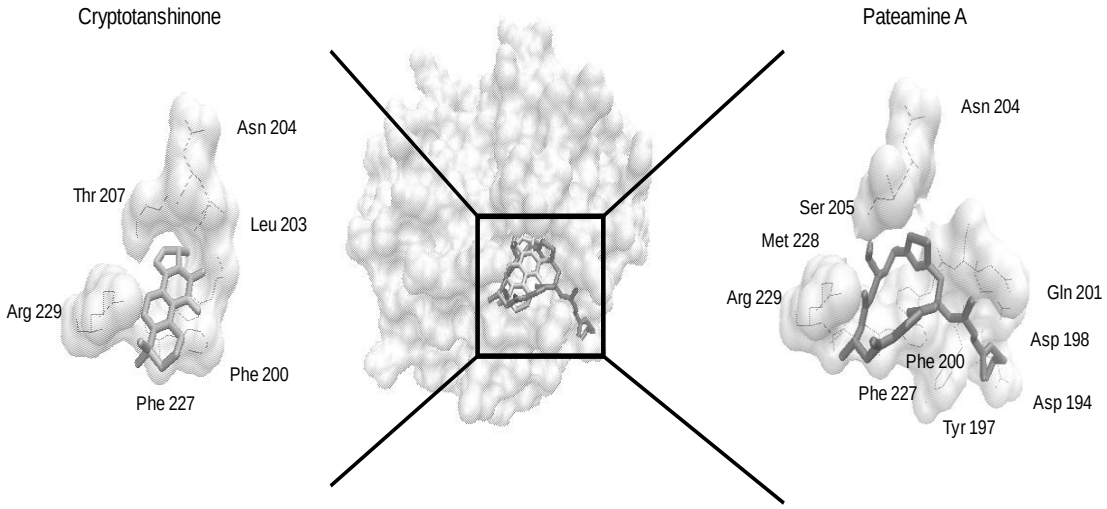

Figure 26. Molecular docking result of CPT (silver) and pateamine A (grey) on eIF-4A (PDB ID: 2G9N, white surface representation). Pateamine A, a specific eIF-4A inhibitor selected as a control drug, was used to compare the docking sites of CPT.

Table 10. Molecular docking of CPT to PI3K (PDB ID: 1E8Y) and eIF4A (PDB ID:2G9N). Docking of control drugs (PI-103 and GSK2126458 for PI3K and pateamine A for eIF4A) was performed for comparison.

Protein	Compound	Lowest energy of docking (kcal/mol)	Mean binding energy (kcal/mol)	Residues hydrogen bond interaction with the ligand	Residues involved in hydrophobic interaction with ligand	[a]PKi (µM)
PI3K	CPT	-8.20±<0.00	-8.20±<0.00	Val882	Met804, Trp812, Tyr867, Ile879, Glu880, Lys890, Met953, Ile963	0.97±<0.00
	PI-103	-8.77±0.01	-8.57±0.03	Val882, Lys890	Met804, Ser806, Trp812, Tyr867, Ile879, Glu880, Ile881, Ala885, Met953	0.37±<0.00
	GSK2126458	-11.20±0.09	-10.78±0.15	Ser806, Lys833, Val882, Asp964	Met804, Ala805, Lys807, Lys808, Pro810, Ile831, Tyr867, Ile879, Glu880, Asp950, Met953, Ile963	0.01±<0.00
eIF-4A	CPT	-8.03±<0.00	-8.03±<0.00		Phe200, Leu203, Asn204, Thr207, Phe227, Arg229	1.31±<0.00
	Pateamine A	-11.51±0.01	-11.27±<0.00		Asp194, Tyr197, Asp198, Phe200, Gln201, Asn204, Ser205, Phe227, Met228, Arg229	0.004±<0.00

[a]**pKi** (predicted Ki): Ki is the inhibition constant for a drug. The pKi value is used to evaluate affinity of drug to a target structure.

4.2.12 Summary: Anticancer activity of cryptotanshinone (CPT) on acute lymphoblastic leukemia cells

In this study, we have shown that CPT exerted strong cytotoxicity towards sensitive and multidrug-resistant ALL cells. Microarray-based mRNA expression profiling of CCRF-CEM cells revealed that CPT predominantly modulated several molecular functions including cell death and survival, cell proliferation, ROS production, cell cycle arrest, DNA damage and cellular movement, and canonical pathways including UPR and eIF2 signaling. These effects were validated by subsequent independent methods to identify the possible mechanisms of CPT-induced cytotoxicity. CPT stimulated ROS production, caused loss of MMP and DNA damage, and activated caspase 3/7 and 9. These results imply that CPT induced cytotoxicity through the mitochondria-mediated intrinsic apoptotic pathway. Down-regulation of p65 translocation might result from a direct binding of CPT to IKKβ, providing supportive evidence for CPT-induced apoptosis. In addition, CPT inhibited cell adhesion to fibronectin. Based on the rapid accumulation of ROS by CPT, it is suggested that CPT-caused apoptosis, inhibition of adhesion and blocking of NFκB signaling may originate from ROS production. In addition, CPT triggered UPR and inhibited protein synthesis via eIF-mediated translation initiation, potentially supporting CPT-induced cytotoxic effects toward acute leukemia cells.

4.3 Miltirone induces G2/M cell cycle arrest and apoptosis in acute lymphoblastic leukemia CCRF-CEM cell line

Interestingly, identified as a tanshinone in 1970s, the pharmaceutical potential of miltirone, in comparison with other tanshinones, is less explored. In addition, the mechanisms of miltirone-induced anti-cancer effects have been reported yet have not been investigated in depth. In this study, we investigated modes of action of miltirone against ALL cells.

4.3.1 Cytotoxicity of miltirone against ALL cells Drug-sensitive CCRF-CEM and P-glycoprotein (P-gp) over-expressing multidrug-resistant CEM/ADR5000 leukemia cells were treated with miltirone concentration ranging from 0.01 to 100 μg/ml) for 72 h and cell viability was measured by the resazurin assay. Miltirone induced cytotoxicity towards both cell lines with IC_{50} values of 2.5 ± 0.1 μM and 1.7 ± 0.17μM, respectively (Figure 27B). Epirubicin, an anthracycline used for leukemia therapy and substrate of P-gp revealed IC_{50} values of 0.001 ± 0.0008 μM in sensitive and 60.727 ± 16.607 μM in resistant cells (Figure 27C). As indicated by the degrees of cross-resistance, epirubicin was more effective in reducing cell viability of sensitive cells, but less active on resistant cells, as it is a known P-gp substrate (Table 11). Taken together, the results implied that miltirone is not transported by P-gp and can be used to treat P-gp overexpressing multidrug-resistant cancer cells.

Miltirone was less active against normal lymphocytes, if compared with the two cancer cell lines. The preferential inhibition of cancer cells indicates that normal cells might be less affected in patients (Figure 27B).

Table 11. IC_{50} Values for miltirone and epirubicin in sensitive wild-type CCRF-CEM and multidrug-Resistant P-glycoprotein overexpressing CEM/ADR5000 cells.

	CCRF-CEM IC50 (μM)	CEM/ADR5000 IC50 (μM)	[a]Degree of cross resistance
epirubicin	0.001 (± 0.0008)	60.727 (± 16.607)	60929.3
miltirone	2.5 (± 0.1)	1.7 (± 0.17)	0.68

[a]Degrees of resistance were calculated by dividing the IC_{50} value of CEM/ADR5000 by the IC_{50} value of CCRF-CEM.

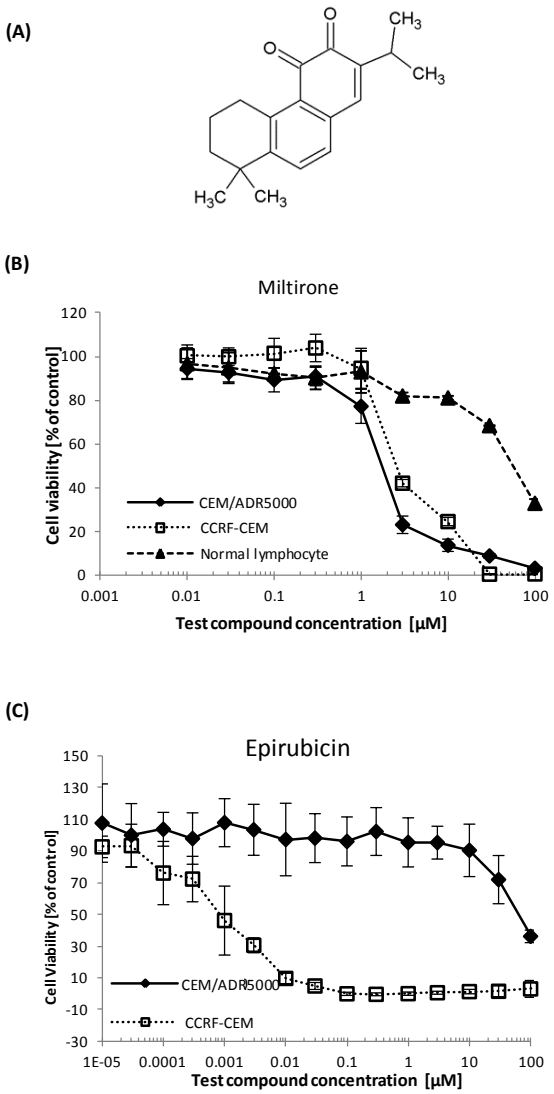

Figure 27. Cell viability of CCRF-CEM and CEM/ADR5000 cells treated with miltirone. (A) Molecular structure of miltirone. (B) Leukemia cells and normal lymphocytes were treated with indicated concentration. After 72h of incubation, resazurin assay was performed. (C) Epirubicin was used as control drug.

4.3.2 Induction of G2/M arrest and apoptosis

Flow cytometric cell cycle analyses were performed after 24, 48 and 96 h of treatment with miltirone. Incubated of CCRF-CEM cells for 24 h arrested cells in the G2/M phase (Figure 28A). After 48 h incubation, miltirone significantly increased the percentage sub-G1 phase (apoptotic) cells in a dose-dependent manner (Figure 28B).

To further investigate miltirone-induced G2/M arrest, mRNA expression of *CDC2* and *CCNB1* (cyclin B1), which control G2/M transition, was measured. Miltirone down-regulated the expression of both genes, though deregulation of *CCNB1* did not reach statistical significance (p<0.05). Expression of *TP53* (tumor suppressor p53), which regulates G1/S and G2/M cell cycle arrest, did not change. *CDKN1A* (p21) expression was induced by miltirone (Figure 28C), indicating that DNA damage response might play a role [204].

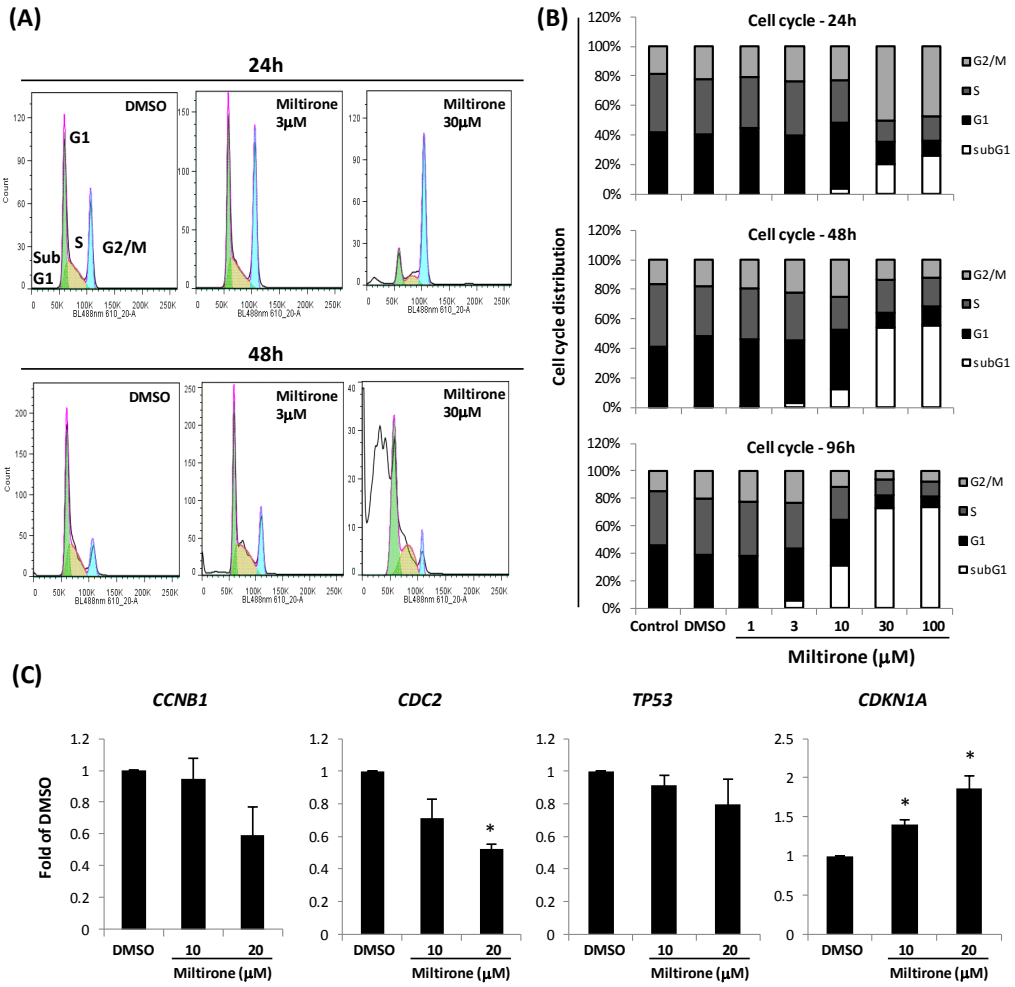

Figure 28. Measurement of cell cycle in CCRF-CEM cells treated with miltirone. (A) DNA histograms of CCRF-CEM cells treated with indicated concentration for 24 and 48 h. (B) Cell cycle distribution was calculated after 24, 48 and 96 h. Results were presented as mean values of three independent experiments. (C) Expression of genes, which regulate G2/M phase. Cells were treated with miltirone for 24 h. The mRNA levels of *CCNB1*, *CDC2*, *TP53* and *CDKN1A* were evaluated by qPCR. *RPS13* was used as a housekeeping gene. *, p<0.05 compared with cells with DMSO group.

4.3.3 Induction of DNA damage

Miltirone-induced G2/M cell cycle arrest and deregulated expression of *CDC2*, *CCNB1* and *CDKN1A* speak for the induction of DNA damage. Therefore, we tested DNA damage using the comet assay (alkaline single cell electrophoresis), as it detects both DNA single- and double-strand breaks and alkali labile DNA adducts [205]. Miltirone significantly increased the percentage of tail DNA with increasing concentration, and in parallel, the percentages of head DNA decreased. DNA migration was observed with increasing concentration of miltirone with tail and Olive tail movements (Figure 29A, B), indicating that miltirone caused DNA damage and inhibited DNA replication.

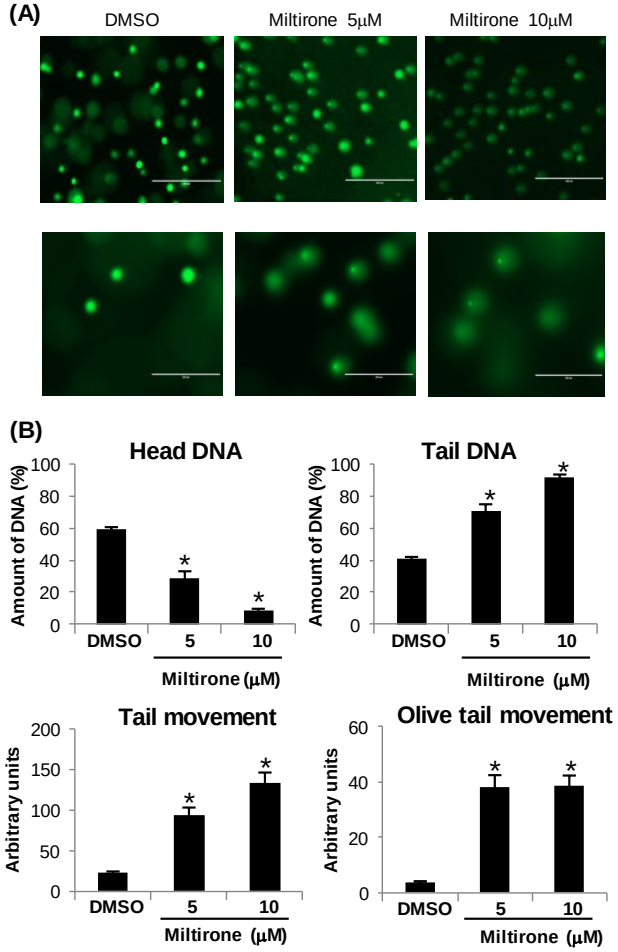

Figure 29. DNA damage induced by miltirone. (A) Cells were incubated with different concentration for 24 h and DNA damage was evaluated by comet assay. Representative pictures (upper panel: 100×; lower panel: 400× magnifications). (B) Head DNA%, tail DNA%, tail movement and Olive tail movement were measured. Tail and Olive tail movements were presented as estimated DNA damage in arbitrary units. Results were presented as mean values ± SD of 25 cells. Statistical significance was calculated by one way ANOVA with Dunnett and Tucky *post hoc* test.

4.3.4 Oxidative stress and MMP disruption

Since miltirone stimulated DNA damage, we hypothesized that ROS may induce DNA damage. Miltirone induced ROS in a dose-dependent manner as measured by flow cytometry and H_2DCFH-DA staining. Statistically significant increased ROS levels were observed after treatment with 1, 3, or 10 µM. ROS generation by miltirone was lower than by 5 mM H_2O_2 , which has been used as control (Figure 30A, B).

CCRF-CEM cells stained with JC-1 after 24 and 48 h of treatment with miltirone led to a shift from red to green fluorescence (Figure 30C, D). This indicates a breakdown of MMP as prerequisite of apoptosis.

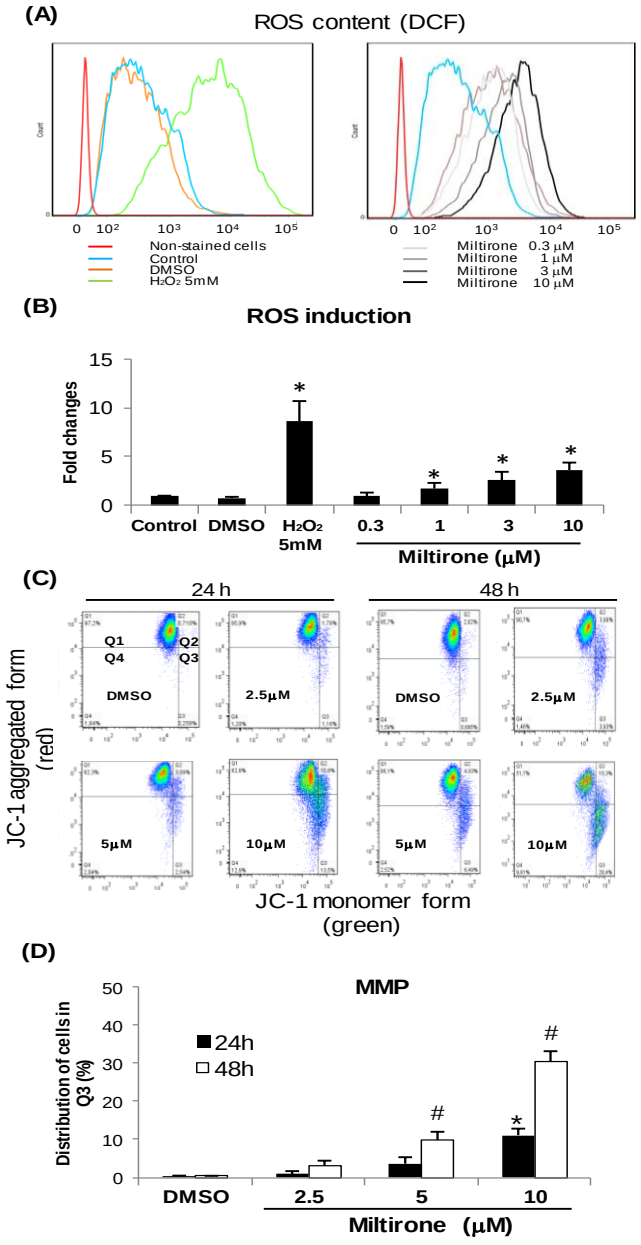

Figure 30. Measurement of ROS and MMP upon miltirone treatment of CCRF-CEM cells. (A) ROS induction in cells treated with miltirone for 1 h or 5mM H_2O_2 as measured by flow cytometry. (B) ROS quantification with fold-changes of mean values ± SD of at least three independent experiments. *: $p<0.05$ if compared with DMSO-treated cells. (C) Cells treated for 24 and 48 h, and stained with JC-1. Untreated cells mainly displayed red-fluorescing J-aggregates, whereas apoptotic cells formed green fluorescing JC-1 monomers. (D) Upon miltirone treatment, a cell population with depolarized MMP appeared in Q3. Results were obtained from three independent experiments. *: $p<0.05$ compared with DMSO after 24 h treatment; #: $p<0.05$ compared with DMSO in 48 h treatment.

4.3.5 Mechanism of miltirone-induced apoptosis

After miltirone treatment, apoptotic bodies appeared as shown by fluorescence microscopy and DAPI staining (Figure 31A). Doxorubicin was used as control drug. Early apoptosis was also detected by flow cytometry and annexin V (AV)-FITC propidium iodide (PI) staining. After incubating with 5 μM miltirone for 48 h, the fraction of apoptotic AV^+PI^- cells considerably increased in contrast to untreated controls (Figure 31B, C).

Since miltirone disrupted MMP and induced apoptosis, miltirone may induce the intrinsic, mitochondrial apoptotic pathway. During intrinsic apoptosis caspase 9 is activated, which subsequently activates the down-stream caspases 3 and 7 [206]. We examined caspases 3/7 and caspase 9 in miltirone-treated CCRF-CEM cells. Indeed, all caspases were significantly activated in a dose-dependent manner upon miltirone treatment (Figure 31D).

PARP, a molecule responding to DNA damage, is cleaved and activated by caspase 3 [207]. Western blotting showed that miltirone induced PARP cleavage (Figure 31E). These data indicate that miltirone induced the intrinsic apoptotic pathway in CCRF-CEM cells.

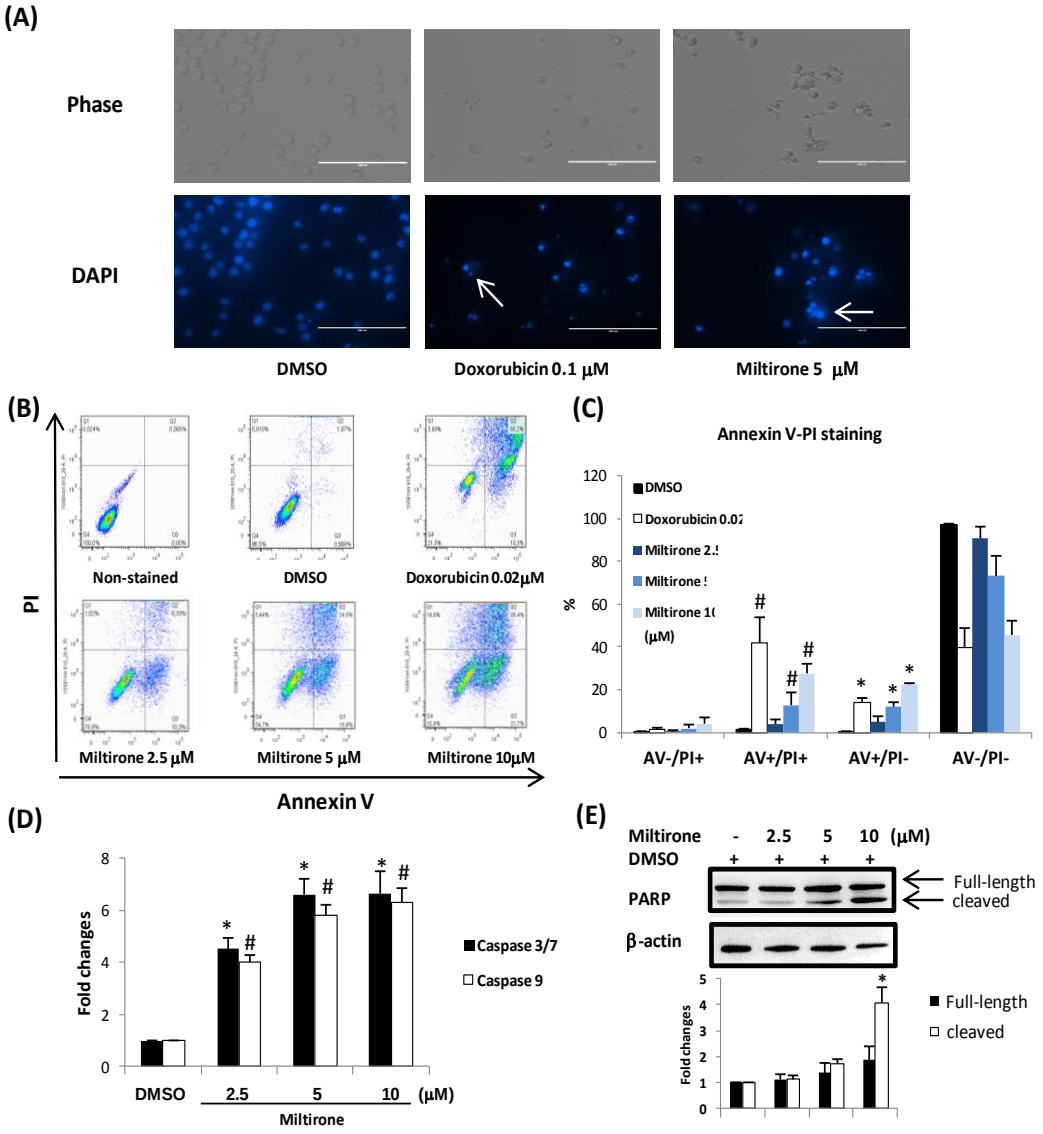

Figure 31. Miltirone-induced apoptosis in CCRF-CEM cells. (A) Cell morphology as shown by phase contrast microscopy (upper panel) and DAPI-stained cells as captured by fluorescence microscopy (lower panel). (B) Cells treated for 48 h. Doxorubicin were used as positive control. AV-FITC binding and PI staining were measured by flow cytometry. (C) Results show fractions of AV^+PI^+ and AV^+PI^- stained cells. *: $p<0.05$ if compared with DMSO treated controls in AV^+PI^- cells; #: $p<0.05$ if compared with the DMSO treated group in AV^+PI^+ cells. (D) Cleavage of caspases upon miltirone treatment. Miltirone affects the activity of caspase 3/7 and caspase 9. Cells were treated for 24 h. Activity of caspase 3/7 and caspase 9 were determined as fold-change of control. The results were obtained from three independent experiments. *: $p<0.05$ if compared with DMSO-treated cells in caspase 3/7 experiments; #: $p<0.05$ if compared with DMSO-treated cells in caspase 9 experiments. (E) PARP expression was detected by western blotting. The expression of inactive (116 kDa) and cleaved PARP forms (89 kDa) were normalized to β-actin. Quantification was shown in the lower panel. *: $p<0.05$ if compared with DMSO treated controls.

4.3.6 Miltirone binds IKK-β and inhibits nuclear p65 expression

Inhibition of NFκB activation represents an attractive therapeutic strategy. Previous studies revealed that NFκB-dependent G2/M arrest correlates with p21 induction following DNA damage highlighting the crucial role of NFκB and DNA repair for drug resistance [208,209]. Since miltirone induced DNA damage and apoptosis, we hypothesized that miltirone may inhibit NFκB signaling. For this reason, we investigated whether miltirone may bind to inhibitor κB kinase-β (IKK-β) by a computational molecular docking approach. IKK-β phosphorylates NFκB inhibitor protein IκB, leading to stimulation of down-stream transcriptional genes in the nucleus.[39] As recently reported, the drug binding residues of IKK-β (Ala42, Val29, Tyr98 and Gly102) are mainly located at ATP binding sites [188]. Leu21, Gly22, Gly24, Val29, Ala42, Tyr98, Lys147 and Ile165 are the interacting hydrophobic residues, while Cys99 acts as hydrogen bond donor [188]. It is well-known that kinase inhibitors tend to form hydrogen-bonds to the hinge motif [210]. Therefore, IKK-β inhibitors are also supposed to interact with the hinge motif, which in case of IKK-β is composed of Glu97 and Cys99. Thereby, inhibitor binding is stabilized contributing to reduced catalytic enzyme activity [211,212]. Remarkably, miltirone showed lower binding energy and predicted Ki values (-8.26 kcal/mol; 0.89 μM) than the known NFκB inhibitor, MG132 [213] (-7.59 kcal/mol; 7.33 μM) (Table 12). This implies that miltirone revealed higher affinity to IKK-β than MG132. Notably, miltirone bound to the same pharmacophore as MG132. Miltirone and MG132 bound to the hinge region by forming a hydrogen bond with Cys99 residue. Meanwhile, miltirone also formed a hydrogen bond at the drug binding residue Gly102, as did MG132 (Figure 32A, B, C). In sum, the results suggested that miltirone may directly bind to IKK-β and seems to be a more potent IKK-β inhibitor than MG132.

We further tested the expression of nuclear p65 protein by Western blotting to clarify, whether miltirone may affect p65 translocation. Translocation of p65 from the cytoplasm to the nucleus was induced by TNFα - a process which was inhibited by miltirone (Figure 32D). Taken together, miltirone inhibited NFκB signaling, which may contribute to cell apoptosis.

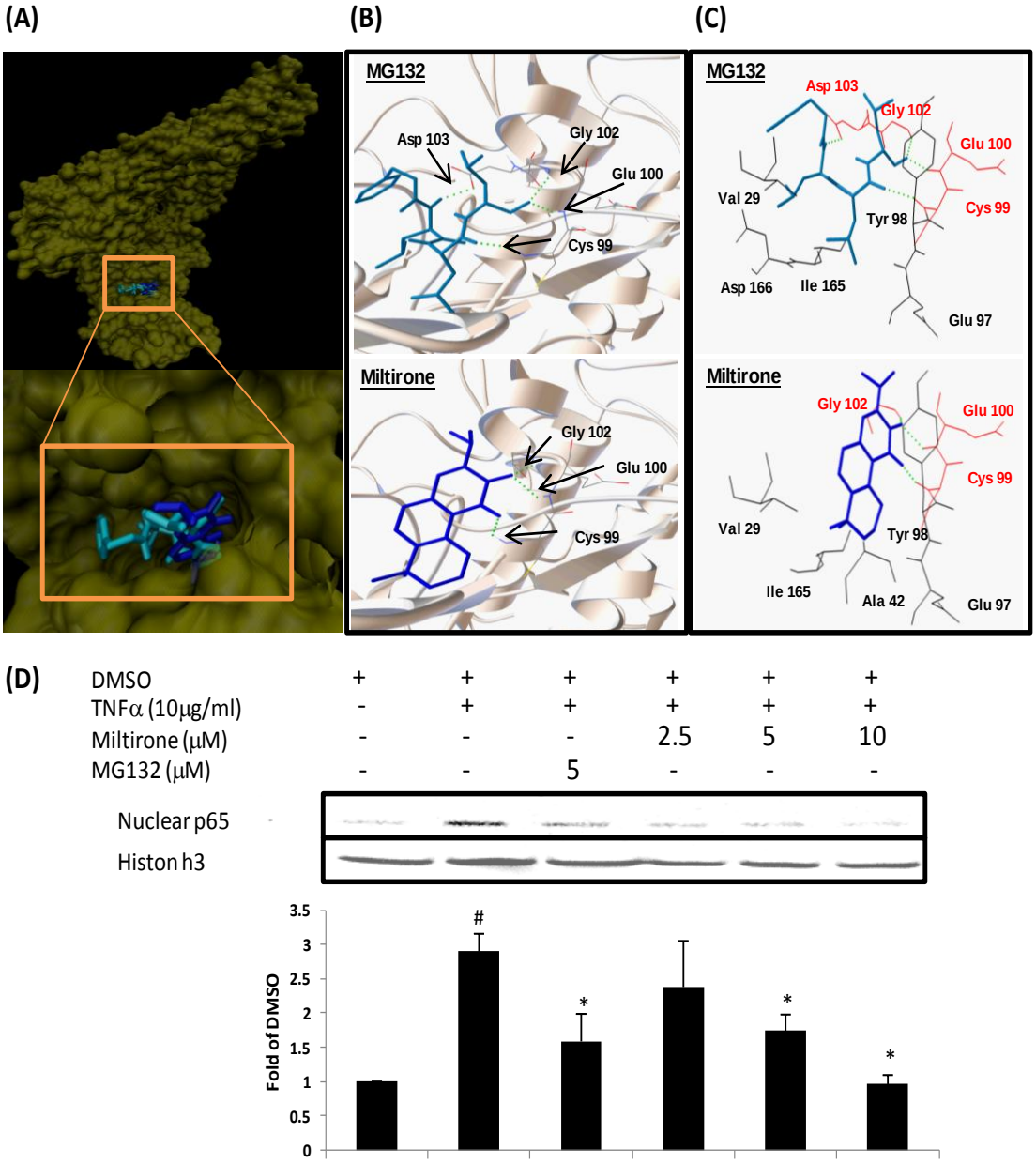

Figure 32. Interaction of miltirone with IKK-β. (A) Docking of miltirone and MG132 to IKK-β. MG-132 was used as control drug. Shown are IKK-β binding sites. VMD files presented the binding site of miltirone (light blue) in comparison with MG132 (dark blue). (B, C) Amino acids interacting with miltirone. Residues participating in hydrogen bonding are labeled in red. Hydrogen bonds are shown as green dots. (D) Prior to TNFα induction for 1 h, cells were treated with miltirone for 24 h or MG132 for 2 h. Cell lysates were collected and nuclear protein was extracted. Nuclear p65 expression was detected by Western blotting. Histon h3 was shown as an internal control. #: $p<0.05$ compared with control; *: $p<0.05$ compared with TNFα.

Table 12. Molecular docking of miltirone to IKK-β.

compound	lowest binding energy (kcal/mol)	mean binding energy (kcal/mol)	residues of hydrogen bond	numbers of residues involved in hydrophobic interaction	pKi values (μM)
MG132 (IKKβ inhibitor)	-7.59	-6.49	**Cys99**, Glu100, **Gly102**, Asp103	16	7.33
Miltirone	-8.25	-8.22	**Cys99**, Glu100, **Gly102**	9	0.89

[a]pKi (predicted Ki): Ki is the inhibition constant for a drug. The pKi value is used to evaluate affinity of drug to a target structure.

[b]Bolded residues are ATP-binding or drug-binding residues.

4.3.7 Inhibition of cell adherence

Transmigrating of leukemia cells from blood to tissue initiates from adherence to blood vessel endothelial cells. Deregulation of adhesion molecules is often found in leukemia cells, which leads to poor prognosis by massive accumulation of leukemia cells in the tissues [214-216]. In addition, NFκB signaling pathway plays an important role in cell adhesion. Blocking of NFκB-mediated transcription leads to down-regulation of adherent molecules on leukemia cells and endothelial cells, which contribute to inhibition of cell adhesion [191,194]. These previous studies revealed that inhibition of cell adhesion represents a crucial step to prevent progression of ALL. Therefore, we investigated whether miltirone may influence cell adhesion. Fibronectin, an important extracellular adhesion glycoprotein, was used to mimic the environment for cell adhesion [217-218]. After 2 h incubation, miltirone dose-dependently suppressed cell adhesion to fibronectin-coated wells, reaching statistical significance at a concentration of 40 μM (Figure 33). The reduction of cell adhesion was not due to cytotoxicity and the cell morphology in miltirone-treated cells remained similar to DMSO-treated control cells. Miltirone decreased cell adhesion, suggesting inhibition of leukemic invasion into tissues.

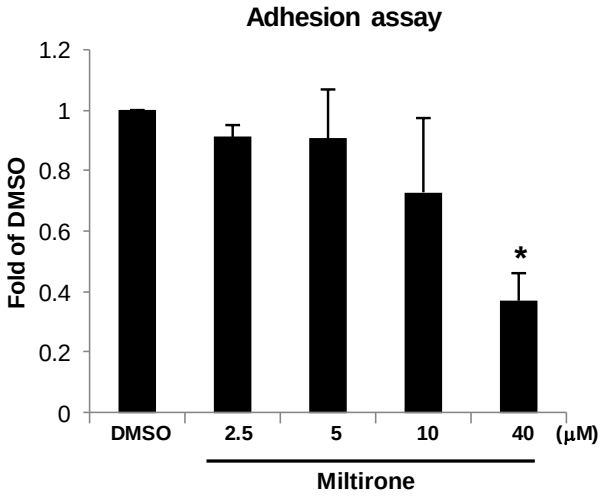

Figure 33. Miltirone inhibited adhesion of CCRF-CEM cells to fibronectin. Cell adhesion was quantified as fold-change in comparison to DMSO-treated control cells. The experiments were performed in triplicate. *: $p<0.05$ compared with DMSO-treated cells.

4.3.8 Summary: Miltirone induces G2/M cell cycle arrest and apoptosis in acute lymphoblastic leukemia CCRF-CEM cell line

Miltirone stimulated ROS generation, disrupted MMP and caused DNA damage leading to the activation of caspases 3/7 and 9. Hence, miltirone was cytotoxic by mitochondria-driven intrinsic apoptosis. Inhibition of nuclear p65 translocation might result from direct binding to IKKβ. Miltirone-induced DNA damage results in G2/M arrest by deregulating *CDC2*, *CCNB1* and *CDKN1A* expression. Furthermore, miltirone inhibited cell adhesion and NFκB signaling. To the best of our knowledge, this is the first report on the mechanisms of miltirone in ALL cells.

4.4 Molecular mechanisms of rosmarinic acid from *Salvia miltiorrhiza* in acute lymphoblastic leukemia cells

Despite its anticancer and chemopreventive properties, the molecular modes of action of RA in cancer cells have not been analyzed in detail, especially on acute lymphoblastic leukemia (ALL). Here, we investigated the inhibitory effects of RA towards sensitive (CCRF-CEM) and multidrug-resistant cell lines (CEM/ADR5000) derived from ALL, which represents an aggressive and malignant form of hematopoietic tumors characterized by uncontrolled growth of abnormal progenitor cells unable to differentiate into T-cells and B-cells. To the best of our knowledge, the detailed mechanisms of RA treatment towards CCRF-CEM and CEM/ADR5000 have not been explored.

4.4.1 Cytotoxicity of RA towards ALL cell lines.

We firstly investigated, whether RA suppresses the growth of sensitive CCRF-CEM cells and the P-gp-overexpressing subline CEM/ADR5000. RA induced cytotoxicity towards CCRF-CEM and CEM/ADR5000 cells with IC_{50} values of 14.6 ± 1.58 µM and 44.5 ± 5.3 µM, respectively (Figure 1B, Table 1). We divided the IC_{50} value of resistant cells by the IC_{50} value of sensitive cells to calculate the degree of resistance. CEM/ADR5000 cells were three-fold more resistant than CCRF-CEM cells (Table 13, Figure 34B). Normal lymphocytes treated with RA showed an IC_{50} value of 77.39 ± 12.2 µM, which was 5-fold and 1.7-fold higher than that of CCRF-CEM and CEM/ADR5000 cells, respectively. For comparison, the clinically established anticancer drug doxorubicin was used as control drug. Doxorubicin revealed IC_{50} values of 0.005 ± 0.0004 µM in sensitive and 16.6 ± 3.48 µM in resistant cells (Figure 34C, Table 13). The degree of resistance of CEM/ADR5000 cells to doxorubicin was 3320 (Table 13). We also tested the cytotoxicity of doxorubicin towards normal lymphocytes and measured an IC_{50} value of 3.97 ± 0.84 µM. This value was 794-fold higher than that of sensitive CCRF-CEM cells, but 4.17-fold lower than that of multidrug-resistant CEM/ADR5000 cells. This indicates that normal cells were able to tolerate RA, but not doxorubicin at doses necessary to kill MDR cells. In sum, RA revealed preferential cytotoxic effects on both sensitive and P-gp overexpressing leukemia cells.

Phase contrast microscopy was applied to study the cellular morphology of CCRF-CEM cells after 24 h treatment of RA or DMSO. As shown in figure 34D, two different types of morphological changes including cell swelling (indicated by arrowhead with solid line) and formation of apoptotic bodies (indicated by arrowhead with dashed line) were observed. This implies that RA simultaneously induced necrotic and apoptotic cell death in CCRF-CEM cells.

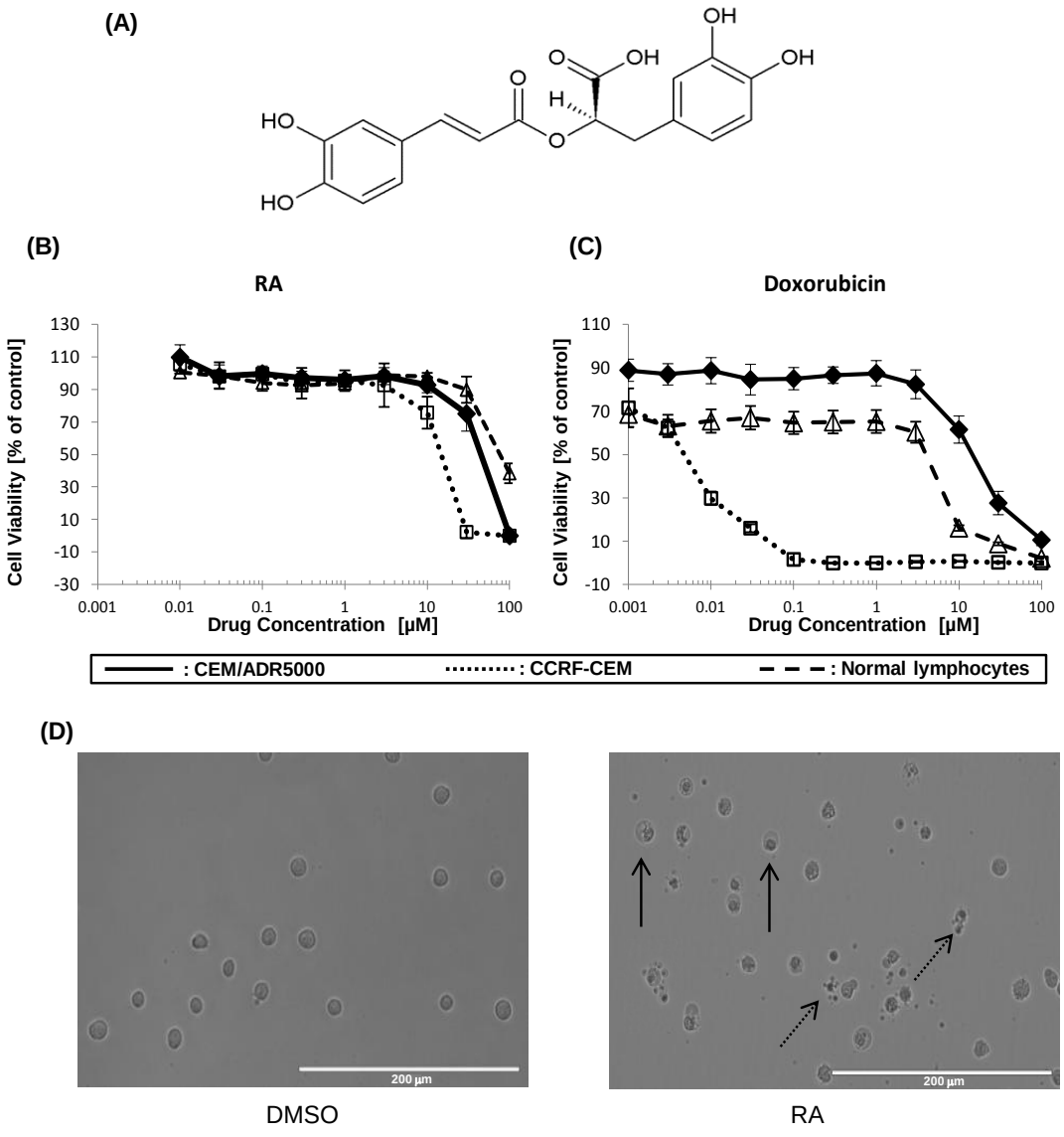

Figure 34. Cytotoxicity of RA towards acute lymphoblastic leukemia cells. (A) Chemical structure of RA. (B, C) CCRF-CEM and resistant CEM/ADR5000 cells were treated with varying concentration of RA and doxorubicin following seeding. Normal lymphocytes were freshly isolated and were treated with RA. After 72 h of incubation, cell viability was performed by resazurin assay. (D) Phase contrast pictures represented morphology of CCRF-CEM cells without or with RA treatment. Arrows with solid lines indicated necrotic cells, while arrows with dotted line indicated apoptotic cells.

Table 13. IC50 values for RA and doxorubicin in sensitive wild-type CCRF-CEM, multidrug-resistant P-glycoprotein overexpression CEM/ADR5000 cells and normal lymphocytes.

	CCRF-CEM IC50 (μM)	CEM/ADR5000 IC50 (μM)	Normal lymphocyte	Degree of cross resistance
Doxorubicin	0.005 (± 0.0004)	16.577 (± 3.478)	3.97(±0.84)	3503.4
RA	14.6 (± 1.58)	44.5 (± 5.3)	77.39±(12.2)	3.06

Degree of cross-resistance: it is calculated by dividing the IC 50 value of CEM/ADR5000 by the IC 50 value of CCRF-CEM.

4.4.2 Microarray profiling of untreated and RA-treated CCRF-CEM cells

CCRF-CEM cells were treated with 30 μM RA or DMSO for 48 h. Using Chipster software, 856 genes were significantly deregulated (p<0.05) upon RA treatment in comparison to DMSO treatment. These genes were subsequently subjected to Ingenuity Pathway Analysis (IPA) to obtain profiles of possibly affected signaling pathways. The most pronounced biological functions identified by IPA were: cellular growth and proliferation, cell death and survival, cell cycle, DNA replication and repair, cellular movement and energy production (Figure 35A).

As a next step, we performed network analysis to prove, whether these deregulated genes act independently or together as a network beyond pathways. A specific molecular network connected with cell death and survival and cell cycle pointed to NFκB complex as a main cellular regulator, implying that RA acts on NFκB (Figure 35B).

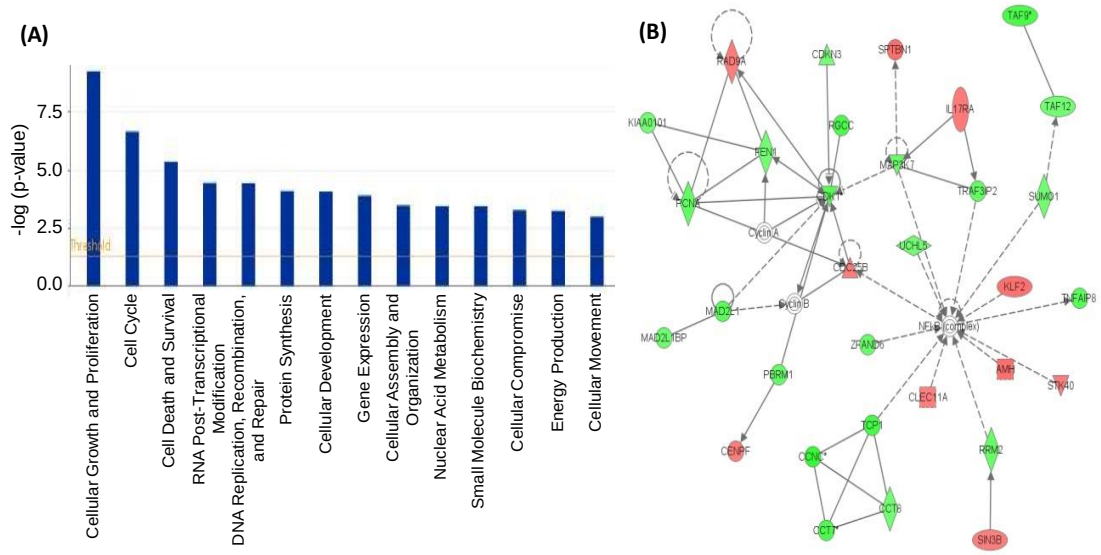

Figure 35. Microarray-based mRNA expression profiling of CCRF-CEM cells treated with RA using Ingenuity Pathway Analysis. Predominant pathways (A) and signaling networks (B) regulated by deregulated genes were identified.

4.4.3 Validation microarray results by qPCR

Five up- or down-regulated genes were exemplarily selected for qPCR analysis (*DDIT3, AKR1C3, TXNIP, IGLL1* and *VPREB1*). Their expression was normalized to *RPS13*. Then, the fold-change values of RA-treated and untreated samples obtained from microarray hybridization and qPCR were subjected to Pearson correlation test. We obtained a correlation coefficient R-value of 0.924, indicating high concordance of microarray and qPCR data (Table 14).

Table 14. Validation of microarray gene expression profiling with selected genes by real-time reverse transcription-PCR.

Gene name	Microarray data	qPCR data
AKR1C3	1.892	3.6425
DDIT3	1.409	1.7455
IGLL1	-1.778	-1.29
TXNIP	2.189	6.315
VPREB1	-2.266	-1.4005

R value= 0.9236

4.4.4 Induction of cell cycle arrest by RA

Based on the pathway analysis of microarray results that cell cycle is affected by RA treatment, we investigated the cell cycle using flow cytometry. As indicated in figure 36, RA induced a slight G2/M arrest after 24 h and also increased the fraction of sub-G1 cells at high concentrations (100 µM) after 48 h incubation. G2/M arrest can be taken as hints that RA treatment is associated with DNA damage, DNA repair and cell survival. Sub-G1 cells imply the induction of cell apoptosis. Therefore, we tested this hypothesis in the next sections.

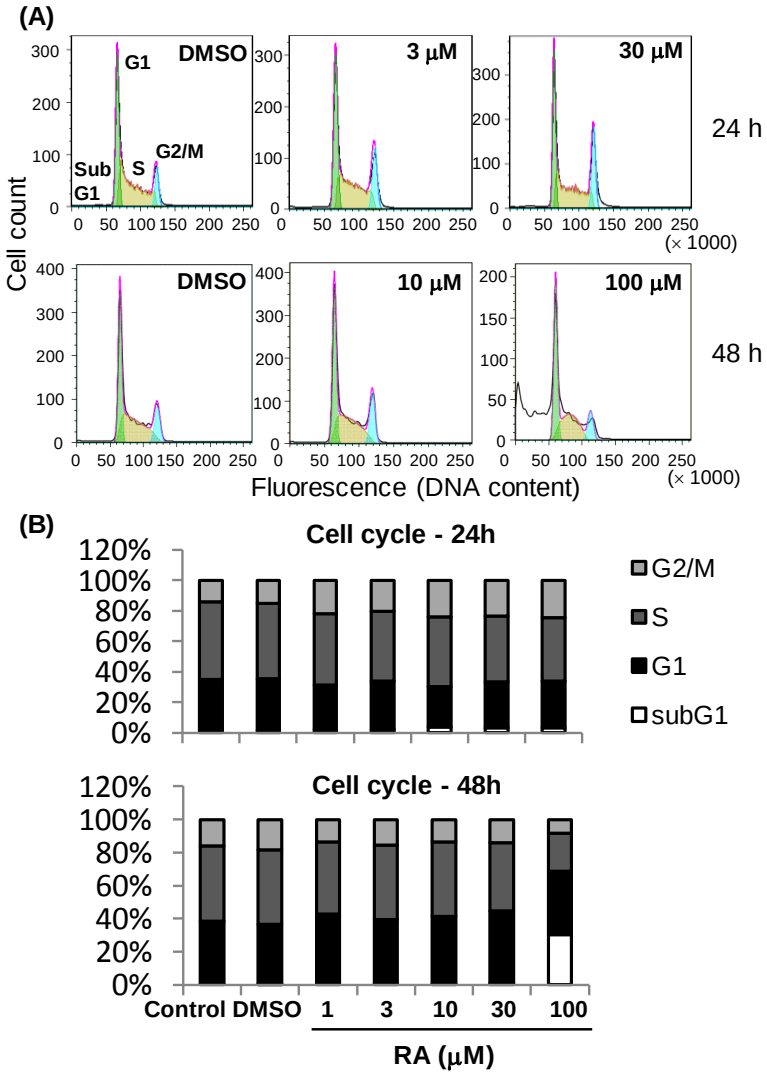

Figure 36. Measurement of cell cycle in CCRF-CEM cells treated with RA. (A) DNA histograms of CCRF-CEM cells treated with indicated concentration for 24 and 48 h. (B) Cell cycle distribution was calculated after 24 and 48 h of treatment.

4.4.5 Induction of apoptotic and necrotic cell death by RA

We performed annexin V (AV) – PI analyses, of RA-treated CCRF-CEM cells to differentiate apoptotic from necrotic cell death. RA significantly increased cell population in the AV(+)PI(-) and AV(-)PI(+) quadrants, indicating that both, early apoptosis and necrosis occurred (Fig. 37A and B). Notably, the statistical evaluation showed that necrotic cell death occurred preferentially compared to apoptotic cell death.

Although it has been initially considered that necrosis is an accidental form of cell death without contribution of a genetic regulatory pathway, recent studies demonstrated the existence of programmed necrotic cell death (termed necroptosis) with RIP1 and RIP3-mediated signaling as major transduction pathway [219-221]. Therefore, we were intrigued by the question, whether RA-induced necrosis could be classified as necroptosis (programmed necrotic cell death) or unregulated necrosis. Necrostatin -1 (Nec-1) was used as a specific RIP1 inhibitor and necroptosis marker. z-VAD-fmk (zVAD) was used as a pancaspase inhibitor. As seen in Figure 37C, incubation with 50 µM Nec-1 did not block RA-induced cell death, suggesting that RA induced unregulated necrosis rather than necroptosis. Cell death was partially rescued by zVAD, implying involvement of caspases in regulating RA-induced cytotoxicity towards ALL cells.

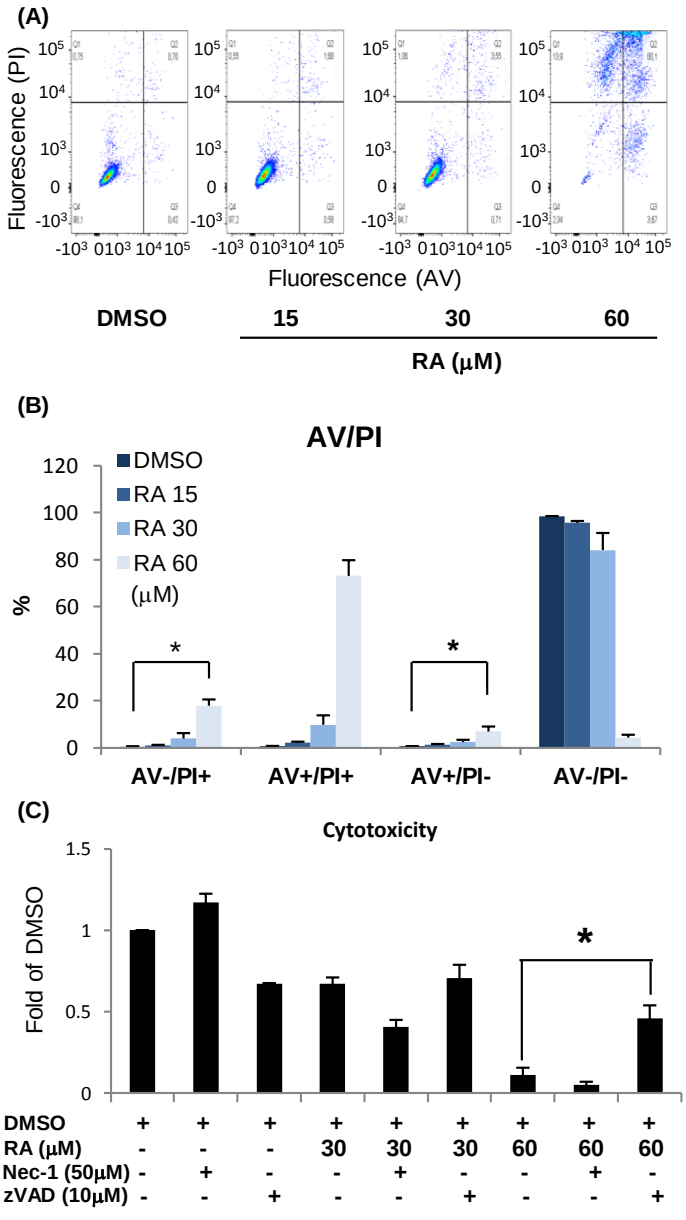

Figure 37. Induction of necrosis and apoptosis by RA in CCRF-CEM cells. (A) Cells were treated with RA or DMSO for 48 h. The signals of AV-FITC binding and PI staining were detected by flow cytometry. (B) Quantification of AV-FITC and PI binding was performed. (C) Cells were treated with nec-1 or zVAD for 2 h prior to 24 h incubation of RA. All treatments contained equal amount of DMSO. Cell viability was determined by resazurin assay. *: $p<0.05$ in comparison between RA alone and RA treatment with zVAD.

4.4.6 Induction of ROS-independent DNA damage

Pathway analysis of microarray results showed that genes associated with DNA replication and repair were significantly deregulated, and additionally, cell cycle assay revealed that G2/M arrest was stimulated by RA. This implies that RA may induce DNA damage. We performed alkaline comet assays to detect single and double-stranded DNA damage. Besides RA decreased the percentage of comet head and increased the percentage of comet tail, DNA migration was observed with tail and Olive tail movements in a dose-dependent manner (Fig. 38A and B). We conclude that RA induced DNA damage and therefore inhibited DNA replication.

DNA damage can result from surplus oxidative stress, which is mediated by overproduction of intracellular ROS [222]. Therefore, we proved, whether RA-induced DNA damage may be associated with increased ROS production. Interestingly, RA did not increase intracellular ROS levels (Figure 38C and D). Taken together, RA-induced DNA damage is not attributed to ROS generation and RA might be involved in a direct interaction with DNA bases.

4.4.7 Disruption of MMP by RA

Mitochondria generate most of the cellular energy supply by regulating adenosine triphosphate (ATP). Mitochondrial dysfunction leads to cell death and causes disruption of membrane integrity by breakdown of ATP synthesis (necrosis) or releasing mitochondrial proteins to activate apoptotic-related caspases (apoptosis) [223-225]. Since the microarray results indicated that energy production was altered by RA, we explored whether RA affected MMP. JC-1-stained CCRF-CEM cells resulted in a shift from red to green fluorescence after RA treatment for 48 h (Figure 39A and B), indicating a depolarization of MMP.

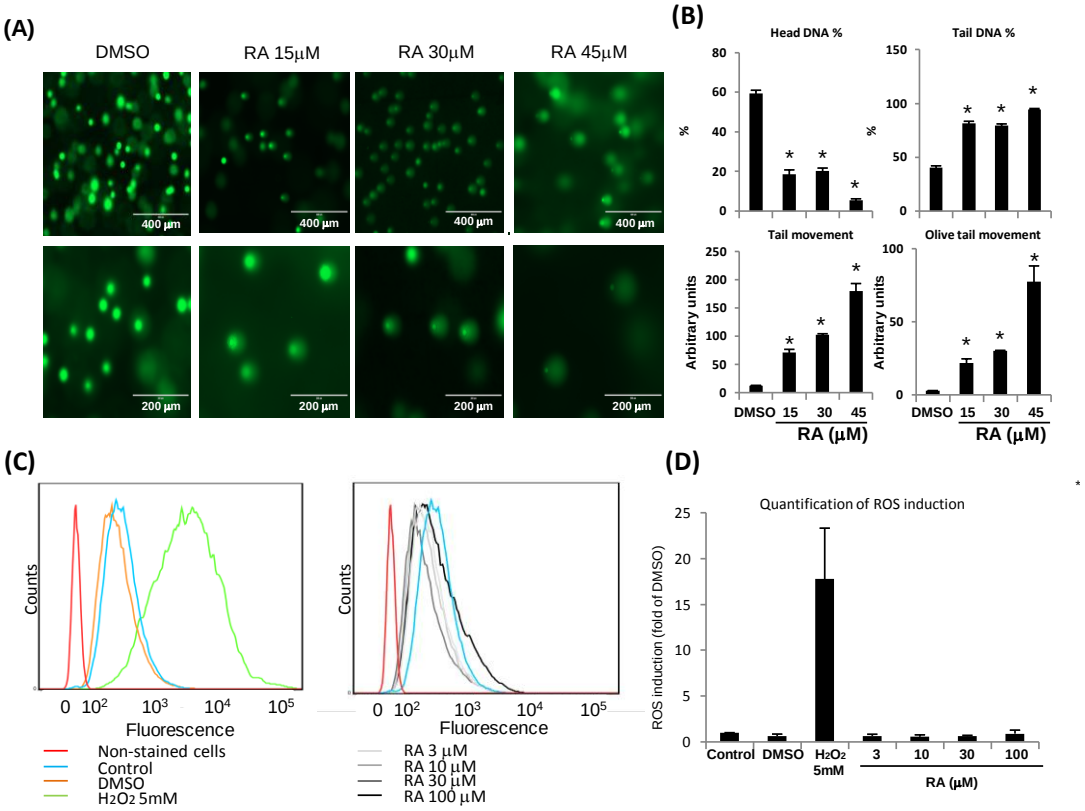

Figure 38. Induction of ROS-independent DNA damage by RA in CCRF-CEM cells. (A) Cells were incubated with different concentration of RA for 24 h. DNA damage was measured by comet assay. Representative pictures of comet assay (upper panel: 100× of magnification; lower panel: 400×). (B) Four parameters were detected including head DNA (%), tail DNA (%), tail movement and Olive tail movement. Tail movement and Olive tail movement were presented in arbitrary units. Results were presented as mean ± SD of 25 cells each. *: $p<0.05$ compared with DMSO. (C) ROS production was measured by flow cytometry after treatment with varying concentration of RA or DMSO for 1 h or 5 mM H_2O_2 for 15 min in CCRF-CEM cells. (D) Statistical quantification of ROS level with mean (fold change) ± SD.

4.4.8 Induction of caspase-independent cell death by RA

We further investigated, whether RA induces the intrinsic, mitochondrial apoptotic pathway in CCRF-CEM cells. Caspase 9 is activated by loss of MMP, which in turn cleaves the effector caspases 3 and 7 and finally leads to cell apoptosis (Kroemer et al., 2007). Therefore, we investigated the activity of caspases 3/7 and caspase 9 in RA-treated CCRF-CEM cells. Western blots revealed no significant cleavage of caspase 3 and 9 upon RA treatment. Caspase 7 showed partially cleaved bands at high RA concentration without reaching statistical significance (Figure 39C and D).

As the next step, we used MCF-7, the cancer cells which do not express caspase-3 [226], to further confirm that caspase 3 is not involved in RA-induced cell apoptosis. As shown in figure 40, RA inhibited MCF-7 cell growth (IC_{50}: 59.88 ± 10.11 µM). Cell population in Sub-G1 phase was upregulated by RA treatment, suggesting RA induced caspase 3-independent apoptosis.

Nuclear PARP is activated after DNA damage. PARP binds to DNA and allows DNA repair-related enzymes access to the damaged DNA [227]. Cleavage of PARP, which typically inactivates PARP, is often associated with apoptosis. Over-activation of PARP results in depletion of ATP and cellular NAD^+ pool, and subsequently to necrosis [228-230]. RA dose-dependently elevated full-length PARP expression (116 kDa), indicative for both, DNA repair and necrotic cell death in response to RA-induced DNA damage. PARP cleavage (89 kDa) upon exposure with high RA concentrations pointed to apoptotic cell death (Figure 39C and D). In sum, RA led to caspase-independent and PARP-mediated cell death in CCRF-CEM cells.

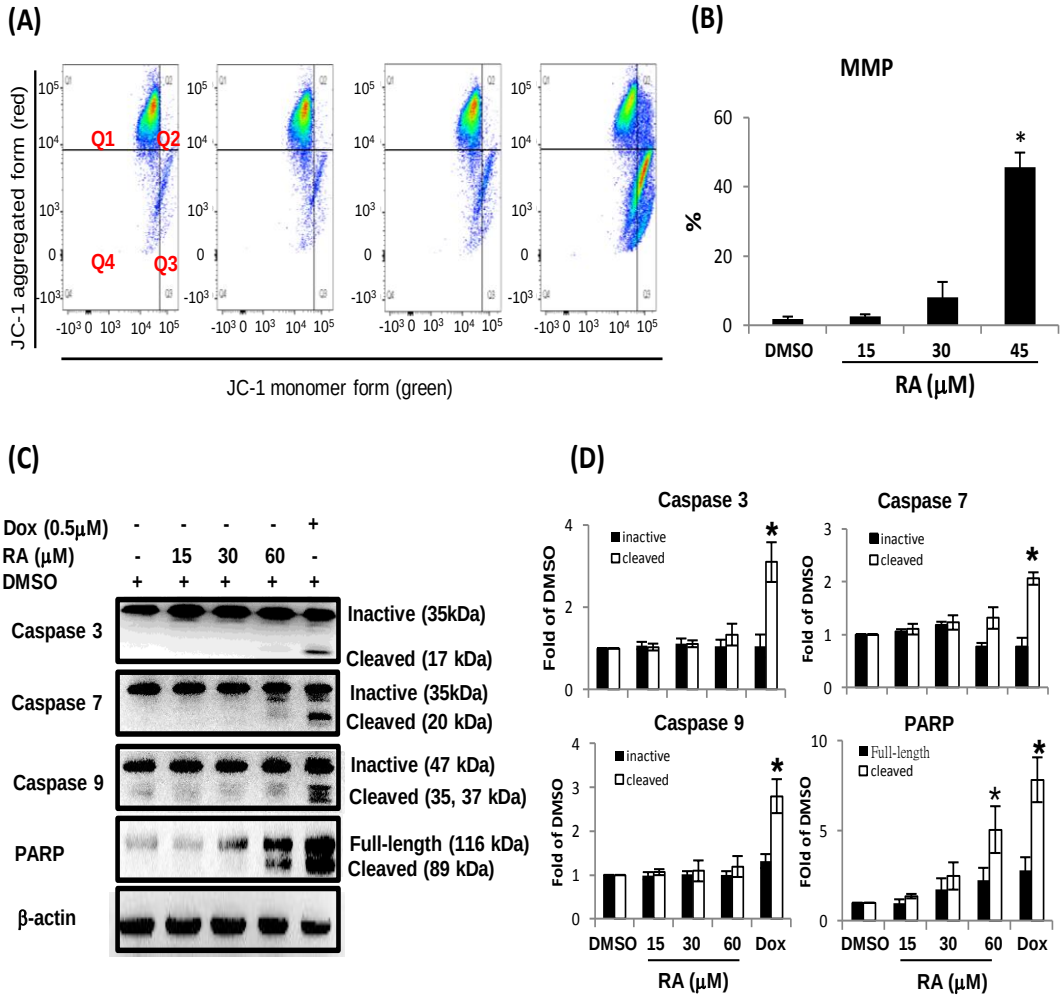

Figure 39. Disruption of MMP and induction of caspase-independent cell death by RA in CCRF-CEM cells. (A) Cells were treated with RA for 48 h, and stained by JC-1. Healthy cells mainly displayed the J-aggregated form with red fluorescence (Q1) and apoptotic cells showed JC-1 monomers with green fluorescence (Q3). (B) Statistical results of the cell population in Q3, which was defined as disruption of mitochondrial membrane potential. *: $p<0.05$ compared with DMSO for 48 h. (C) Cells were treated with RA for 24 h. All treatments contained equal amount of DMSO. Cell lysates were collected and the extracted protein was then subjected to western blotting to detect cleavage of caspase 3/7, caspase 9 and PARP. β-actin was used as an internal control. (D) Quantified results were shown as fold-change of DMSO.

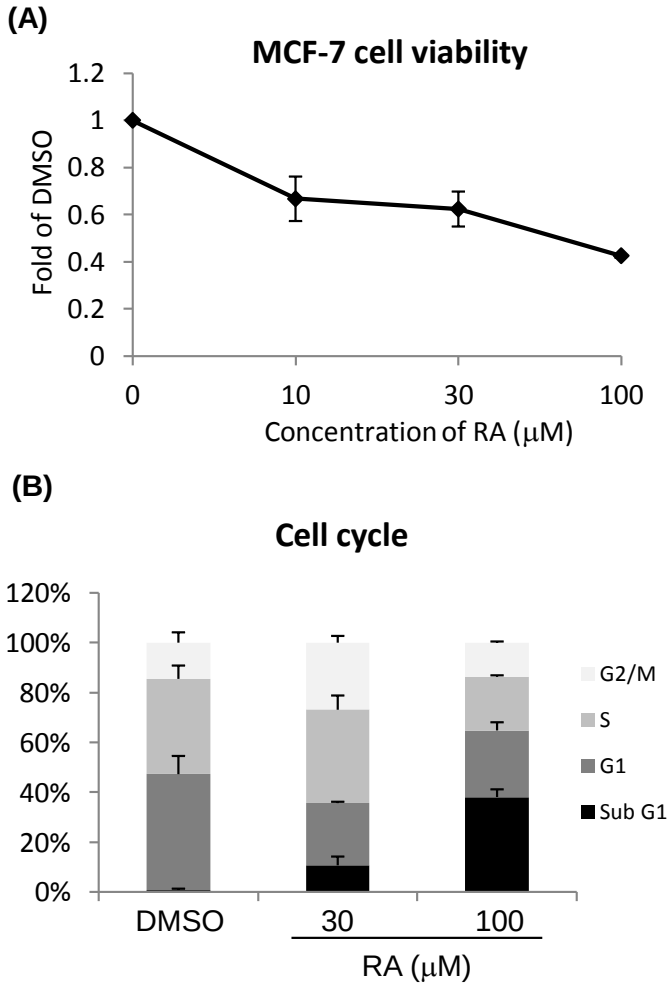

Figure 40. Measurement of cytotoxicity and cell cycle distribution upon RA treatment towards MCF-7 cells. (A) MCF-7 cells were seeded for 24h and subsequently treated with varying concentration of RA. After 72 h of incubation, cell viability was performed by MTT assay. (B) Cell cycle distribution was calculated after 48 h of treatment.

4.4.9 Inhibition of cell adhesion by RA

Microarray data showed that genes involved in cellular movement were deregulated by RA. Thus, we performed an *in vitro* cell adhesion assay. Indeed, RA dose-dependently down-regulated cell adhesion to fibronectin after 2 h RA treatment (Figure 41). This result implies that RA may inhibit extravascular invasion of leukemia cells.

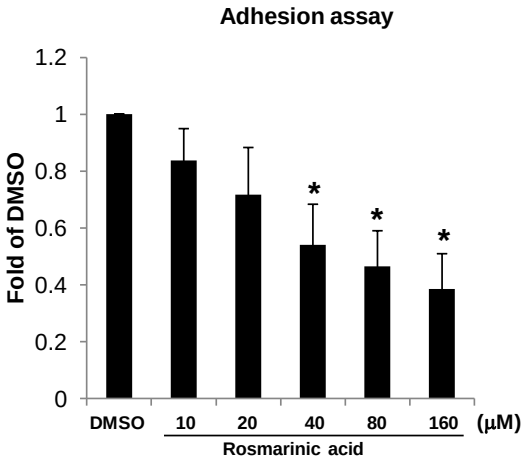

Figure 41. Inhibition of cell adhesion by RA in CCRF-CEM cells. Cells were incubated with different RA doses in fibronectin-coated wells and were allowed to adhere for 2 h at 37°C. Attached cells were determined by resazurin assay. *: $p<0.05$ compared with DMSO.

4.4.10 RA interferes with NFκB signaling

Based on the results in figure 35B that NFκB complex may act as transcriptional regulator of genes associated with cell death and survival and cell cycle, we assumed that NFκB at least partly mediates the activity of RA towards CCRF-CEM cells. Firstly, differentially expressed genes of the most pronounced networks from microarray data (cell death and survival, cellular growth and proliferation, and cell cycle genes) were selected for gene promoter binding motif analysis. The rationale was that genes with high frequency of binding motifs in their promoters for NFκB may be tightly regulated by this transcription factor. As shown in table 15, NFκB elements including NFκB1 and c-Rel were indeed found in these genes, emphasizing that motifs of NFκB complex were important transcriptional factor binding sites for RA-induced deregulated genes.

Table 15. Binding motif analysis for transcription factors in promoter sequences of genes that were differentially expressed upon RA treatment.

$Cluster	Motif	Z score	-log10 (p-val)
1	FOXO3A|FOXO3	-7.283	294.416
2	*REL	-6.503	239.564
	*c-Rel|REL	-5.048	153.155
	*NFKB1	-3.478	82.824
3	POU4F3	-5.871	199.475
	SCMH1	-3.443	81.529
4	SOAT1	-5.799	195.205
5	STAT1|Stat1	-5.602	183.63
6	GZF1|Gzf1	-5.482	176.787
7	Oct-1|POU2F1	-5.064	153.973
8	STAT3	-5.039	152.69
9	TSNAX	-4.9	145.536
	E2F1	-3.182	72.213
	STAT4	-3.118	70.023
10	Ypr015c	-4.877	144.339

*: proteins of the NFκB complex

$: Genes that appear with similar motifs were classified into the same cluster. Ranking was numbered according to t –log10 (p-val) of the first motif of each cluster.

Subsequently, we speculated that RA may interact with NFκB signaling. If the NFκB pathway is activated, inhibitor κB kinase-β (IKK-β) phosphorylates NFκB inhibitor protein and then degrades IκB, which liberates p50 (*NFKB1*)/p65 (*RELA*) complex. This complex in turn enters the nucleus, leading to the transcriptional activation of downstream genes [231]. Thus, we proposed that RA may directly bind to IKK-β and performed *in silico* molecular docking. IKK-β inhibitors interact with the hinge motif, which forms hydrogen bonds with Glu97 and Cys99 [188]. Remarkably, RA bound to the same pharmacophore as MG132, a reference compound for IKK-β inhibition. MG132 and RA formed hydrogen bonds to the ATP binding sites at binding residue Cys99 and Glu97 (Figure 42A and B, Table 16). Additionally, RA also formed hydrogen bond with Asp166 and Leu167, which are located in the N-terminal activation segment in the ATP binding site [232]. Interestingly, RA showed a higher binding energy than MG132 (-6.98 kcal/mol *vs*. -7.59 kcal/mol), but a lower predicted Ki value (7.33 *vs*. 5.75 μM).

NFκB activation is associated with its translocation from the cytosol to the nucleus. Therefore, we investigated, whether RA binding to IKK-β was associated with decreased nuclear p65 translocation. We performed Western blotting to detect nuclear expression p65 protein. TNF-α was used as inducer of NFκB signaling. Indeed, RA inhibited TNFα-induced translocation of p65 from the cytoplasm to the nucleus (Figure 42C). Taken together, we conclude that RA binds to IKK-β and decreases nuclear p65 translocation. The inactivation of NFκB transcriptional activity may then lead to the deregulation of genes involved in cell cycle regulation, cell death, DNA damage and invasion.

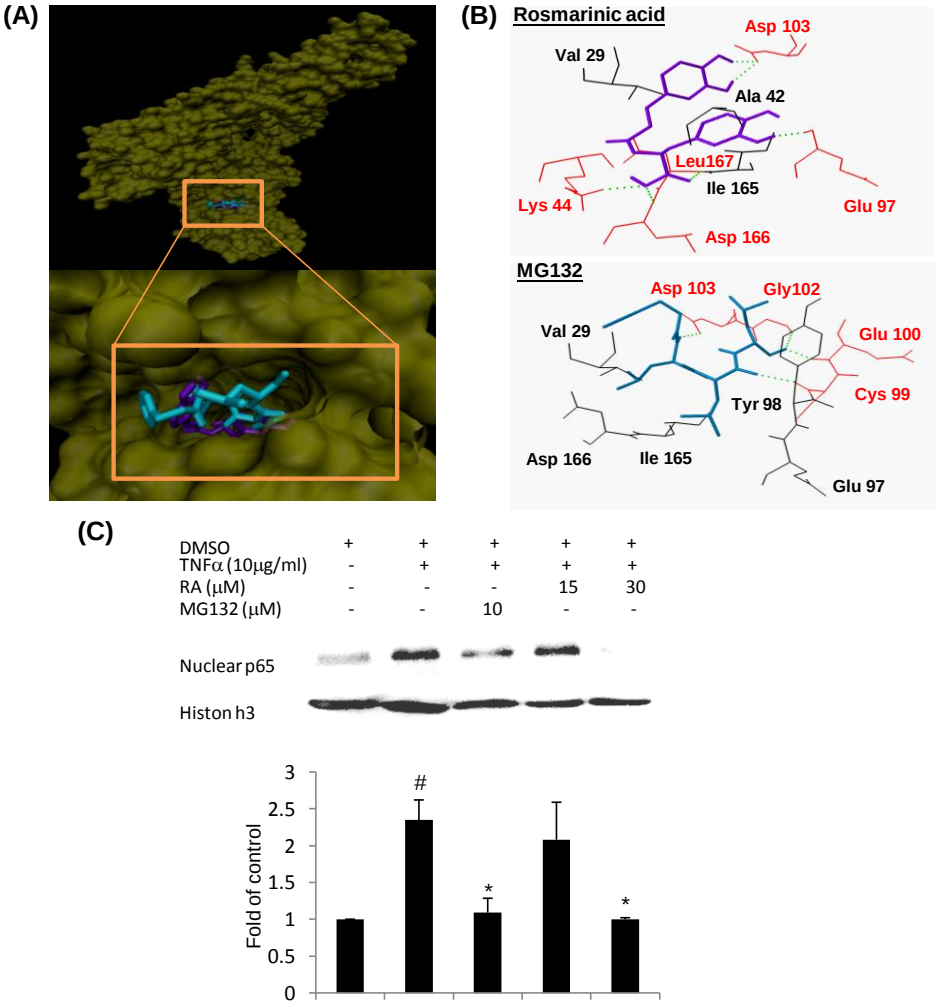

Figure 42. RA interacts with NFκB signaling. (A) Molecular docking of RA to IKK-β. VMD files presented the binding site of RA (purple) in comparison with the control drug, MG132 (blue). (B)The residues included in hydrogen bond binding are labeled in red, and hydrogen bonds are shown as green dots. (C) Incubation CCRF-CEM cells with RA for 24 h or MG132 for 2 h prior to 1 h induction of TNFα. All treatments contained equal amount of DMSO. Western blot analysis was used to detect expression of nuclear p65 and histon h3 (internal control). #: $P<0.05$ compared with DMSO; *: $p<0.05$ compared with TNFα.

Table 16. Molecular docking of rosmarinic acid on IKK-β. The frame performed the lowest binding energy and name of hydrogen bond.

Compound	Lowest binding energy (kcal/mol)	Mean binding energy (kcal/mol)	Residues of hydrogen bond	Numbers of residues involved in hydrophobic interaction	PKi value (μM)
MG132 (IKKβ inhibitor)	-7.59	-6.49	**CYS99**, GLU100, **GLY102**, ASP103	16	7.33
Rosmarinic acid	-6.98	-6.98	LYS44 **GLU97** ASP103 **ASP166** **LEU167**	11	5.75

4.4.11 *TP53* as a regulator gene upon RA treatment

In response to DNA damage by RA treatment, G2/M arrest and subsequently appearance of sub-G1 peak were stimulated, which indicates the induction of apoptosis. The microarray data depicted a series of deregulated genes associated with control of G2/M arrest, which might support the phenomenon of RA-induced G2/M arrest (Figure 43). The tumor suppressor gene and stress sensor p53 induces cell cycle arrest and apoptosis following multiple stresses [233]. It blocks damaged cells at G2 checkpoints, if cells enter the G2 phase with damaged DNA. A recent study revealed that p53 regulated not only apoptosis, but also necrosis by forming mitochondrial permeability transition pores upon interaction of cyclophilin D [234]. Our microarray results implied that p53 might be also a regulator gene upon RA treatment-induced DNA damage.

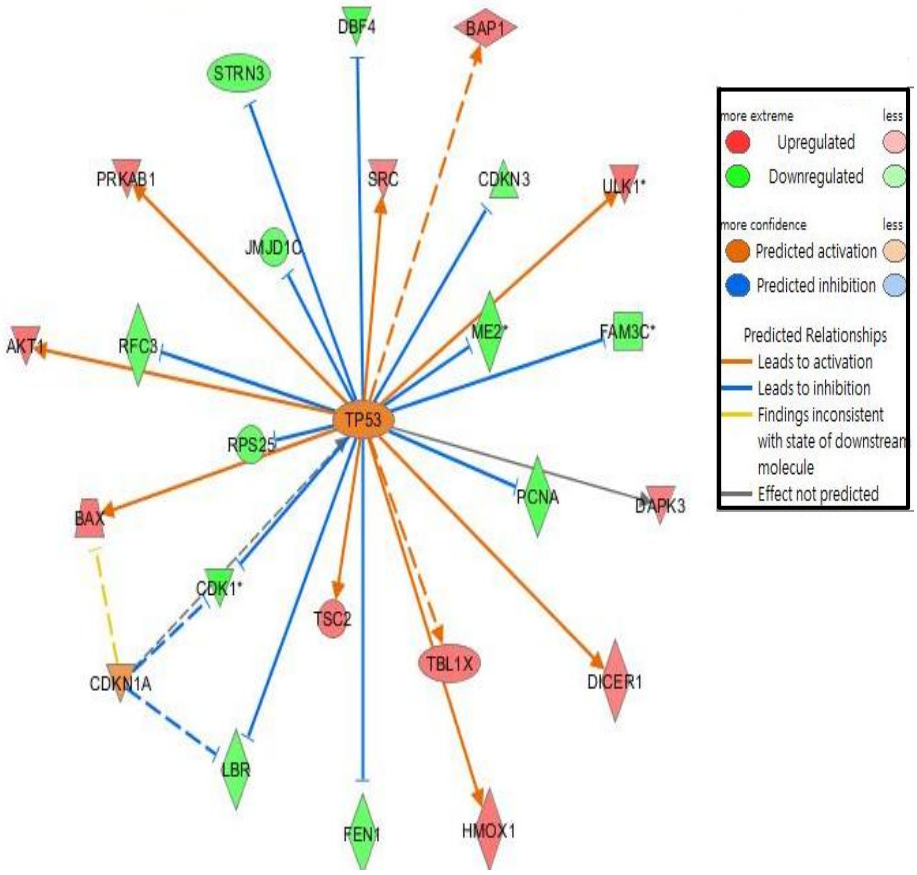

Figure 43. Deregulated genes under the influence of *TP53* in CCRF-CEM cells treated with RA. The arrows indicate effects of deregulated genes on other genes. Continuous lines show a direct interaction, dotted lines an indirect interaction.

4.4.12 Summary: Molecular mechanisms of rosmarinic acid from *Salvia miltiorrhiza* in acute lymphoblastic leukemia cells

It has been demonstrated that RA induced necrosis and apoptosis through DNA damage and disruption of MMP in a ROS- and caspase-independent manner. Additionally, RA also inhibits NFκB signaling and cell adhesion. This study provides additional insights into novel modes of cell death. These results may contribute to the rationale use of RA and *Salvia miltiorhizza* in traditional medicine to treat leukemia.

4.5 Production of rosmarinic acid and salvianolic acid B from callus culture of *Salvia miltiorrhiza* with cytotoxicity towards acute lymphoblastic leukemia cells

Plant tissue cultures serve as useful and convenient models for the mass production of valuable secondary metabolites, particularly from rare or slow-growing plant species. It is known that the highest contents of bioactive hydrophilic and hydrophobic compounds can be found in the roots of *S. miltiorrhiza*, however, the number of studies employing cultures of SM leaf and stem callus as source of bioactive compounds is very limited. In this investigation, we established a solid medium callus culture system for stem and leaf from SM and detected the major components from the extracts by HPLC analysis. Thereafter, the cytotoxic effects of callus cultures toward the acute lymphoblastic CCRF-CEM leukemia cells were determined.

4.5.1 Callus induction from stem and leaf explants

A variety of modifications of medium for stem and leaf callus culture have been tested to identify the most effective culture medium for stem or leaf callus production. Stem explants from SM producing callus on a nutrient AM1 medium supplemented with 1 mg/l 2,4-D combined with 0.45 mg/l kinetin and 0.01 mg/l 1-naphtylacetic acid was found the best condition, which generated the highest amounts of stem calli. Using AM1, a biomass of 4.0 ± 0.75 g was accumulated (Table 17). Leaf explants cultured in MS medium supplemented with 0.022 mg/l of kinetin generated 2.9 ± 0.31 g of calli. The results indicated that SM stems potentially produced more calli than leaves did.

Figure 44. Callus formation from leaf and stem of SM.

4.5.2 Qualitative and quantitative analysis of RA and Sal B

The qualitative and quantitative HPLC analyses of the individual phenolic compounds in plant and callus extracts are given in Table 1. Representative chromatograms at 330 nm are shown in figure 45 and 46. The constituents were identified by comparison their retention times (Rt), UV spectra and MS data with those of authentic standards and confirmed by comparison of the data reported the literature [235]. Briefly, the major components were RA (Rt 14 min) and Sal B (Rt 19.5 min). RA UV spectra displayed λmax at 225, 290 (sh), and 330 nm, while for Sal B λmax were at 218, 238, 290, 210 (sh) nm. Both negative and positive ionization mode was tried to detect mass fragmentation of the constituents. The results indicated that negative mode was sensitive to RA and Sal B and the quasi-molecular peak $[M-H]^-$ was always present. Specifically, RA displayed the fragments at 359 $[M-H]^-$ and 719 $[2M-H]^-$, while Sal B fragments were at 717 $[M-H]^-$, 519 $[M-H\text{-}198]^-$, 321 $[M-H\text{-}198\text{-}198]^-$. The fragments at 519 *m/z* and 321 *m/z* indicated the loss of one or two units of danshensu. Quantitative data were calculated on the basis of the peak area of each compound in the chromatograms at 330 nm for RA and at 290 for Sal B. In accordance with the values of dry biomass, calli from stem explants produced higher amount of RA (1.27 ± 0.38 % *vs*. 0.28 ± 0.02 %) and Sal B (0.87 ± 0.20 % *vs.* 0.07 ± 0.03 %) than leaves did. Similarly, the phenomenon that stem samples yielded higher amounts of these two constituents than leaves was also seen in plants.

Table 17. Biosynthetic parameters of SM plant and callus extracts

Sample	Starting materials (g)	Fresh biomass (g)	Dry biomass (g)	RA (%)	Sal B (%)
Callus stem	0.086 (± 0.01)	120.4 (± 5.02)	4.0 (± 0.75)	*1.27 (± 0.38)	*0.87 (± 0.20)
Callus leaf	0.061 (± 0.01)	130.3 (± 17.6)	2.9 (± 0.31)	0.28 (± 0.02)	0.07 (± 0.03)
Plant stem				*1.12 (± 0.31)	*0.50 (± 0.25)
Plant leaf				0.06 (± 0.02)	0.01 (± 0.01)

*Values from callus or plant stem extracts significantly differ at a significance level of $p <$ 0.05 in comparison with respective callus or plant leaf.

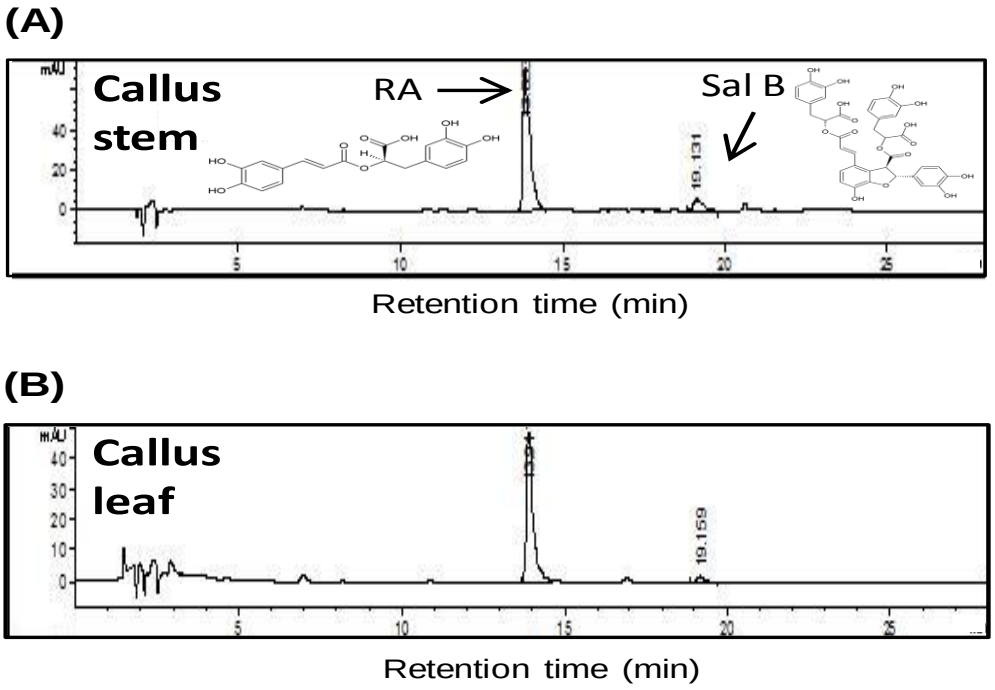

Figure 45. HPLC chromatogram at 330 nm of RA and Sal B from callus stem (A) and leaf (B) extracts of SM. The peak shown at a retention time of 14 min indicated RA, and at 19.5 min Sal B.

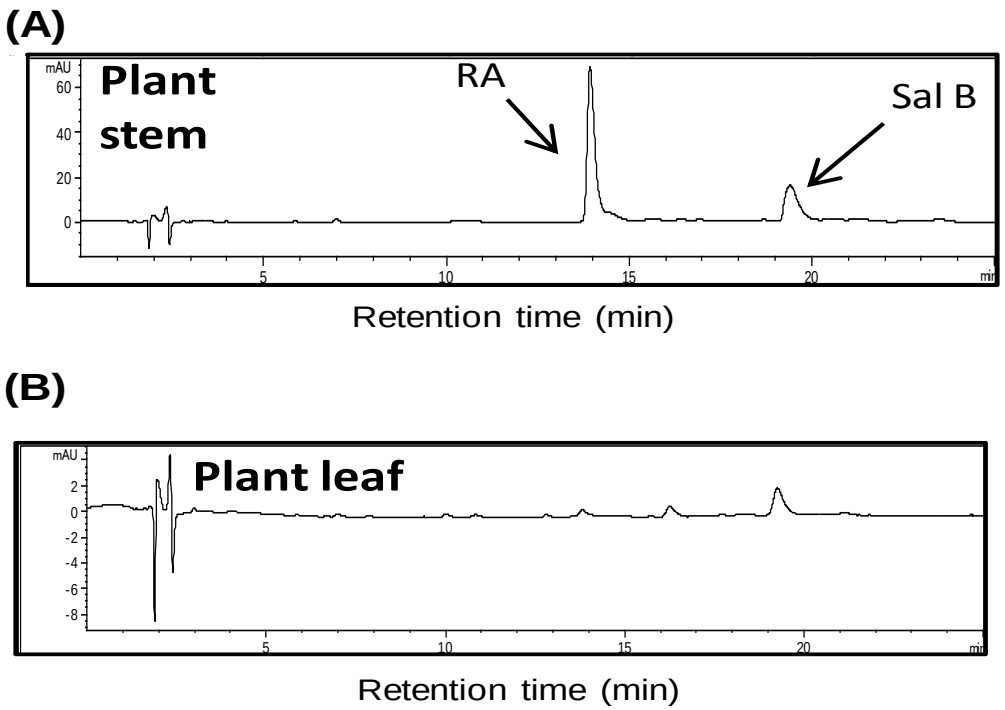

Figure 46. HPLC chromatogram at 330 nm of RA and Sal B from plant stem (A) and leaf (B) extracts of SM. The peak shown at a retention time of 14 min indicated RA, and at 19.5 min Sal B.

4.5.3 Linearity, LOD, LOQ, precision

All calibration curves showed good linearity. The following r^2 values were obtained: Sal B r^2=0.9996 (regression curve: y=0.0004x−0.0591); RA r^2=0.9999 (regression curve: y=9× 10^{-4}−0.0006). LOD for Sal B was 1.89 ng (0.94 μg/ml, 2μl of injection) and LOQ was 6.6 ng (3.3 μg/ml, 2 μl of injection). For RA, LOD was calculated as 1.86 ng (0.93 μg/ml, 2 μl of injection) and LOQ was 5.8 ng (2.9 μg/ml, 2 μl of injection). The overall intra- and inter-day time variations of the standards were less than 3.64% and 2.34% for Sal B and less than 2.13% and 3.44% for RA, respectively. In addition, both Sal B and RA remained stable (not less than 93% residual percentage) during the three days of inter-day variability tests.

4.5.4 Cytotoxicity of stem and leaf callus extracts towards ALL cells

In general, extracts from callus cultures contained higher amounts of RA and Sal B than plant extracts (Table 17). Therefore, we further tested cytotoxic effects of extracts from callus cultures. CCRF-CEM cells were treated with stem or leaf callus extract in a concentration ranging from 0.01 to 100 μg/ml for 72 h and the cell viability was measured by the resazurin assay. Stem and leaf callus extracts cytotoxic towards both cell lines with IC_{50} values of 13.1 ± 0.90 and 18.1 ± 0.33 μg/ml, respectively (Figure 47A, Table 18). In comparison, stem extracts with higher amounts of RA and Sal B inhibited cell growth more than leaf extracts. Treatment with RA or Sal B revealed IC_{50} values of 13.1 ± 0.81 and 4.4 ± 2.41 μM, indicating that Sal B was more potent than RA in killing CCRF-CEM cells.

The combination of RA and Sal B resulted in a synergetic effect towards inhibition of CCRF-CEM cells as validated by Loewe additivity model (Fig 47B). CCRF-CEM cells were treated with varying concentration of RA and indicated concentration (1 or 2 μM) of Sal B for 72 h. In table 18, it was shown that the IC_{50} value of RA decreased with increasing doses of Sal B to 2 μM, 2.42 to 3.03-fold less than RA treatment alone.

Table 18. IC50 values for callus extracts from SM and 2 compounds (RA and Sal B) towards CCRF-CEM cells as determined by resazurin assay.

Extract/Compound	CCRF-CEM IC_{50} (extract: μg/ml; compound: μM)	95% confidence interval
Stem	*13.1 (± 0.90)	10.87 – 15.33
Leaf	18.1 (± 0.33)	17.28 – 18.92
RA	13.1 (± 0.81)	11.09 – 15.11
Sal B	4.4 (± 0.41)	3.38 – 5.42
RA + 1 μM Sal B	5.41 (± 0.76)	3.52 – 7.30
RA + 2 μM Sal B	4.32 (± 0.35)	3.45 – 5.19

*Values significantly differ at a significance level of $p < 0.05$ in comparison with callus leaf

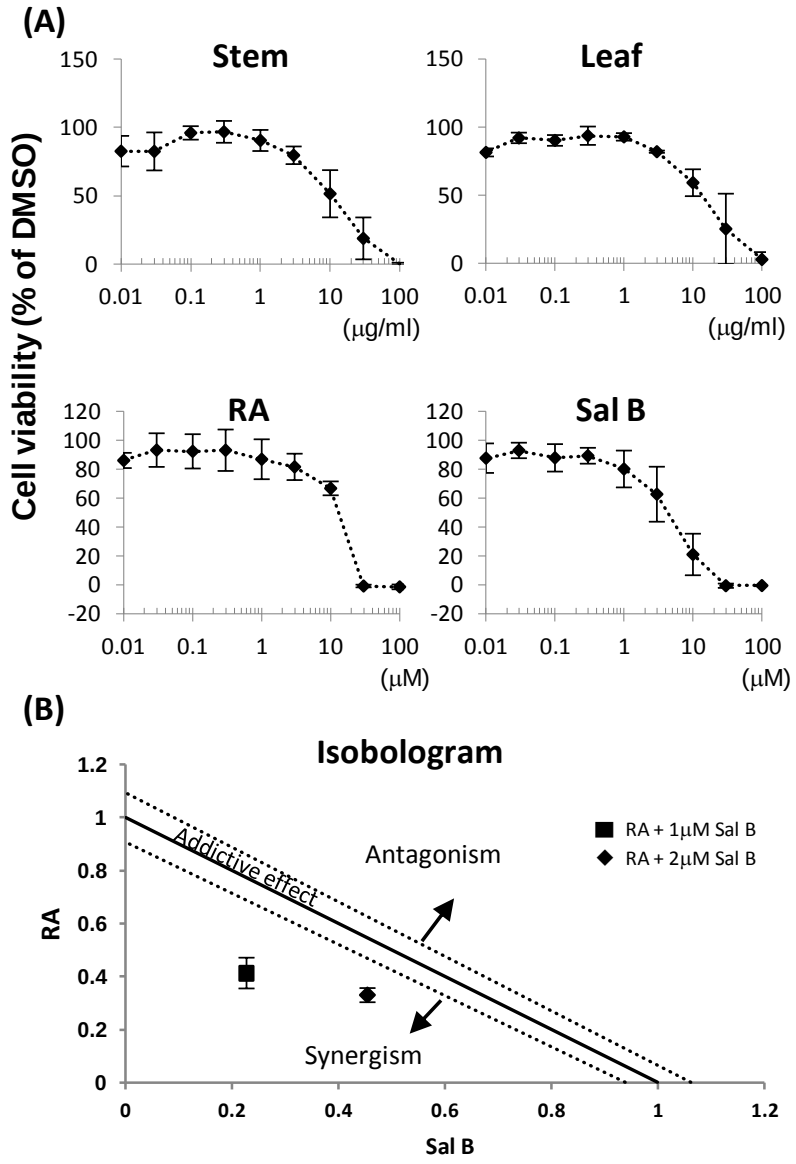

Figure 47. Cell viability of CCRF-CEM cells treated with callus culture extracts from SM, RA and Sal B. (A) The cells were treated with indicated concentrations following seeding. After 72 h of incubation, resaruzin assays were performed. At least three independent experiments each with six parallel measurements were performed. (B) Combined effects of RA and Sal B were illustrated by isobologram analysis. The concentrations of RA and Sal B were normalized with the dose of their IC_{50} on x and y-axes. Dash lines represented the standard deviation for IC_{50} values of each drug. The results were displayed as with mean SD.

4.5.5 Summary: Production of rosmarinic acid and salvianolic acid B from callus culture of *Salvia miltiorrhiza* with cytotoxicity towards acute lymphoblastic leukemia cells

In this study, the chemical constituents and anticancer potential of *Salvia miltiorrhiza* (SM) stem and leaf were examined with those of respective callus cultures. The callus culture for stem and leaf explants was initiated in modified Murashige and Skoog (MS) medium. Active constituents of respective extracts were analyzed by high performance liquid chromatography coupled with DAD and MS (HPLC-DAD-MS). Rosmarinic acid (RA) and salvianolic acid B (Sal B) were determined to be the main phenolic compounds. Quantitative analyses revealed that callus stem extracts produced higher amount of RA and Sal B. Stem and leaf callus extracts exerted cytotoxic effects towards CCRF-CEM cells. As expected, stem extract with higher amount of RA and Sal B showed lower IC_{50} value than leaf extract. These findings suggest the possibility to isolation bioactive constituents with anti-cancer properties from *in vitro* callus cultures of stem and leaf of SM.

5. Discussion

5.1 Anticancer effects of *S. miltiorrhiza*

5.1.1 *S. miltiorrhiza* overcomes drug resistance

Acute lymphoblastic leukemia (ALL) is featured by uncontrolled proliferation of lymphoid progenitor cells, which are unable to differentiate into T cells and B cells. Since conventional chemotherapy frequently fails to cure relapsed ALL patients and results in severe complications, new therapeutic drugs are needed to improve the treatment [7,44].

Clinical trials testing compounds, which inhibit ABC transporter-mediated MDR, revealed high toxicity of these inhibitors in normal tissues limiting their clinical use [236]. Thus, cytotoxic agents, which are able to bypass MDR or selectively kill the MDR cells (by collateral sensitivity) represent an attractive alternative concept to treat otherwise drug-resistant tumors [25]. Collateral sensitivity can be understood as a kind of synthetic lethality, in which the genetic alterations in MDR cells is accompanied by hypersensitivity to certain compounds that the parental cells are not that much sensitive to [237,238]. The mechanisms that result in collateral sensitivity can be either P-gp-mediated or non-P-gp-mediated [237, 239-241]. Specific genetic alterations in MDR cells, which otherwise confer resistance, can be specifically exploited to preferentially kill MDR cells. Miltirone inhibited multidrug-resistant CEM/ADR5000 cells with even higher efficacy than wild-type CCRF-CEM cells as indicated by degree of resistance below 1.0, referring to a significant collateral sensitivity. This represents an attractive approach to kill unresponsive tumors and is a remarkable result in light of the extremely high resistance of CEM/ADR5000 cells to epirubicin. In this context it is worth mentioning that miltirone affected normal lymphocytes less than multidrug-resistant CEM/ADR5000 cells, indicating that the collateral sensitivity of milrirone against MDR is not accompanied by increased toxicity towards normal cells. The mechanisms how miltirone exerts collateral sensitivity warrants further investigation.

In contrast to doxorubicin and epirubicin, which are well-known P-gp substrates and which exert high cross-resistance in P-gp-overexpressing, resistant CEM/ADR5000 cells, *S. miltiorrhiza* root extract, CPT and RA exerted similar cytotoxic efficacy in CEM/ADR5000 cells and parental CCRF-CEM cells. This is a strong clue that *S. miltiorrhiza* root extracts displayed cell death independent of P-gp.

Moreover, *S. miltiorrhiza* root extracts conferred greater sensitivity towards resistant HCT116 (*p53*$^{-/-}$) and U87.MGΔEGFR cells compared to their parental counterparts, showing the potential of *S. miltiorrhiza* root extracts for inducing collateral sensitivity. This investigation confirmed the multifactorial properties of *S. miltiorrhiza* roots to overcome drug resistance in diverse cancer cell lines.

5.1.2 Discussion of CPT, miltirone and RA on NFκB signaling and cell invasion

Activation of NFκB signaling leads to anti-apoptotic effects and drug resistance of cancer cells. In ALL, inhibition of NFκB-mediated transcription contributed to downregulated molecules referred to cell adhesion [191,194]. CPT and RA-deregulated genes by motif analysis have yielded clues that NFκB may be a crucial transcriptional regulator upon treatment. Our molecular docking analysis revealed that CPT, miltirone and RA bound to the same pharmacophore but with higher affinity (lower binding energy and pKi value) than the well-known IKK-β inhibitor MG132. These three compounds down-regulated p65 translocation was induced by TNF-α, suggesting that they may target NFκB and inhibit NFκB signaling in ALL cells.

Notably, 5 μM CPT slightly, but not statistical significantly enhanced p65 translocation compared with TNF-α treatment alone. This undesired effect implied that low dose of CPT might potentially trigger NFκB on CCRF-CEM cells. As mentioned previously, activation of NFκB stimulated drug resistance and expression of anti-apoptotic molecules in cancer cells. Thus, low-dose CPT-induced NFκB might be related to drug resistance. The phenomenon is similarly reported toward doxorubicin-treated cervical carcinoma cells [242]. The mechanism of NFκB induction by low-dose CPT and whether low-dose CPT-induced NFκB activation directly regulates drug resistance required further elucidation.

Leukemia cells can leave the blood vessel system and permeate into various organs. This is also well documented for acute lymphoblastic leukemia (ALL) cells. Infiltrated organs include urinary bladder, eyes, ovary, breast, lung and others [243-252]. Treatment of leukemic infiltration is frequently difficult and therapeutic improvements are warranted. The fact that CPT, miltirone and RA indeed inhibited adhesion of CCRF-CEM cells is a clue that these compounds might be suited to treat extravascular infiltration of organs by ALL cells.

5.1.3 *S. miltiorrhiza* initiates DNA damage and ROS-mediated apoptosis

Reactive oxygen species (ROS) is a collective term that summarizes O_2-derived free radicals such as superoxide anions ($O_2^{\bullet-}$), hydroxyl radicals (HO•), peroxyl (RO_2•), alkoxyl (RO•), as well as O_2-derived non-radical species such as hydrogen peroxide (H_2O_2) [253]. They are considered as side products of anaerobe metabolisms with the feature of instability. At low level, ROS act as "redox messenger" to regulate intracellular signaling and maintain physiological function, while excess ROS interacts with different component of DNA to modify DNA bases and generate strand breaks, which seriously alters cellular function and determines cell fate, termed as oxidative stress [222]. Mitochondria are the primary source of endogenous ROS, as they supply approximately 90% of cellular energy in the form of ATP, in which the respiration process generates free radicals. Therefore, mitochondria are also major targets of unfavorable effects from ROS, which lead to mitochondrial dysfunction and activitation of the mitochondrial-mediated intrinsic apoptotic pathway [254,255]. Agents inducing ROS-production and apoptosis gained interests to inhibit cancer cell growth. These drugs produce excess ROS mostly in mitochondria and stimulate oxidative DNA damage. Caspase-dependent intrinsic (mitochondria-mediated) pathway is mediated by mitochondrial dysfunction and release of cytochrome c, which determines apoptotic cell death. In this investigation, *S. miltiorrhiza* root extract has been shown to induce ROS-mediated apoptotic cancer cell death. Furthermore, activation of caspase 9 suggested that the upstream mitochondrial dysfunction was initiated. Cleavage of the effectors caspase 3 and 7 ensured caspase-dependent apoptotic pathway was activated. The phenomenon was also observed in the results of CPT and miltirone-induced cytotoxic effects, suggesting that tanshinones are the main active compounds of *S. miltiorrhiza* against growth of ALL cells.

In response to genotoxic stress caused by environmental or endogenous insults such as ultraviolet radiation, various chemicals and reactive cellular metabolites, cell cycle checkpoints can be initiated to slow down or arrest cell cycle progression, allowing the cell to repair or prevent the transmission of damaged chromosomes. Cell cycle checkpoint regulation can also activate pathways leading to apoptosis to remove damaged cells from tissues. Defects in these processes may lead to formation of cancer cells which summarize hypersensitivity to cellular stress, and susceptibility to DNA damage, genomic defects, and resistance to apoptosis [256].The DNA-damage response network is highly complex and involves a multitude of proteins that sense the damage, transduce signals into cells and execute cellular responses. DNA

double-strand break “sensor” proteins constitute NBS1/Mre11/Rad50 multiprotein complexes recruited at DNA damage sites, where they create rapidly-expanding nuclear foci referred to as DNA damage heterochromatin foci. The “transducer” protein of DNA double-strand breaks is the phosphoinositide 3-kinase-related ataxia-telangiectasia-mutated (ATM) kinase, which, in turn, activates multiple “effector” proteins, including p53, Mdm2, and CHK2. Activation of these “effector” proteins influences cell-cycle progression and arrest, cellular senescence and apoptosis activation [257,258]. Cell cyle transition is regulated by cyclin-dependent kinases (CDK), cyclin proteins and CDK inhibitors. In general, DNA damage in the G2 phase prevents transition into mitosis. P53 is activated by ATM and ATM- and Rad3-related (ATR) protein kinases in response to DNA damage, resulting in increase of p21(Cip/Kip family of CDK inhibitors). This protein inhibits cdc2 activity (also known as CDK1) - cyclin B1 complex. Down-regulation of this complex halts cell cycle at the G2/M checkpoint [204,259]. Taken miltirone as an example, miltirone-induced G2/M arrest was validated by up-regulation of *CDKN1A* (p21) and down-regulation of *CDC2/CCNB1*. Interestingly, *TP53* (p53) gene expression was not significantly changed In previous reports, G2/M arrest and p21 expression were regulated in a p53-independent way [260,261]. A possible explanation is that ATM and ATR inhibited CDC2 by phosphorylating tyrosine 15 and threonine 14, thereby stimulating G2/M arrest [233].

PARP is another important DNA damage sensor. It binds at sites of single- or double-strand DNA breaks and initiates repair process. Activated PARP can deplete the ATP of a cell in an attempt to repair the damaged DNA. Once cells undergo apoptosis, PARP is cleaved by caspases, which in turn inactivate PARP. Therefore, cleavage of PARP is associated with caspase-dependent apoptotic pathway [184]. PARP cleavage that mediated by caspases in intrinsic pathway and G2/M arrest stimulated by CPT and miltirone implied that they are potentially a DNA-damaging inducer.

RA induced DNA damage, PARP cleavage and dusfunction of mitochondria, howener, it generated ROS-independent and caspase-dependent cell death. The underlying mechanisms of RA against ALL cell growth are discussed in detail in the seperated chapter below.

5.2 Molecular basis of CPT-mediated anticancer effects

Compare analysis

It is well documented that the cancer cells' response to chemotherapeutic agents is determined by multiple factors [262]. To gain insight into the determinants of cellular sensitivity and resistance towards *S. miltiorrhiza* root extract, we selected CPT as main constituent and performed a microarray-based transcriptome-wide COMPARE analysis for 60 cancer cell lines to identify genes, whose mRNA expression correlated with the $\log_{10} IC_{50}$ values of CPT. As listed in Table 5, the encoded proteins exerted diverse function, including cellular adhesion (*HAPLN3*) [263], cell proliferation (*OPTN*, *PARD3*) [264-266], DNA methylation (*GNAS*, *PRKD1*) [267,268], mitochondrial biogenesis and components (*DCTN6*, *MRPL44*) [269], and signal transduction and transcriptional regulators (*NMT2*, *ZCCHC9*, *ZEB2*, *ZMIZ2*) [270,271]. Among these genes, Zinc finger E-box-binding homeobox 2 (*ZEB2*) and N-myristoyltransferase 2 (*NMT2*) are determinants, which are known to render cells resistant to drugs. ZEB2 is involved in apoptotic regulation, which contributes to MDR associated with E2F1 overexpression. This transcription factor up-regulates P-gp [272,273]. *NMT2* is known to inhibit cancer cell apoptosis [274]. Induction of the *NMT2* gene in drug-resistant osteosarcoma cell lines suggested a role for drug resistance [275]. The other genes are not reported as of yet to be involved in drug resistance. However, the function or pathways, which these genes are assigned to are known to be relevant for drug resistance, *e.g.* cell-cell adhesion [276-278], DNA methylation [279-281], cell death mechanisms [282,283], and signal transduction [284-286]. The results draw a diverse picture of different gene functions and cancer-associated mechanisms. This implies that CPT exerts multifactorially determined cytotoxicity towards cancer cells, as most natural products do. It deserves further studies to unravel the full range of molecular mechanisms that determine the responsiveness of tumor cells to CPT.

CPT initiates UPR and interferes protein translation

Based on the microarray and bioinformatic results, treatment of CPT on CCRF-CEM cells induced ER stress mainly through deregulation of IRE1-XBP1 and ATF4-CHOP pathways. Transcription of the *CHOP* gene has been reported to be activated by XBP1, ATF4 and ATF6 [148]. It is worth mentioning that CHOP induced GADD34 expression, which regulates restoration of protein synthesis via a negative feedback loop by dephosphorylation of eIF-2α. The recovery of protein translation might be in favor of synthesis of pro-apoptotic molecules [144, 287]. Expression of GADD34 is

associated with increased sensitivity to apoptosis [146]. Previous reports showed that CPT induced ROS and CHOP expression, and contributed to apoptosis of human hematoma, melanoma and breast cancer cells [288,289]. Combined with the data which unraveled the ROS-dependent intrinsic apoptotic pathway upon CPT treatment, the present investigation suggested that ER stress is potentially involved in CPT-induced apoptosis in ALL cells.

Inhibitors targeting PI3K/mTOR signaling are under evaluation in human clinical trials, including BEZ235 (phase II) and GSK2126458 (phase I) showing anticancer activity in a variety of cancers, such as metastatic breast cancer, lymphoma and advanced solid tumors [290]. Previous investigations also revealed that CPT inhibited signaling pathways of PI3K and mTOR, and regulated expression of downstream molecules, which led to attenuation of cancer development [291,292]. Our docking approach revealed that CPT may target PI3K/mTOR, which corroborates these findings. However, it is also reported that mTOR inhibitors or PI3K/mTOR dual inhibitors led to resistance by MYC-driven elevation of eIF4F complex [293]. Therefore, the combination of such inhibitors with those targeting the eIF4F complex may be expected as improved anticancer strategy. Here we showed that CPT potentially bound to eIF4A, one of the components of eIF4F. Hence, CPT may be a suitable component for such combination treatments.

5.3 Anticancer mechanisms of RA

RA has been recognized as important natural antioxidant, which possesses antioxidant activities by scavenging free radicals, increasing antioxidant enzymes such as superoxide dismutase (SOD) and glutathione peroxidase and decreasing malondialdehyde (MDA) resulting from lipid peroxidation [294-296]. Furthermore, RA acts in an anti-inflammatory manner and prevents from oxidative injuries [297,298]. Our result showed that RA was not capable of generating ROS, which might be attributed to the feature of RA as antioxidant. In this regard, RA-induced DNA damage did not result from excess ROS generation. Rather, RA acts potentially as a genotoxin through other mechanisms involving intercalation of DNA and/or inhibition of topoisomerase, DNA polymerase and ribonucleotide reductase [299,300]. Other antioxidants such as epigallocatechin gallate (EGCG) exert not only genotoxic, but also mutagenic effects with reductive DNA damage in normal cells [301]. Therefore, it warrants more investigation to figure out, whether RA treatment generates genotoxic or mutagenic effect.

As mentioned above, PARP activity is regulated by many factors, such as DNA damage, caspases, and intracellular NAD^+ concentrations. Activation of PARP represents DNA damage is sensed and DNA repair is initiated. Cleavage of PARP is mediated by caspase 3, which results in PARP inactivation and subsequently apoptosis . Overexpression of PARP not only refers to DNA repair, but also implies necrotic cell death for depletion of ATP and cellular NAD^+ pool [184, 228-230]. AV-PI analysis revealed that RA caused apoptotic and necrotic cell death. The results are in accordance with the expression of PARP, which depicted cleavage of PARP from 116 to 89 kDa and activation of full-length PARP simultaneously. Activation of PARP has been observed in lower concentration of RA, meaning that treatment of RA triggered process of DNA repair. Concerning the comet assay and cell cycle assay, it further confirms that low dose of RA caused DNA insults and triggered DNA repair system protected cells from damages by showing unchanged cell cycle regulation.

Apoptosis and necrosis are by definition two extremes of possible types of cell death. It seems that the availability of ATP is decisive for the mode of cell death [302]. In particular, DNA-damaging compounds lead to activation of the energy-consuming DNA repair machinery in cells and thus to extensive exhaustion of cellular NAD^+ and ATP pools caused by PARP activation [303]. As a consequence cells are no longer able to perform the energy-requiring molecular and structural changes (e.g. nuclear condensation and DNA degradation) necessary for apoptosis, and necrosis will occur instead [228]. The mechanism that RA simultaneously induced apoptotic and necrotic cell death remains unclear. Indeed, in various cell types, a narrow range of ATP depletion (15–25% of basal levels) has been found to represent a threshold that determines whether a cell dies by apoptosis or by necrosis, and below this threshold necrosis is the dominant cell death pathway [304]. It seems that DNA damage leads to extensive PARP activity and thus to a rapid consumption of NAD^+ and ATP, which subsequently leads to a necrotic mode of ALL cell death *in vitro*. To further confirm RA-induced necrotic cell death warrants investigations involving morphologic identification by electron microscopy and analysis of ATP depletion.

Western blotting and luminescence assays (data not shown) confirmed that caspases 3, 7 and 9, which play a vital role in mitochondrial apoptosis, were not activated by RA. In addition, RA also induced cytotoxic effects towards caspase 3-null MCF-7 cell line, confirming caspase 3-independent cell death mode by RA. Our result was supported by the authors Xavier et al., who have shown that RA- promoted apoptosis on colon

cancer cells is not dependent on caspase 3 and 9 [112]. One report revealed that caspases are involved in RA-induced mitochondrial-dependent apoptotic pathway in HepG2 and Jurkat cells [305-306]. Therefore, induction of apoptosis by RA might be cell type specific. In light with the result that pancaspase inhibitor zVAD reversed RA-induced cell death, it is reasonable to speculate that cleavage of PARP may be mediated by other caspases [307,308]. Considering that RA induced DNA damage, mitochondrial dysfunction and caspases-independent pathway, it is worth mentioning that these effects caused by RA might be related to apoptosis inducing factor (AIF) and endonuclease G (ENDOG), which translocate to the nucleus and mediate large-scale DNA fragmentation [127].

Due to genetic alternations, cancer cells develop the capacity to circumvent apoptotic cell death and resistance to chemotherapeutic agents [309], which leads to failure of anti-cancer treatment. Therefore, other types of cell death such as necrosis, autophagy and mitotic catastrophe against apoptosis-resistant cancer cells have gained much attention [310,311]. Necrosis shows morphological changes by random DNA fragmentation, increase in cell volume, swelling of organelles, loss of plasma membrane integrity, and leakage of intracellular contents. Necrotic cell death has been thought to be a cause of inflammatory reactions. However, necrotic cells are not always proinflammatory and occasionally can also inhibit inflammatory responses [312,313], implying the complexity of necrosis-induced inflammation. ROS production and NFκB signaling are important for inflammatory processes [314,315]. Since the NFκB activity was repressed and ROS generation was unchanged upon RA treatment, RA may be less harmful to healthy tissues by conquering inflammatory response induced by necrotic death. Of note, several reports revealed that ROS generation and NFκB activation leads to up-regulation of P-gp [316-318]. Moreover, increased ROS generation upon chemotherapeutic agents induced mitochondrial DNA mutations, resulting in resistance of leukemia cells to anti-cancer drug [319]. Thus, the occurrence of MDR might be avoided by RA treatment. Additionally, necrotic cell death is thought to be immunogenic, and to stimulate immune responses against cancer cells [320-322]. Taken together, the mode of cell death induced by RA is worth considering as novel anti-cancer strategy.

5.4 Callus produces RA and Sal B from *S. miltiorrhiza* leaf and stem

In this study, callus cultures were successfully generated from *S. miltiorrhiza* leaves

and stems on modified MS solid medium with optimized concentration of growth regulators. Our results are in good agreement with other reports that 2,4-D in combination with kinetin favors callus growth and the production of secondary metabolites [323,324].

HPLC analysis revealed that RA and Sal B were the major components in plant and callus extracts. Both of the detected constituents are caffeic acid derivatives. The establishment of productive callus culture systems to gain desired phytochemicals results from plant materials originally having high-yield potential [325]. In accordance with previous research, our results showed that, plant and callus stem produced greater amounts of RA and Sal B than plant and callus leaf extracts did. The callus culture system allows growth in a medium containing more carbon source and growth hormones than in the normal atmosphere. The nutrient-rich environment might promote higher biosynthesis of phenols. Therefore, it is not surprising that *S. miltiorrhiza* stem and leaf extracts from callus cultures generated higher amounts of RA and Sal B than field-cultivated plants. The phenomenon seen in our investigation is in agreement with other studies [326,327]. In addition, different combinations of nutrition additives in the medium may also influence the yield production of the desired compounds. This has been reported for RA synthesis [326]. Thus, the composition of nutrients in the culture medium needs to be optimized to obtain the maximum amount of desired compounds.

The variations in the distribution of individual phenolic compounds in the plant parts remain unclear. Previous studies revealed that leaves contain the second highest amounts of bioactive components after roots, and most of these compounds are water-soluble [328,329]. Accumulation of phenolics in the leaves may serve as defense strategy against UV-B radiation. UV-sensitized phenolics activate specific antioxidant systems and prevent the plant from DNA damage and cell death [330,331]. These finding are in agreement with data of Modarres et al., [332], showing that superior yields of caffeic acid derivatives in the leaves of *Salvia leriifolia*. Interestingly, our results indicated that leaves contained less active components than stems. This phenomenon might be attributed to geographical or climate-related factors. A recent study suggested that the distribution of phenolics in SM differs at different stages. Phenolic compounds are transported from leaves through the stem and ultimately to the root during growth [333]. Therefore, the harvest time may considerably determine the quantities of phenolic components in SM.

We have shown that the extracts containing RA and Sal B inhibited CCRF-CEM cell growth. In addition, a synergetic growth inhibitory effect was by the combination of RA and Sal B in CCRF-CEM cells, suggesting the chemotherapeutic potential of callus or plant stem and leaf extracts from *S. miltiorrhiza*.

6. Summary and conclusion

The goal of the study is to identify the mode of actions that underlie the anticancer effects of *S. miltiorrhiza* and its major compounds including cryptotanshinone, miltirone and rosmarinic acid. *S. miltiorrhiza* root extract exerted cytotoxicity towards various sensitive and resistant cancer cells. CEM/ADR5000 cells were shown nearly identical sensitive to CCRF-CEM cells, while HCT116 ($p53^{-/-}$) and U87.MGΔEGFR cells were hypersensitive (collateral sensitive) compared to their parental cells. *S. miltiorrhiza* root extract stimulated ROS generation, cell cycle S phase arrest and triggered intrinsic apoptotic pathway on CCRF-CEM cells. To develop new chemotherapeutic agents against resistant cancer cells, it is worthwhile to further investigate the selective cytotoxicity towards EGFR-overexpressing and p53-mutant cell lines by SM root extract, giving hope for development of new anti-cancer drugs which confer sensitivity to tumors resistant to conventional chemotherapy.

Guided by HPLC analysis of *S. miltiorrhiza*, we illustrated the mechanisms of cryptotanshinone, miltirone and rosmarinic acid towards CCRF-CEM cells as follows:

(1) Cryptotanshinone stimulated ROS generation and induced DNA damage. It arrested cells in G2/M phase of the cell cycle and induced mitochondrial-mediated intrinsic apoptosis. DNA-binding motif analysis of the microarrary-retrived deregulated genes in the promoter region revealed NFκB as potential transcription factor involved in cryptothanshinone's mode of action. Molecular docking and western blotting provided supportive evidence suggesting that cryptotanshinone binds to IKK-β and inhibits the translocation of p65 from the cytosol to the nucleus. In addition, cryptotanshonone inhibited cellular movement, indicating that this compound exerts anti-invasive features. In addition, cryptotanshinone triggered genes (e.g. *DDIT3*, *XBP1*, *GADD34* and *ATF4*) related to UPR and cell apoptosis. Molecular docking suggested inhibitory effects of crptotanshinone by binding to eIF-4A and PI3K providing evidence for a role of crptotanshinone's in the disruption of protein synthesis via eIF-mediated translation initiation. These findings potentially support cryptotanshinone-induced cytotoxic effects toward acute leukemia cells.

(2) Miltirone inhibited multidrug-resistant CEM/ADR5000 cells better than drug-sensitive CCRF-CEM wild-type cells – a phenomenon termed collateral sensitivity. Furthermore, miltirone showed less active against normal lymphocytes, indicating normal cells might be less affected in patients. Flow cytometric analyses revealed that miltirone induced G2/M arrest and apoptosis. Down-regulation of *CCNB1* (cyclin B1) and *CDC2* mRNA and up-regulation of *CDKN1A* (p21) mRNA

were in accord with miltirone-induced G2/M arrest. Furthermore, miltirone stimulated ROS generation and MMP disruption, which in turn induced DNA damage and activation of caspases and PARP. Moreover, miltirone decreased cell adherence to fibronectin. Molecular docking revealed that miltirone bound to the ATP binding site of IKK-β.

(3) Rosmarinic acid dose-dependently inhibited CCRF-CEM and CEM/ADR5000 cells, but caused less cytotoxicity towards normal lymphocytes. RA simultaneously induced apoptosis and necrosis. DNA damage was dose-dependently induced without ROS generation, which subsequently led to cell cycle arrest. Rosmarinic acid-stimulated MMP dysfunction activated PARP-cleavage and caspase-independent apoptosis. In accordance with molecular docking and gene promoter binding motif analyses, p65 translocation from the cytosol to the nucleus was blocked, indicating a mechanistic role of the NFκB pathway to explain rosmarinic acid's action. Rosmarinic acid affected cellular movement as evaluated by ameliorating cell adhesion to fibronectin.

In an additional project, rosmarinic acid and salvianolic acid B were identified as the main constituents with therapeutic effects in extracts and callus culture of *S. miltiorrhiza* leaf and stem parts. Extracts from respective callus culture showed cytotoxic effects towards CCRF-CEM cells. These established experimental approaches pave a way to utilize leaf and stem parts of *S. miltiorrhiza*, which are considered as a waste of the medicinal plant, to generate rosmarinic acid and salvianolic acid B in the industry.

In conclusion, these results suggest that crptotanshinone, miltirone and rosmarinic acid may serve as potential chemotherapeutic agents in anti-leukemia therapy, and may contribute to the rationale use of *Salvia miltiorhizza* in traditional medicine of cancer.

7. References

[1] Fitzmaurice C, Dicker D, Pain A et al. Global burden of disease cancer collaboration. The global burden of cancer 2013. *JAMA Oncology* 2015, 1: 505- 527.

[2] Bray F. Transitions in human development and the global cancer burden. In:Wild CP, Stewart B, eds. *World cancer report 2014*. Lyon: International Agency for Research on Cancer, 2014.

[3] Anand P, Kunnumakara AB, Sundaram C, Harikumar KB, Tharakan ST, Lai OS, Sung B, Aggarwal BB. Cancer is a preventable disease that requires major lifestyle changes. *Pharmaceutical Research* 2008, 25: 2097–2116.

[4] Hanahan D, Weinberg RA. Hallmarks of cancer: the next generation. *Cell* 2011, 144: 646-674.

[5] Lichtman MA. Battling the hematological malignancies: the 200 years' war. *Oncologist* 2008, 13: 126-138.

[6] Pillar GJ. John Hughes Bennett and the discovery of leukaemia. In: Pillar GJ, eds. *Proceedings of the royal college of physicians of Edinburgh*: Supplement 3. 1997, 27: 1-49.

[7] Pui CH, Robison LL, Look AT. Acute lymphoblastic leukaemia. *Lancet* 2008, 371: 1030–1043.

[8] Kaatsch P. Epidemiology of childhood cancer. *Cancer Treatment Reviews* 2010, 36: 277-285.

[9] Nigro LL. Biology of childhood acute lymphoblastic leukemia. *Journal of Pediatric Hematology/Oncology* 2013, 35: 245-252.

[10] Inaba H, Greaves M, Mullighan CG. Acute lymphoblastic leukaemia. *Lancet* 2013, 381: 1943-1955.

[11] Locatelli F, Schrappe M, Bernardo ME, Rutella S. How I treat relapsed childhood acute lymphoblastic leukemia. *Blood* 2012, 120: 2807-2816.

[12] DeVita VT, Jr., Chu E. A history of cancer chemotherapy. *Cancer Research* 2008, 68:8643-53.

[13] DeVita VT Jr, Rosenberg SA. Two hundred years of cancer research. *The New England Journal of Medicine*. 2012, 366: 2207-2214.

[14] Housman G, Byler S, Heerboth S, Lapinska K, Longacre M, Snyder N, Sarkar S. Drug Resistance in Cancer: An Overview**.** *Cancers (Basel)*. 2014, 6: 1769–1792.

[15] Gottesman MM. Mechanisms of cancer drug resistance. *Annual Reiew Medicine* 2002, 53: 615-627.

[16] Martinez L, Falson P. Multidrug resistance ATP-binding cassette membrane transporters as targets for improving oropharyngeal candidiasis treatment. *Advances in Cellular and Molecular Otolaryngology* 2014, 2: 23955.

[17] Efferth T. The human ATP-binding cassette transporter genes: from the bench to the bedside. *Current Molular Medcine* 2001, 1: 45-65.

[18] Gillet JP, Efferth T, Remacle J. Chemotherapy-induced resistance by ATP-binding cassette transporter genes. *Biochimca et Biophysica Acta* 2007, 1775: 237-262.

[19] Borst P, Schinkel AH. P-glycoprotein ABCB1: a major player in drug handling by mammals. *The Journal of Clinical Investigation* 2013, 123: 4131-4133.

[20] Gottesman MM, Pastan I. Biochemistry of multidrug resistance mediated by the multidrug transporter. Annual Review of Biochemistry 1993, 62: 385-427.

[21] Scala S, Akhmed N, Rao US, Paull K, Lan LB, Dickstein B, Lee JS, Elgemeie GH, Stein WD, Bates SE. P-glycoprotein substrates and antagonists cluster into two distinct groups. *Molular Pharmacology* 1997, 51:1024-1033.

[22] O'Brien FE, Clarke G, Dinan TG, Cryan JF, Griffin BT. Human P-glycoprotein differentially affects antidepressant drug transport: relevance to blood-brain barrier permeability. *International Journal of Neuropsychopharmacology* 2013, 16:2259-2272.

[23] Yague E, Armesilla AL, Harrison G, Elliott J, Sardini A, Higgins CF, Raguz S. P-glycoprotein (MDR1) expression in leukemic cells is regulated at two distinct steps, mRNA stabilization and translational initiation. *The Journal of Biological Chemistry* 2003, 278:10344-10352.

[24] Szakács G, Paterson JK, Ludwig JA, Booth-Genthe C, Gottesman MM. Targeting multidrug resistance in cancer. *Nature Reviews Drug Discovory* 2006, 5: 219-34.

[25] Zahreddine H, Borden KL. Mechanisms and insights into drug resistance in cancer. *Frontiers in Pharmacology* 2013, 4: 28.

[26] Lynch TJ, Bell DW, Sordella R, Gurubhagavatula S, Okimoto RA, Brannigan BW, Harris PL, Haserlat SM, Supko JG, Haluska FG, Louis DN, Christiani DC, Settleman J, Haber DA. Activating mutations in the epidermal growth factor receptor underlying responsiveness of non-small-cell lung cancer to gefitinib. The *New England Journal of Medicine* 2004, 350: 2129-2139.

[27] Amann J, Kalyankrishna S, Massion PP, Ohm JE, Girard L, Shigematsu H, Peyton M, Juroske D, Huang Y, Stuart Salmon J, Kim YH, Pollack JR, Yanagisawa K, Gazdar A, Minna JD, Kurie JM, Carbone DP. Aberrant epidermal growth factor receptor signaling and enhanced sensitivity to EGFR inhibitors in lung cancer. *Cancer Research* 2005, 65: 226-235.

[28] Tomas A, Futter CE, Eden ER. EGF receptor trafficking: consequences for signaling and cancer. *Trends in Cell Biology* 2014, 24: 26-34.

[29] Lee J, Moon C. Current status of experimental therapeutics for head and neck cancer. *Experimental Biology and Medicine* 2011, 236:375-389.

[30] Zhang Z, Stiegler AL, Boggon TJ, Kobayashi S, Halmos B. EGFR-mutated lung cancer: a paradigm of molecular oncology. Oncotarget 2010, 1:497-514.

[31] Liu J, Zhang C, Hu W, Feng Z. Tumor suppressor p53 and its mutants in cancer metabolism. *Cancer Letters* 2015 356(2 Pt A):197-203.

[32] Harris SL, Levine AJ. The p53 pathway: positive and negative feedback loops. *Oncogene* 2005, 24:2899-2908.

[33] Giono LE, Manfredi JJ. The p53 tumor suppressor participates in multiple cell cycle checkpoints. *Journal of Cellular Physiology* 2006, 209:13-20.

[34] Smith ML, Seo YR. p53 regulation of DNA excision repair pathways. *Mutagenesis* 2002 17:149-156.

[35] Amaral JD, Xavier JM, Steer CJ, Rodrigues CM. The role of p53 in apoptosis. *Discovery Medicine* 2010, 9:145-152.

[36] Ben-Porath I, Weinberg RA. The signals and pathways activating cellular senescence. *The International Journal of Biochemistry & Cell Biology* 2005, 37:961-976.

[37] Levine AJ, Oren M. The first 30 years of p53: growing ever more complex. *Nature Reviews Cancer* 2009, 9:749-758.

[38] McCurrach ME, Connor TMF, Knudson CM, Korsmeyer SJ, Lowe SW. Bax-deficiency promotes drug resistance and oncogenic transformation by attenuating p53-dependent apoptosis. *Proceedings of the National Academy of Science of the United States of America* 1997, 94: 2345–2349.

[39] Giménez-Bonafé P, Tortosa A, Pérez-Tomás R. Overcoming drug resistance by enhancing apoptosis of tumor cells. *Current Cancer Drug Targets* 2009, 9: 320-340.

[40] Fojo, T. Commentary: Novel therapies for cancer: why dirty might be better. *Oncologist* 2008, 13: 277-283.

[41] Garraway LA, Jänne PA. Circumventing cancer drug resistance in the era of personalized medicine. *Cancer Discovery* 2012, 2: 214-226.

[42] Malhotra V, Perry MC. Classical chemotherapy: mechanisms, toxicities and the therapeutic window. *Cancer biology & therapy.* 2003, 2:S2-4.

[43] Siddik ZH. Mechanisms of action of cancer chemotherapeutic agents: DNA-interactive alkylating agents and antitumour platinum-based drugs. In: Alison MR, Ed, *The cancer handbook*, Nature Publishing Group, London. 2002, 1295–1313.

[44] Pui CH, Jeha S. New therapeutic strategies for the treatment of acute lymphoblastic leukaemia. *Nature Reviews Drug Discovery* 2007, 6: 149-165.

[45] Evans BE, Rittle KE, Bock MG, DiPardo RM, Freidinger RM, Whitter WL, Lundell GF, Veber DF, Anderson PS, Chang RSL, Lotti VJ, Cerino DJ, Chen TB, Kling PJ, Kunkel KA, Springer JP, Hirshfield J. Methods for drug discovery: development of potent, selective, orally effective cholecystokinin antagonists. *Journal of Medicinal Chemistry* 1988, 31:2235-2246.

[46] Bailly C. Ready for a comeback of natural products in oncology. *Biochemical Pharmacology* 2009, 77: 1447–1457.

[47] Basmadjian C, Zhao Q, Bentouhami E, Djehal A, Nebigil CG, Johnson RA, Serova M, de Gramont A, Faivre S, Raymond E, Désaubry LG. Cancer wars: natural products strike back. *Frontiers in Chemistry* 2014, 2:20.

[48] Luo F, Gu J, Chen L, Xu X.Systems pharmacology strategies for anticancer drug discovery based on natural products. *Molecular Biosystems* 2014, 10:1912-1917.

[49] Swinney DC, Anthony J. How were new medicines discovered? *Nature Reviews Drug Discovery* 2011, 10: 507-19.

[50] Newman DJ, Cragg GM. Natural products as sources of new drugs over the 30 years from 1981 to 2010. *Journal of Natural Products* 2012, 75:311-335.

[51] Efferth T, Kahl S, Paulus K, Adams M, Rauh R, Boechzelt H, Hao X, Kaina B, Bauer R. Phytochemistry and pharmacogenomics of natural products derived from traditional Chinese medicine and Chinese materia medica with activity against tumor cells. *Molecular Cancer Therapeutics* 2008, 7:152-161.

[52] Ruan WJ, Lai MD, Zhou JG. Anticancer effects of Chinese herbal medicine, science or myth? *Journal of Zhejiang University Science B* 2006, 7:1006-1014.

[53] Xue T, Roy R. Studying traditional Chinese medicine. Science 2003, 300:740–741.

[54] Youns M, Hoheisel JD, Efferth T. Traditional Chinese medicines (TCMs) for molecular targeted therapies of tumours. Curr ent Drug Discovery Technologies 2010, 7:37-45.

[55] Zhang YH, Qin X, Xu J. Analysis of Chinese medical syndrome features of patients with primary liver cancer before and after transcatheter arterial chemo-embolization. *Zhongguo Zhong Xi I Jie He Za Zhi* 2012, 32: 111-1174.

[56] Hu B, Wang SS, Du Q. Traditional Chinese medicine for prevention and treatment of hepatocarcinoma: From bench to bedside. *World Journal of Hepatology* 2015, 7: 1209-1232.

[57] Chen X, Guo J, Bao J, Lu J, Wang Y. The anticancer properties of Salvia miltiorrhiza Bunge (Danshen): a systematic review. *Medicinal Research Reviews* 2014, 34: 768-794.

[58] Du G, Zhang J. Overview of modern research on Danshen. In: Yan X, eds. *Danshen (Salvia miltiorrhiza) in Medicine*. Springer, Dordrecht, 2014, 3-17.

[59] Zhou L, Zuo Z, Chow MS. Danshen: an overview of its chemistry, pharmacology, pharmacokinetics, and clinical use. The Journal of Clinical Pharmacology 200, 45: 1345-1359.

[60] Liu AH, Li L, Xu M, Lin Y H, Guo HZ, Guo DA. Simultaneous quantification of six major phenolic acids in the roots of *Salvia miltiorrhiza* and four related traditional Chinese medicinal preparations by HPLC –DAD method. *Journal of Pharmaceutical and Biomedical Analysis*, 2006, 41: 48-56.

[61] Li HB, Chen F. Preparative isolation and purification of six diterpenoids from the Chinese medicinal plant Salvia miltiorrhiza by high-speed counter-current chromatography. *Journal of Chromatography A*, 2001, 925: 109-114.

[62] Lin TH, Hsieh CL. Pharmacological effects of Salvia miltiorrhiza (Danshen) on cerebral infarction. *Chinese Mdicine* 2010, 5: 22.

[63] Zhang XZ, Qian SS, Zhang YJ, Wang RQ. Salvia miltiorrhiza: A source for anti-Alzheimer's disease drugs. *Pharmaceutical Biology* 2015, 10: 1-7.

[64] Cheng TO. Cardiovascular effects of Danshen. *International Journal of Cardiology* 2007, 121: 9-22.

[65] Liu M, Wang Q, Liu F, Cheng X, Wu X, Wang H, Wu M, Ma Y, Wang G, Hao H. UDP-glucuronosyltransferase 1A compromises intracellular accumulation and anti-cancer effect of tanshinone IIA in human colon cancer cells. *PLoS One* 2013, 8: e79172.

[66] Wang L, Wu J, Lu J, Ma R, Sun D, Tang J. Regulation of the cell cycle and PI3K/Akt/mTOR signaling pathway by tanshinone I in human breast cancer cell lines. *Molecular Medicine*

*Report*s 2015, 11: 931-939.

[67] Li S, Wang H, Hong L, Liu W, Huang F, Wang J, Wang P, Zhang X, Zhou J. Cryptotanshinone inhibits breast cancer cell growth by suppressing estrogen receptor signaling. *Cancer Biology & Therapy* 2015, 16:176-184.

[68] Chen X, Guo J, Bao J, Lu J, Wang Y. The anticancer properties of Salvia miltiorrhiza Bunge (Danshen): a systematic review. *Medicinal Research Reviews* 2014, 34: 768-794.

[69] Lam FF, Yeung JH, Chan KM, Or PM. Mechanisms of the dilator action of cryptotanshinone on rat coronary artery. *European Journal of Pharmacology* 2008, 578:253-260.

[70] Ang KP, Tan HK, Selvaraja M, Kadir AA, Somchit MN, Akim AM, Zakaria ZA, Ahmad Z. Cryptotanshinone attenuates in vitro oxLDL-induced pre-lesional atherosclerotic events. *Planta Medica* 2011, 77:1782-1787.

[71] Liu Z, Xu S, Huang X, Wang J, Gao S, Li H, Zhou C, Ye J, Chen S, Jin ZG, Liu P. Cryptotanshinone, an orally bioactive herbal compound from Danshen, attenuates atherosclerosis in Apolipoprotein E-Deficient Mice: role of LOX-1. *British Journal of Pharmacology* 2015, 172:5661-5675.

[72] Mei Z, Zhang F, Tao L, Zheng W, Cao Y, Wang Z, Tang S, Le K, Chen S, Pi R, Liu P. Cryptotanshinone, a compound from Salvia miltiorrhiza modulates amyloid precursor protein metabolism and attenuates beta-amyloid deposition through upregulating alpha-secretase in vivo and in vitro. 2009, *Neuroscience Letters* 2009, 452:90-95.

[73] Yoo KY, Park SY. Terpenoids as potential anti-Alzheimer's disease therapeutics. *Molecules* 2012, 17:3524-3538.

[74] Mothana RAA, Jansen R, Gruenert R, Bednarski PJ, Lindequist U. Antimicrobial and cytotoxic abietane diterpenoids from the roots of Meriandera benghalensis (Roxb.) Benth. *Pharmazie* 2009, 64:613-615.

[75] Tang Y, Chen Y, Chu Z, Yan B, Xu L. Protective effect of cryptotanshinone on lipopolysaccharide-induced acute lung injury in mice. *European Journal of Pharmacology* 2014, 723:494-500.

[76] Wang Y, Wang S, Li Y, Jiang J, Zhou C, Li C, Li D, Lu L, Liu P, Huang M, Shen X. Therapeutic effect of Cryptotanshinone on collagen-induced arthritis in rats via inhibiting nuclear factor kappa B signaling pathway. *Translational Research* 2015, 165:704-716.

[77] Kim EJ, Jung SN, Son KH, Kim SR, Ha TY, Park MG, Jo IG, Park JG, Choe W, Kim SS, Ha J. Antidiabetes and antiobesity effect of cryptotanshinone via activation of AMP-activated protein kinase. *Molecular Pharmacology* 2007, 72:62-72.

[78] Guo Y, Li Y, Xue L, Severino RP, Gao S, Niu J, Qin LP, Zhang D, Brömme D. Salvia miltiorrhiza: an ancient Chinese herbal medicine as a source for anti-osteoporotic drugs. *Journal of Ethnopharmacology* 2014, 155:1401-1416.

[79] Lee SY, Choi DY, Woo ER. Inhibition of osteoclast differentiation by tanshinones from the root of Salvia miltiorrhiza bunge. *Archives of Pharmaceutical Research* 2005, 28:909-913.

[80] Chen L, Wang HJ, Xie W, Yao Y, Zhang YS, Wang H. Cryptotanshinone inhibits lung tumorigenesis and induces apoptosis in cancer cells in vitro and in vivo. *Molecular Medicine Reports* 2014, 9:2447-2452.

[81] Park IJ, Yang WK, Nam SH, Hong J, Yang KR, Kim J, Kim SS, Choe W, Kang I, Ha J. Cryptotanshinone induces G1 cell cycle arrest and autophagic cell death by activating the AMP-activated protein kinase signal pathway in HepG2 hepatoma. *Apoptosis* 2014, 19:615-628.

[82] Hayashi T, Kakisawa H, Hsu HY, Chen YP. The structure of miltirone, a new diterpenoid quinone. *Journal of Chemical Society D: Chemical Communications* 1970, 5: 299.

[83] Zhou X, Wang Y, Hu T, Or PM, Wong J, Kwan YW, Wan DC, Hoi PM, Lai PB, Yeung JH. Enzyme kinetic and molecular docking studies for the inhibitions of miltirone on major human cytochrome P450 isozymes. *Phytomedicine* 2013, 20: 367-374.

[84] Lee CM, Wong HN, Chui KY, Choang TF, Hon PM, Chang HM. Miltirone, a central benzodiazepine receptor partial agonist from a Chinese medicinal herb Salvia miltiorrhiza. *Neuroscience Letters* 1991, 127: 237–241.

[85] Colombo G, Serra S, Vacca G, Orrù A, Maccioni P, Morazzoni P, Bombardelli E, Riva A, Gessa GL, Carai MA. Identification of miltirone as active ingredient of Salvia miltiorrhiza responsible for the reducing effect of root extracts on alcohol intake in rats. *Alcoholism: Clinical and Experimental Research* 2006, 30: 754-762.

[86] Mostallino MC, Mascia MP, Pisu MG, Busonero F, Talani G, Biggio G. Inhibition by miltirone of up-regulation of GABAA receptor alpha4 subunit mRNA by ethanol withdrawal in hippocampal neurons. *European Journal of Pharmacology* 2004, 494: 83-90.

[87] Slusarczyk S, Zimmermann S, Kaiser M, Matkowski A, Hamburger M, Adams M. Antiplasmodial and antitrypanosomal activity of tanshinone-type diterpenoids from Salvia miltiorrhiza. *Planta Medica* 2011, 77: 1594-1596.

[88] Miura, K.; Kikuzaki, H.; Nakatani, N. Antioxidant activity of chemical components from sage (Salvia officinalis L.) and thyme (Thymus vulgaris L.) measured by the oil stability index method. *Journal of Agricultural and Food Chemistry* 2002, 50: 1845-1851.

[89] Huang W, Li J, Zhang W, Zhou Y, Xie C, Luo Y, Li Y, Wang J, Li J, Lu W. Synthesis of miltirone analogues as inhibitors of Cdc25 phosphatases. *Bioorganic & Medicinal Chemistry Letters* 2006, 16: 1905-1908.

[90] Ryu SY, Lee CO, Choi SU. In vitro cytotoxicity of tanshinones from Salvia miltiorrhiza. *Planta Medica* 1997, 63: 339-342.

[91] Zhou X, Wang Y, Lee WY, Or PM, Wan DC, Kwan YW, Yeung JH.Miltirone is a dual inhibitor of P-Glycoprotein and cell growth in doxorubicin-resistant HepG2 cells. *Journal of Natural Products* 2015, 78:2266-2275.

[92] Petersen M, Simmonds MS. Rosmarinic acid. *Phytochemistry* 2003, 62: 121-125.

[93] Hur YG, Suh CH, Kim S, Won J. Rosmarinic acid induces apoptosis of activated T cells from rheumatoid arthritis patients via mitochondrial pathway. *Journal of Clinical Immunology* 2007, 27: 36-45.

[94] Mesaik MA, Jabeen A, Halim SA, Begum A, Khalid AS, Asif M, Fatima B, Ul-Haq Z, Choudhary MI. In silico and in vitro immunomodulatory studies on compounds of Lindelofia stylosa. *Chemical Biology & Drug Design* 2012, 79: 290-299.

[95] Falcao RA, do Nascimento PL, de Souza SA, da Silva TM, de Queiroz AC, da Matta CB, Moreira MS, Camara CA, Silva TM. Antileishmanial phenylpropanoids from the leaves of *Hyptis pectinata* (L.) Poit. *Evidenced-Based Complementary and Alternative Medicine* 2013, 2013: 460613.

[96] Mašković P, Solujić S, Mihailović V, Mladenović M, Cvijović M, Mladenović J, Aćamović-Đoković G, Kurćubić V. Phenolic compounds and biological activity of *Kitaibelia vitifolia*. *Journal of Medicinal Food* 2011, 14: 1617-1623.

[97] Hooker CW, Lott WB, Harrich D. Inhibitors of human immunodeficiency virus type 1 reverse transcriptase target distinct phases of early reverse transcription. *Journal of Virology* 2001, 75: 3095–3104.

[98] Astani A, Navid MH, Schnitzler P. Attachment and penetration of acyclovir-resistant herpes simplex virus are inhibited by *Melissa officinalis* extract. *Phytotherapy Research* 2014, 28: 1547-1552.

[99] Abedini A, Roumy V, Mahieux S, Biabiany M, Standaert-Vitse A, Riviere C, Sahpaz S, Bailleul F, Neut C, Hennebelle T. Rosmarinic Acid and Its Methyl Ester as Antimicrobial Components of the Hydromethanolic Extract of Hyptis atrorubens Poit. (Lamiaceae). *Evidence- Based Complementary and Alternative Medicine* 2013, 2013: 604536.

[100] Chung YC, Hsieh FC, Lin YJ, Wu TY, Lin CW, Lin CT, Tang NY, Jinn TR. Magnesium lithospermate B and rosmarinic acid, two compounds present in Salvia miltiorrhiza, have potent antiviral activity against enterovirus 71 infections. European Journal of Pharmacology 2015, 755: 127-133.

[101] Ghaffari H, Venkataramana M, Jalali Ghassam B, Chandra Nayaka S, Nataraju A, Geetha NP, Prakash HS. Rosmarinic acid mediated neuroprotective effects against H_2O_2-induced neuronal cell damage in N2A cells. *Life Science*s 2014, 113: 7-13.

[102] Govindaraj J, Sorimuthu Pillai S. Rosmarinic acid modulates the antioxidant status and protects pancreatic tissues from glucolipotoxicity mediated oxidative stress in high-fat diet: streptozotocin-induced diabetic rats. *Molecular and Cellular Biochemistry* 2015, 404: 143-159.

[103] Huang SS, Zheng RL. Rosmarinic acid inhibits angiogenesis and its mechanism of action *in vitro*. *Cancer Letters* 2006, 239: 271–280.

[104] Osakabe N, Yasuda A, Natsume M, Yoshikawa T. Rosmarinic acid inhibits epidermal inflammatory responses: Anti-carcinogenetic effects of *Perilla frutescens* extract in the murine two-stage skin mode. *Carcinogenesis* 2004, 25: 549–557.

[105] Jiang WL, Chen XG, Qu GW, Yue XD, Zhu HB, Tian JW, Fu FH. Rosmarinic acid protects against experimental sepsis by inhibiting proinflammatory factor release and ameliorating hemodynamics. *Shock* 2009, 32: 608-613.

[106] Chu X, Ci X, He J, Jiang L, Wei M, Cao Q, Guan M, Xie X, Deng X, He J. Effects of a natural prolyl oligopeptidase inhibitor, rosmarinic acid, on lipopolysaccharide-induced acute lung injury in mice. *Molecules* 2012, 17: 3586-3598.

[107] Hamaguchi T, Ono K, Murase A, Yamada M. Phenolic compounds prevent Alzheimer's pathology through different effects on the amyloid-beta aggregation pathway. *American Journal of Pathology* 2009, 175: 2557-2565.

[108] Hasanein P, Mahtaj AK. Ameliorative effect of rosmarinic acid on scopolamine-induced memory impairment in rats. *Neuroscience Letters* 2015, 585: 23-27.

[109] Hossan MS, Rahman S, Bashar ABMA, Jahan R, Al-Nahain A, Rahmatullah M. Rosmarinic acid: a review of its anticancer action. *World Journal of Pharmaceutical Sciences* 2014, 3: 57-70.

[110] Scheckel KA, Degner SC, Romagnolo DF. Rosmarinic acid antagonizes activator protein-1-dependent activation of cyclooxygenase-2 expression in human cancer and nonmalignant cell lines. *Journal of Nutrition* 2008, 138: 2098-2105.

[111] Tao L, Wang S, Zhao Y, Sheng X, Wang A, Zheng S, Lu Y. Phenolcarboxylic acids from medicinal herbs exert anticancer effects through disruption of COX-2 activity. *Phytomedicine* 2014, 21: 1473-1482.

[112] Xavier CP, Lima CF, Fernandes-Ferreira M, Pereira-Wilson C. Salvia fruticosa, Salvia officinalis, and rosmarinic acid induce apoptosis and inhibit proliferation of human colorectal cell lines: the role in MAPK/ERK pathway. *Nutrition and Cancer* 2009, 61: 564-571.

[113] Xu Y, Xu G, Liu L, Xu D, Liu J. Anti-invasion effect of rosmarinic acid via the extracellular signal-regulated kinase and oxidation-reduction pathway in Ls174-T cells. *Journal of Cellular Biochemistry* 2010,111: 370-379.

[114] Paluszczak J, Krajka-Kuźniak V, Baer-Dubowska W. The effect of dietary polyphenols on the epigenetic regulation of gene expression in MCF7 breast cancer cells. *Toxicology Letters* 2010, 192: 119-125.

[115] Moon DO, Kim MO, Lee JD, Choi YH, Kim GY. Rosmarinic acid sensitizes cell death through suppression of TNF-alpha-induced NF-kappaB activation and ROS generation in human leukemia U937 cells. *Cancer Letters* 2010, 288: 183-191.

[116] Huang CY, Chen SY, Fu RH, Huang YC, Chen SY, Shyu WC, Lin SZ, Liu SP. Differentiation of embryonic stem cells into cardiomyocytes used to investigate the cardioprotective effect ofsalvianolic acid B through BNIP3 involved pathway. *Cell Transplantation* 2015, 24: 561-571.

[117] Guo HD, Cui GH, Tian JX, Lu PP, Zhu QC, Lv R, Shao SJ. Transplantation of salvianolic acid B pretreated mesenchymal stem cells improves cardiac function in rats with myocardial infarction through angiogenesis and paracrine mechanisms. *International Journal of Cardiology* 2014, 177: 538-542.

[118] Xu L, Deng Y, Feng L, Li D, Chen X, Ma C, Liu X, Yin J, Yang M, Teng F, Wu W, Guan S, Jiang B, Guo D. Cardio-protection of salvianolic acid B through inhibition of apoptosis network. *PLoS One* 2011, 6:e24036.

[119] Xu H, Zhou Y, Lu C, Ping J, Xu LM. Salvianolic acid B lowers portal pressure in cirrhotic rats and attenuates contraction of rat hepatic stellate cells by inhibiting RhoA signaling pathway. *Laboratory Investigation* 2012, 92: 1738-1748.

[120] Hou J, Tian J, Jiang W, Gao Y, Fu F. Therapeutic effects of SMND-309, a new metabolite of salvianolic acid B, on experimental liver fibrosis. *European Journal of Pharmacology* 2011, 650: 390-395.

[121] Tang Y, Jacobi A, Vater C, Zou X, Stiehler M. Salvianolic acid B protects human endothelial progenitor cells against oxidative stress-mediated dysfunction by modulating Akt/mTOR/4EBP1, p38 MAPK/ATF2, and ERK1/2 signaling pathways. *Biochemical Pharmacology* 2014, 90: 34-49.

[122] Tian J, Fu F, Li G, Wang Y, Gao Y, Liu Z, Zhang S. SMND-309, a novel derivate of salvianolic acid B, ameliorates cerebral infarction in rats: characterization and role. *Brain Research* 2009, 1263: 114-121.

[123] Zhao Y, Guo Y, Gu X. Salvianolic acid B, a potential chemopreventive agent, for head and neck squamous cell cancer. *Journal of Oncology* 2011, 2011:534548.

[124] Wang M, Sun G, Wu P, Chen R, Yao F, Qin M, Luo Y, Sun H, Zhang Q, Dong X, Sun, X. Salvianolic Acid B prevents arsenic trioxide-induced cardiotoxicity in vivo and enhances its anticancer activity *in vitro*. *Evidenced-Based Complementary and Alternative Medicine* 2013, 2013:759483.

[125] Lowe SW, Lin AW. Apoptosis in cancer. *Carcinogenesis* 2000, 21: 485-495.

[126] Kerr JF, Wyllie AH, Currie AR. Apoptosis: a basic biological phenomenon with wide-ranging implications in tissue kinetics. *British Journal of Cancer* 1972, 26: 239-257.

[127] Galluzzi L, Vitale I, Abrams JM, Alnemri ES, Baehrecke EH, Blagosklonny MV, Dawson TM, Dawson VL, El-Deiry WS, Fulda S, Gottlieb E, Green DR,Hengartner MO, Kepp O, Knight RA, Kumar S, Lipton SA, Lu X, Madeo F, Malorni W, Mehlen P, Nuñez G, Peter ME, Piacentini M, Rubinsztein DC, Shi Y, Simon HU, Vandenabeele P, White E, Yuan J, Zhivotovsky B, Melino G, Kroemer G. Molecular definitions of cell death subroutines: recommendations of the Nomenclature Committee on Cell Death 2012. *Cell Death and Differentiation* 2012, 19:107-120.

[128] Reed JC. Bcl-2 family proteins: regulators of apoptosis and chemoresistance in hematologic malignancies. *Seminars in Hematology* 1997, 34: 9-19.

[129] Wong RS. Apoptosis in cancer: from pathogenesis to treatment. *Journal of Experimental & Clinical Cancer Research* 2011, 30: 87.

[130] LaCasse EC, Mahoney DJ, Cheung HH, Plenchette S, Baird S, Korneluk RG. IAP-targeted therapies for cancer. *Oncogene* 2008, 27: 6252-6275.

[131] Hayden MS, Ghosh S. NF-κB, the first quarter-century: remarkable progress and outstanding questions. Genes & Development 2012, 26:203-234.

[132] Prasad S, Ravindran J, Aggarwal BB. NF-kappaB and cancer: how intimate is this relationship. *Molecular and Cellular Biochemistry* 2010, 336: 25-37.

[133] Kim HJ, Hawke N, Baldwin AS. NF-κB and IKK as therapeutic targets in cancer *Cell Death and Differentiation* 2006, 13: 738-747.

[134] Hoesel B, Schmid JA. The complexity of NF-κB signaling in inflammation and cancer. *Molecular Cancer* 2013, 12: 86.

[135] Sun Z, Andersson R. NF-kappaB activation and inhibition: a review. *Shock* 2002 18: 99-106.

[136] Anto R, Mukhopadhyay A, Denning K, Aggarwal BB. Curcumin induces apoptosis through activation of caspase-8, Bid cleavage, and cytochrome *c*release: it suppression by ectopic expression of Bcl-2 and Bcl-xL.*Carinogenesis* 2002, 23: 143–150.

[137] García MG, Alaniz L, Lopes EC, Blanco G, Hajos SE, Alvarez E.Inhibition of NF-kappaB activity by BAY 11-7082 increases apoptosis in multidrug resistant leukemic T-cell lines. Leukemia Research 2005, 29:1425-1434.

[138] Frelin C, Imbert V, Griessinger E, Peyron A-C, Rochet N, Phillip P, Dageville C, Sirvent A, Hummelsberger M, Berard E, Dreano M, Sirvent N, Peyron JF. Targeting NF-kappaB activation via pharmacologic inhibition of IKK2-induced apoptosis of human acute myeloid leukemia cells. *Blood* 2005, 105: 804–811.

[139] Guzman M, Rossi R, Karnischky L, Li X, Peterson D, Howard, Jordan CT. The sesquiterpene lactone parthenolide induces apoptosis of human acute myelogenous leukemia stem and progenitor cells. *Blood* 2005, 105: 4163–4169.

[140] Braakman I, Hebert DN. Protein folding in the endoplasmic reticulum. *Cold Spring Harbor Perspectives in Biology* 2013, 5: a013201.

[141] Ruggiano A, Foresti O, Carvalho P. Quality control: ER-associated degradation: protein quality control and beyond. *The Journal of Cell Biology* 2014, 204: 869-879.

[142] Plongthongkum N, Kullawong N, Panyim S, Tirasophon W. Ire1 regulated XBP1 mRNA splicing is essential for the unfolded protein response (UPR) in Drosophila melanogaster. Biochemical and Biophysical Research Communications 2007, 354: 789-794.

[143] Yan W, Frank CL, Korth MJ, Sopher BL, Novoa I, Ron D, Katze MG. Control of PERK eIF2alpha kinase activity by the endoplasmic reticulum stress-induced molecular chaperone P58IPK. *Proceedings of the National Academy of Sciences of the United States of America* 2002, 99: 15920-15925.

[144] Han J, Back SH, Hur J, Lin YH, Gildersleeve R, Shan J, Yuan CL, Krokowski D, Wang S, Hatzoglou M, Kilberg MS, Sartor MA, Kaufman RJ. ER-stress-induced transcriptional regulation increases protein synthesis leading to cell death. *Nature Cell Biology* 2013, 15: 481-490.

[145] Li M, Baumeister P, Roy B, Phan T, Foti D, Luo S, Lee AS. ATF6 as a transcription activator of

the endoplasmic reticulum stress element: thapsigargin stress-induced changes and synergistic interactions with NF-Y and YY1. *Molecular and Cellular Biology* 2000, 20: 5096-5106.

[146] Gorman AM, Healy SJ, Jäger R, Samali A. Stress management at the ER: regulators of ER stress-induced apoptosis. *Pharmacology & Therapeutics* 2012, 134: 306-316.

[147] Weston RT, Puthalakath H. Endoplasmic reticulum stress and BCL-2 family members. *Advances in Experimental Medicine and Biology* 2010, 687: 65-77.

[148] Oyadomari S, Mori M. Roles of CHOP/GADD153 in endoplasmic reticulum stress. *Cell Death and Differentiation* 2004, 11: 381-389.

[149] Walter P and Ron D. The Unfolded Protein Response: From Stress Pathway to Homeostatic Regulation. *Science* 2011, 334: 1081-1086.

[150] Bhat M, Robichaud N, Hulea L, Sonenberg N, Pelletier J, Topisirovic I. Targeting the translation machinery in cancer. *Nature Reviews Drug Discovery* 2015, 14:261-278.

[151] Grzmil M, Hemmings BA. Translation regulation as a therapeutic target in cancer. *Cancer Research* 2012, 72: 3891-3900.

[152] Gebauer F, Hentze MW. Molecular mechanisms of translational control. *Nature Reviews Molecular Cell Biology* 2004, 5:827-835.

[153] Sonenberg N and Hinnebusch AG. Regulation of Translation Initiation in Eukaryotes: Mechanisms and Biological Targets. *Cell* 2009, 136: 731–745.

[154] Zhang L, Pan X, Hershey JW. Individual overexpression of five subunits of human translation initiation factor eIF3 promotes malignant transformation of immortal fibroblast cells. *The Journal of Biological Chemistry* 2007, 282:5790–5800.

[155] Graff JR, Konicek BW, Vincent TM, Lynch RL, Monteith D, Weir SN, Schwier P, Capen A, Goode RL, Dowless MS, Chen Y, Zhang H, Sissons S, Cox K, McNulty AM, Parsons SH, Wang T, Sams L, Geeganage S, Douglass LE, Neubauer BL, Dean NM, Blanchard K, Shou J, Stancato LF, Carter JH, Marcusson EG. Therapeutic suppression of translation initiation factor eIF4E expression reduces tumor growth without toxicity. *The Journal of Clinical Investion* 2007, 117:2638-2648.

[156] Bordeleau ME, Cencic R, Lindqvist L, Oberer M, Northcote P, Wagner G, Pelletier J. RNA-mediated sequestration of the RNA helicase eIF4A by Pateamine A inhibits translation initiation. *Chemistry & Biology* 2006, 13:1287-1295.

[157] Cencic R, Carrier M, Galicia-Vázquez G, Bordeleau ME, Sukarieh R, Bourdeau A, Brem B, Teodoro JG, Greger H, Tremblay ML, Porco JA Jr, Pelletier J. Antitumor activity and mechanism of action of the cyclopenta[b]benzofuran, silvestrol. *PLoS One* 2009, 4:e5223.

[158] Werzowa J, Koehrer S, Strommer S, Cejka D, Fuereder T, Zebedin E, Wacheck V. Vertical inhibition of the mTORC1/mTORC2/PI3K pathway shows synergistic effects against melanoma in vitro and in vivo. *The Journal of Investigative Dermatology* 2011, 131:495-503.

[159] Bennett RN, Wallsgrove RM. Secondary metabolites in plant defense mechanisms. *New Phytologist* 1994, 127: 617-633.

[160] Ramakrishna A, Ravishankar GA. Influence of abiotic stress signals on secondary metabolites in plants. *Plant Signaling & Behavior* 2011, 6: 1720-1731.

[161] Khojasteh A, Mirjalili MH, Hidalgo D, Corchete P, Palazon J. New trends in biotechnological production of rosmarinic acid. *Biotechnology Letters* 2014, 36: 2393-2406.

[162] Achamlale S, Rezzonico B, Grignon-Dubois M. Rosmarinic acid from beach waste: Isolation and HPLC quantification in *Zostera* detritus from Arcachon lagoon. *Food Chemistry* 2009, 113: 878-883.

[163] Verpoorte R. Secondary metabolism. In: Verpoorte R, Alferman AW, eds. *Metabolic engineering of plant secondary metabolism*. The Netherlands: Springer Netherlands. 2000, 1-29.

[164] Hussain M, Fareed S, Ansari S, Rahman M, Ahmad IZ, Saeed M. Current approaches toward production of secondary plant metabolites. *Journal of Pharmacy and Bioallied Sciences* 2012, 4: 10–20.

[165] Burgess J. Hormones and cell differentiation. In: Burgess J, eds. *Introduction of plant cell development.* The Press Syndicate of the University of Cambridge, NY, USA. 1985, 129-153.

[166] Ikeuchi M, Sugimoto K, Iwase A. Plant callus: mechanisms of induction and repression. *The Plant Cell* 2013, 25: 3159-3173.

[167] Bourgaud F, Gravot A, Milesi S, Gontier E. Production of plant secondary metabolites: a historical perspective. *Plant Science* 2001, 161: 839-851.

[168] Stafford A, Morris P, Fowler MW. Plant cell biotechnology: A perspective. *Enzyme and Microbial Technology* 1986, 8: 578-586.

[169] Murashige T, Skoog F. A revised medium for rapid growth and bioassays with tobacco tissue cultures. *Physiologia Plantarum* 1962, 15: 473–497.

[170] Dong J, Liu Y, Liang Z, Wang W. Investigation on ultrasound-assisted extraction of salvianolic acid B from Salvia miltiorrhiza root. *Ultrasonics Sonochemistry* 2010, 17: 61-65.

[171] Fitzgerald JB, Schoeberl B, Nielsen UB, Sorger PK. Systems biology and combination therapy in the quest for clinical efficacy. *Nature Chemical Biology* 2006, 2: 458-466.

[172] Zhao L, Au JL, Wientjes MG. Comparison of methods for evaluating drug-drug interaction. *Frontiers in Bioscience (Elite Ed)* 2010, 2: 241-249.

[173] Gérard E, Meulle A,Feron O, Marchand-Brynaert J. LDV peptidomimetics equipped with biotinylated spacer-arms: synthesis and biological evaluation on CCRF-CEM cell line. *Bioorganic & Medicinal Chemistry Letters* 2012, 22: 586-590.

[174] Morris GM, Huey R, Lindstrom W, Sanner MF, Belew RK, Goodsell DS, Olson AJ. AutoDock4 and AutoDockTools4: Automated docking with selective receptor flexibility. *Journal of Computational Chemistry* 2009, 30: 2785-2791.

[175] Liu T, Ortiz JA, Taing L, Meyer CA, Lee B, Zhang Y, Shin H, Wong SS, Ma J, Lei Y, Pape UJ, Poidinger M, Chen Y, Yeung K, Brown M,Turpaz Y, Liu XS. Cistrome: an integrative platform for transcriptional regulation studies. *Genome Biology* 2011, 12: R83.

[176] Hamm R, Chen YR, Seo EJ, Zeino M, Wu CF, Müller R, Yang NS, Efferth T. Induction of

cholesterol biosynthesis by archazolid B in T24 bladder cancer cells. *Biochemical Pharmacology* 2014, 91:18-30.

[177] Eberwine J, Yeh H, Miyashiro K, Cao Y, Nair S, Finnell R, Zettel M, Coleman P. Analysis of gene expression in single live neurons. *Proceedings of the National Academy of Science of the United States of America* 1992, 89:3010–3014.

[178] Grill C, Gheyas F, Dayananth P, Jin W, Ding W, Qiu P, Wang L, Doll RJ, English JM. Analysis of the ERK1,2 transcriptome in mammary epithelial cells. *The Biochem Journal* 2004, 381: 635-644.

[179] Saeed M, Khalid H, Sugimoto Y, Efferth T. The lignan, (-)-sesamin reveals cytotoxicity toward cancer cells: pharmacogenomic determination of genes associated with sensitivity or resistance. *Phytomedicine* 2014, 21: 689-696.

[180] Efferth T, Konkimalla VB, Wang YF, Sauerbrey A, Meinhardt S, Zintl F, Mattern J, Volm M. Prediction of broad spectrum resistance of tumors towards anticancer drugs. *Clinical Cancer Research* 2008, 14: 2405-2412.

[181] Efferth T, Koch E. Complex interactions between phytochemicals. The multitarget therapeutic concept of phytotherapy. *Current Drug Targets* 2011, 12: 122–132.

[182] Barzilai A, Yamamoto K. DNA damage responses to oxidative stress. *DNA Repair* 2004, 3: 1109-1115.

[183] Rolli V, Ruf A, Augustin A, Schulz GE, Ménissier-de Murcia J, de Murcia G. Poly(ADP-ribose) polymerase: Structure and function. In: de Murcia G, Shall S, Eds. *From DNA damage and stress signalling to cell death: Poly ADP-ribosylation reactions*, Oxford University Press: New York 2000: 35-79.

[184] Decker P, Isenberg D, Muller S. Inhibition of caspase-3-mediated poly (ADP- ribose) polymerase (PARP) apoptotic cleavage by human PARP autoantibodies and effect on cells undergoing apoptosis. *Journal of Biological Chemistry* 2000, 275: 9043-9046.

[185] Okinaga T, Kasai H, Tsujisawa T, Nishihara T. Role of caspases in cleavage of lamin A/C and PARP during apoptosis in macrophages infected with a periodontopathic bacterium. *Journal of Medicinal Microbiology* 2007, 56: 1399-1404.

[186] Boucher D, Blais V, Denault JB. Caspase-7 uses an exosite to promote poly (ADP ribose) polymerase 1 proteolysis. *Proceedings of the National Academy of Science of the United States of America* 2012, 109: 5669-5674.

[187] Cullen SP, Martin SJ. Caspase activation pathways: some recent progress. *Cell Death and Differentiation.* 2009, 16: 935-938.

[188] Kalia M, Kukol A. Structure and dynamics of the kinase IKK-β--A key regulator of the NF-kappa B transcription factor. *Journal of Structual Biology* 2011, 176: 133-142.

[189] Chiarini F, Lonetti A, Evangelisti C, Buontempo F, Orsini E, Evangelisti C, Cappellini A, Neri LM, McCubrey JA, Martelli AM. Advances in understanding the acute lymphoblastic leukemia bone marrow microenvironment: From biology to therapeutic targeting. *Biochimica et*

Biophysica Acta 2015, doi: 10.1016/j.bbamcr.2015.08.015.

[190] Lockyer JM, Colladay JS, Alperin-Lea WL, Hammond T, Buda AJ. Inhibition of nuclear factor-kappaB-mediated adhesion molecule expression in human endothelial cells. *Circulation Research* 1998, 82: 314-320.

[191] Eck SL, Perkins ND, Carr DP, and Nabel GJ. Inhibition of phorbol ester-induced cellular adhesion by competitive binding of NF-kappa B in vivo. *Molecular and Cellular Biology* 1993, 13: 6530–6536.

[192] Juliano RL, Haskill S. Signal transduction from the extracellular matrix. *The Journal of Cell Biology* 1993, 120: 577-585.

[193] Wrighton CJ, Hofer-Warbinek R, Moll T, Eytner R, Bach FH, de Martin R. Inhibition of endothelial cell activation by adenovirus-mediated expression of IkBa, an inhibitor of the transcription factor NF-kB. *The Journal of Experimental Medicine* 1996, 183:1013–1022.

[194] Jacamo R, Chen Y, Wang Z, Ma W, Zhang M, Spaeth EL, Wang Y, Battula VL, Mak PY, Schallmoser K, Ruvolo P, Schober WD, Shpall EJ, Nguyen MH, Strunk D, Bueso-Ramos CE, Konoplev S, Davis RE, Konopleva M, Andreeff M. Reciprocal leukemia-stroma VCAM-1/VLA-4-dependent activation of NF-κB mediates chemoresistance. *Blood* 2014, 123: 2691-2702.

[195] Averous J, Bruhat A, Jousse C, Carraro V, Thiel G, Fafournoux P. Induction of CHOP expression by amino acid limitation requires both ATF4 expression and ATF2 phosphorylation. *The Journal of Biological Chemistry* 2004, 279: 5288-5297.

[196] Hollander MC, Zhan Q, Bae I, Fornace AJJ. Mammalian GADD34, an apoptosis- and DNA damage-inducible gene. *The Journal of Biological Chemistry* 199, 272: 13731-13737.

[197] Peterson EA, Andrews PS, Be X, Boezio AA, Bush TL, Cheng AC, Coats JR, Colletti AE, Copeland KW, DuPont M, Graceffa R, Grubinska B, Harmange JC, Kim JL, Mullady EL, Olivieri P, Schenkel LB, Stanton MK, Teffera Y, Whittington DA, Cai T, La DS. Discovery of triazine-benzimidazoles as selective inhibitors of mTOR. *Bioorganic & Medicinal Chemistry Letters* 2011, 21: 2064-2070.

[198] Knight ZA, Gonzalez B, Feldman ME, Zunder ER, Goldenberg DD, Williams O, Loewith R, Stokoe D, Balla A, Toth B, Balla T, Weiss WA, Williams RL, Shokat KM. A pharmacological map of the PI3-K family defines a role for p110alpha in insulin signaling. *Cell* 2006, 125: 733-747.

[199] Knight SD, Adams ND, Burgess JL, Chaudhari AM, Darcy MG, Donatelli CA, Luengo JI, Newlander KA, Parrish CA, Ridgers LH, Sarpong MA, Schmidt SJ, Van Aller GS, Carson JD, Diamond MA, Elkins PA, Gardiner CM, Garver E, Gilbert SA, Gontarek RR, Jackson JR, Kershner KL, Luo L, Raha K, Sherk CS, Sung CM, Sutton D, Tummino PJ, Wegrzyn RJ, Auger KR, Dhanak D. Discovery of GSK2126458, a highly potent inhibitor of PI3K and the mammalian target of rapamycin. *ACS Medicinal Chemistry Letters* 2010, 1: 39-43.

[200] Park S, Chapuis N, Bardet V, Tamburini J, Gallay N, Willems L, Knight ZA, Shokat KM, Azar

N, Viguié F, Ifrah N, Dreyfus F, Mayeux P, Lacombe C, Bouscary D. PI-103, a dual inhibitor of Class IA phosphatidylinostide 3- kinase and mTOR, has antileukemic activity in AML. *Leukemia* 2008, 22: 1698-1706.

[201] Spriggs KA, Bushell M, Willis AE. Translational regulation of gene expression during conditions of cell stress. *Molecular Cell* 2010, 40: 228-237.

[202] Chu J, Pelletier J. Targeting the eIF4A RNA helicase as an anti-neoplastic approach. *Biochimica et Biophysica Acta* 2015, 1849: 781-791.

[203] Wolfe AL, Singh K, Zhong Y, Drewe P, Rajasekhar VK, Sanghvi VR, Mavrakis KJ, Jiang M, Roderick JE, Van der Meulen J, Schatz JH, Rodrigo CM, Zhao C, Rondou P, de Stanchina E, Teruya-Feldstein J, Kelliher MA, Speleman F, Porco JAJ, Pelletier J, Rätsch G, Wendel HG. RNA G-quadruplexes cause eIF4A-dependent oncogene translation in cancer. *Nature* 2014, 513 : 65-70.

[204] Vermeulen K, Van Bockstaele DR, Berneman ZN. The cell cycle: a review of regulation, deregulation and therapeutic targets in cancer. *Cell Proliferation* 2003, 36: 131-149.

[205] Olive PL, Banáth JP. The comet assay: a method to measure DNA damage in individual cells. *Nature Protocols* 2006, 1: 23-29.

[206] Orrenius S, Nicotera P, Zhivotovsky B. Cell death mechanisms and their implications in toxicology. *Toxicological Sciences* 2011, 119: 3-19.

[207] Le Rhun Y, Kirkland JB, Shah GM. Cellular responses to DNA damage in the absence of Poly(ADP-ribose) polymerase. *Biochemical and Biophysical Research Communications* 1998, 245: 1-10.

[208] Wuerzberger-Davis SM, Chang PY, Berchtold C, Miyamoto S. Enhanced G2/M arrest by NF-kB-dependent p21waf1/cip1 induction. *Molecular Cancer Research* 2005, 3: 345-353.

[209] Hellin AC, Bentires-Alj M, Verlaet M, Benoit V, Gielen J, Bours V, Merville MP. Roles of nuclear factor-kappaB, p53, and p21/WAF1 in daunomycin-induced cell cycle arrest and apoptosis. The *Journal of Pharmacology and Experimental Therapeutics* 2000, 295: 870-878.

[210] Ghose AK, Herbertz T, Pippin DA, Salvino JM, Mallamo JP. Knowledge based prediction of ligand binding modes and rational inhibitor design for kinase drug discovery. *Journal of Medicinal Chemistry* 2008, 51: 5149-5171.

[211] Lauria A, Ippolito M, Fazzari M, Tutone M, Di Blasi F, Mingoia F, Almerico AM. IKK-beta inhibitors: an analysis of drug-receptor interaction by using molecular docking and pharmacophore 3D-QSAR approaches. *Journal of Molecular Graphics & Modelling* 2010, 29: 72-81.

[212] Nagarajan S, Choo H, Cho YS, Oh KS, Lee BH, Shin KJ, Pae AN. IKKbeta inhibitors identification part II: ligand and structure-based virtual screening. *Bioorganic & Medicinal Chemistry* 2010, 18: 3951-3960.

[213] Ortiz-Lazareno PC, Hernandez-Flores G, Dominguez-Rodriguez JR, Lerma-Diaz JM, Jave-Suarez LF, Aguilar-Lemarroy A, Gomez-Contreras PC, Scott-Algara D, Bravo-Cuellar A.

MG132 proteasome inhibitor modulates proinflammatory cytokines production and expression of their receptors in U937 cells: involvement of nuclear factor-κB and activator protein-1. *Immunology* 2008, 124: 534-541.

[214] Stupack DG. The biology of integrins. *Oncology* 2007, 21: 6–12.

[215] Uchiyama T, Ishikawa T, Imura A. Adhesion properties of adult T cell leukemia cells. *Leukemia & Lymphoma* 1995, 16: 407–412.

[216] Chung EJ, Hwang SG, Nguyen P, Lee S, Kim JS, Kim JW, Henkart PA, Bottaro DP, Soon L, Bonvini P, Lee SJ, Karp JE, Oh HJ, Rubin JS, Trepel JB. Regulation of leukemic cell adhesion, proliferation, and survival by beta-catenin. *Blood* 2002, 100: 982-990.

[217] Young TH, Tu HR, Chan CC, Huang YC, Yen MH, Cheng NC, Chiu HC, Lin SJ. The enhancement of dermal papilla cell aggregation by extracellular matrix proteins through effects on cell-substratum adhesivity and cell motility. *Biomaterials* 2009, 30: 5031–5040.

[218] Pankov R, Yamada KM. Fibronectin at a glance. *Journal of Cell Science* 2002, 115: 3861-3863.

[219] Han J, Zhong CQ, Zhang DW. Programmed necrosis: backup to and competitor with apoptosis in the immune system. *Nature Immunology* 2011, 12: 1143-1149.

[220] Linkermann A, Green DR. Necroptosis. *The New England Journal of Medicine* 2014, 370: 455-465.

[221] Zong WX, Thompson CB. Necrotic death as a cell fate. *Genes & Development* 2006, 20: 1-15.

[222] Cooke MS, Evans MD, Dizdaroglu M, Lunec J. Oxidative DNA damage: mechanisms, mutation, and disease. *The FASEB Journal* 2003, 17: 1195-1214.

[223] Bernardi P, Petronilli V, Di Lisa F, Forte M. A mitochondrial perspective on cell death. *Trends in Biochemical Science* 2001, 26: 112-117.

[224] Eguchi Y, Shimizu S, Tsujimoto Y. Intracellular ATP levels determine cell death fate by apoptosis or necrosis. *Cancer Research* 1997, 57: 1835-1840.

[225] Kroemer G, Galluzzi L, Brenner C. Mitochondrial membrane permeabilization in cell death. *Physiological Reviews* 2007, 87: 99-163.

[226] Kagawa S, Gu J, Honda T, McDonnell TJ, Swisher SG, Roth JA, Fang B. Deficiency of caspase-3 in MCF7 cells blocks Bax-mediated nuclear fragmentation but not cell death. Clin. *Cancer Research* 2001, 7: 1474-1480.

[227] de Murcia G, Menissier de Murcia J. Poly(ADP-ribose) polymerase: a molecular nick-sensor. *Trends in Biochemical Science* 1994, 19: 172-176.

[228] Ha HC, Snyder SH. Poly(ADP-ribose) polymerase is a mediator of necrotic cell death by ATP depletion. *Proceedings of the National Academy of Science of the United States of America* 1999, 96: 13978-13982.

[229] Kim MY, Zhang T, Kraus WL. Poly(ADP-ribosyl)ation by PARP-1: 'PAR-laying' NAD+ into a nuclear signal. *Genes & Development* 2005, 19: 1951-1967.

[230] Yang H, Rivera Z, Jube S, Nasu M, Bertino P, Goparaju C, Franzoso G, Lotze MT, Krausz T, Pass HI, Bianchi ME, Carbone M. Programmed necrosis induced by asbestos in human

mesothelial cells causes high-mobility group box 1 protein release and resultant inflammation. *Proceedings of the National Academy of Science of the United States of America* 2010, 107: 12611-12616.

[231] Gilmore TD. Introduction to NF-kappaB: players, pathways, perspectives. *Oncogene* 2006, 25: 6680-6684.

[232] Xu G, Lo YC, Li Q, Napolitano G, Wu X, Jiang X, Dreano M, Karin M, Wu H. Crystal structure of inhibitor of kappaB kinase beta. *Nature* 2011, 472: 325-330.

[233] Taylor WR, Stark GR. Regulation of the G2/M transition by p53. *Oncogene* 2001, 20: 1803-1815.

[234] Vaseva AV, Marchenko ND, Ji K, Tsirka SE, Holzmann S, Moll UM. p53 opens the mitochondrial permeability transition pore to trigger necrosis. *Cell* 2012, 149: 1536-1548.

[235] Liu AH, Li L, Xu M, Lin YH, Guo HZ, Guo DA. Simultaneous quantification of six major phenolic acids in the roots of *Salvia miltiorrhiza* and four related traditional Chinese medicinal preparations by HPLC –DAD method. *Journal of Pharmaceutical and Biomedical Analysis*, 2006, *41*: 48-56.

[236] Binkhathlan Z, Lavasanifar A. P-glycoprotein inhibition as a therapeutic approach for overcoming multidrug resistance in cancer: current status and future perspectives. *Current Cancer Drug Targets* 2013, 13: 326-346.

[237] Hall MD, Handley MD, Gottesman MM. Is resistance useless? Multidrug resistance and collateral sensitivity. *Trends in Pharmacological Sciences* 2009, 30: 546-556.

[238] Chan DA, Giaccia AJ. Harnessing synthetic lethal interactions in anticancer drug discovery. *Nature Reviews Drug Discovery* 2011, 10: 351-364.

[239] Hall, M. D.; Marshall, T. S.; Kwit, A. D.; Miller Jenkins, L. M.; Dulcey, A. E.; Madigan, J. P.; Pluchino, K. M.; Goldsborough, A. S.; Brimacombe, K. R.; Griffiths, G. L.; Gottesman, M. M. Inhibition of glutathione peroxidase mediates the collateral sensitivity of multidrug-resistant cells to tiopronin. The *Journal of Biological Chemistry* 2014, 289: 21473-21489.

[240] Marks KM, Park ES, Arefolov A, Russo K, Ishihara K, Ring JE, Clardy J, Clarke AS, Pelish HE. The selectivity of austocystin D arises from cell-line-specific drug activation by cytochrome P450 enzymes. *Journal of Natural Products* 2011, 74: 567-573.

[241] Laberge RM, Ambadipudi R, Georges E. P-glycoprotein (ABCB1) modulates collateral sensitivity of a multidrug resistant cell line to verapamil. *Archives of Biochemistry and Biophysics* 2009, *491*, 53-60.

[242] Yeh PY, Chuang SE, Yeh KH, Song YC, Cheng AL. Involvement of nuclear transcription factor-kappa B in low-dose doxorubicin-induced drug resistance of cervical carcinoma cells. *Biochemical Pharmacology* 2003, 66: 25-33.

[243] Kovalski R, Hansen-Flaschen J, Lodato RF, Pietra GG. Localized leukemic pulmonary infiltrates. Diagnosis by bronchoscopy and resolution with therapy. *Chest* 1990, 97: 674-678.

[244] Pinkel D, Woo S. Prevention and treatment of meningeal leukemia in children. *Blood* 1994, 84:

355-366.

[245] Cortes J. Central nervous system involvement in adult acute lymphocytic leukemia. *Hematology/Oncology Clinics North America* 2001, 15: 145-162.

[246] Gordon KB, Rugo HS, Duncan JL, Irvine AR, Howes ELJ, O'Brien JM, Carter SR. Ocular manifestations of leukemia: leukemic infiltration versus infectious process. *Ophthalmology* 2001, 108: 2293-2300.

[247] Terek MC, Ozkinay E, Zekioglu O, Erhan Y, Cagirgan S, Pehlivan M, Mgoyi L. Acute leukemia in pregnancy with ovarian metastasis: a case report and review of the literature. *International Journal of Gynecological Cancer* 2003, 13: 904-908.

[248] Chang CY, Chiou TJ, Hsieh YL, Cheng SN. Leukemic infiltration of the urinary bladder presenting as uncontrollable gross hematuria in a child with acute lymphoblastic leukemia. *Journal of Pediatric Hematology/Oncology* 2003, 25: 735-739.

[249] Yumuk PF, Aydiner A, Topuz E, Cabioglu N, Dogan O. T-cell lymphoblastic lymphoma presenting with a breast mass. *Leukemia & Lymphoma* 2004, 45: 833-836.

[250] Taylor CW, Taylor RE, Kinsey SE. Leukemic infiltration of the orbit: report of three cases and literature review. *Journal of Pediatric Hematology/Oncology* 2005, 22: 415-422.

[251] Benson RE, Rodd HD, North S, Loescher AR, Farthing PM, Payne M. Leukaemic infiltration of the mandible in a young girl. *International Journal of Paediatric Dentistry* 2007, 17: 145-150.

[252] Karbasian-Esfahani M, Wiernik PH, Yeddu M, Abebe L. Leukemic infiltration of the breast in acute lymphocytic leukemia (ALL). *Hematology* 2008, 13: 101-106.

[253] Halliwell B, Cross CE. Oxygen-derived species: their relation to human disease and environmental stress. *Environmental Health Perspectives* 1994, 102(Suppl 10):5–12.

[254] Sabharwal SS, Schumacker PT. Mitochondrial ROS in cancer: initiators, amplifiers or an Achilles' heel? *Nature Reviews Cancer* 2014, 14: 709-721.

[255] Marchi S, Giorgi C, Suski JM, Agnoletto C, Bononi A, Bonora M, De Marchi E, Missiroli S, Patergnani S, Poletti F, Rimessi A, Duszynski J, Wieckowski MR, Pinton P. Mitochondria-ros crosstalk in the control of cell death and aging. *Journal of Signal Transduction* 2012, 2012: 329635.

[256] Ishikawa K, Ishii H, Saito T. DNA damage-dependent cell cycle checkpoints and genomic stability.*DNA and Cell Biology* 2006, 25: 406-411.

[257] Zhou BB, Elledge SJ. The DNA damage response: putting checkpoints in perspective. *Nature* 2000 408: 433-439.

[258] Shiloh Y. The ATM-mediated DNA-damage response: taking shape. *Trends in Biochemical Sciences* 2006 , 31: 402-410.

[259] Allan LA, Clarke PR. Phosphorylation of caspase-9 by CDK1/cyclin B1 protects mitotic cells against apoptosis. *Molecular Cell* 2007, 26: 301–310.

[260] Takagaki N, Sowa Y, Oki T, Nakanishi R, Yogosawa S, Sakai T. Apigenin induces cell cycle

arrest and p21/WAF1 expression in a p53-independent pathway. *International Journal of Oncology* 2005, 26: 185-189.

[261] Ma S, Tang J, Feng J, Xu Y, Yu X, Deng Q, Lu Y. Induction of p21 by p65 in p53 null cells treated with Doxorubicin. *Biochimica et Biophysica Acta* 2008, 1783: 935-940.

[262] Efferth T, Grassmann R. Impact of viral oncogenesis on responses to anti-cancer drugs and irradiation. *Critical Reviews in Oncogenesis* 2000, 11: 165-187.

[263] Kuo SJ, Chien SY, Lin C, Chan SE, Tsai HT, Chen DR. Significant elevation of CLDN16 and HAPLN3 gene expression in human breastcancer. *Oncology Reports* 2010, 24: 759-766.

[264] Zhu G, Wu CJ, Zhao Y, Ashwell JD. Optineurin negatively regulates TNFalpha-induced NF-kappaB activation by competing with NEMO for ubiquitinated RIP. *Current Biology* 2007, 17: 1438-1443.

[265] Iden S, van Riel WE, Schäfer R, Song JY, Hirose T, Ohno S, Collard JG. Tumor type-dependent function of the par3 polarity protein in skin tumorigenesis. *Cancer Cell* 2012, 22: 389-403.

[266] Liu Z, Chen P, Gao H, Gu Y, Yang J, Peng H, Xu X, Wang H, Yang M, Liu X, Fan L, Chen S, Zhou J, Sun Y, Ruan K, Cheng S, Komatsu M,White E, Li L, Ji H, Finley D, Hu R. Ubiquitylation of autophagy receptor Optineurin by HACE1 activates selective autophagy for tumor suppression. *Cancer Cell* 2014, 26: 106-120.

[267] Borges S, Döppler H, Perez EA, Andorfer CA, Sun Z, Anastasiadis PZ, Thompson E, Geiger XJ, Storz P. Pharmacologic reversion of epigenetic silencing of the PRKD1 promoter blocks breast tumor cell invasion and metastasis. *Breast Cancer Research* 2013, 15: R66.

[268] Brim H, Abu-Asab MS, Nouraie M, Salazar J, Deleo J, Razjouyan H, Mokarram P, Schaffer AA, Naghibhossaini F, Ashktorab H. An integrative CGH, MSI and candidate genes methylation analysis of colorectal tumors. *PLoS One* 2014, 9: e82185.

[269] Lee J, Seol MY, Jeong S, Lee CR, Ku CR, Kang SW, Jeong JJ, Shin DY, Nam KH, Lee EJ, Chung WY, Jo YS. A metabolic phenotype based on mitochondrial ribosomal protein expression as a predictor of lymph node metastasis in papillary thyroid carcinoma. *Medicine (Baltimore)* 2015, 94: e380.

[270] Zhou A, Zhou J, Yang L, Liu M, Li H, Xu S, Han M, Zhang J. A nuclear localized protein ZCCHC9 is expressed in cerebral cortex and suppresses the MAPK signal pathway. *Journal of Genetics and Genomics* 2008, 35: 467-472.

[271] Lee SH, Zhu C, Peng Y, Johnson DT, Lehmann L, Sun Z. Identification of a novel role of ZMIZ2 protein in regulating the activity of the Wnt/β-catenin signaling pathway. The *Journal of Biological Chemistry* 2013, 288: 35913-35924.

[272] Fang S, Zeng X, Zhu W, Tang R, Chao Y, Guo L. Zinc finger E-box-binding homeobox 2 (ZEB2) regulated by miR-200b contributes to multi-drug resistance of small cell lung cancer. *Experimental and Molecular Pathology* 2014, 96: 438-444.

[273] Yan LH, Wei WY, Cao WL, Zhang XS, Xie YB, Xiao Q. Overexpression of E2F1 in human gastric carcinoma is involved in anti-cancer drug resistance. *BMC Cancer* 2014, 14: 904.

[274] Ducker CE, Upson JJ, French KJ, Smith CD. Two N-myristoyltransferase isozymes play unique roles in protein myristoylation, proliferation, and apoptosis. *Molecular Cancer Research* 2005, 3: 463-476.

[275] Walters DK, Steinmann P, Langsam B, Schmutz S, Born W, Fuchs B. Identification of potential chemoresistance genes in osteosarcoma. *Anticancer Research* 2008, 28: 673-679.

[276] Stein WD, Bates SE, Fojo T. Intractable cancers: the many faces of multidrug resistance and the many targets it presents for therapeutic attack. *Current Drug Targets* 2004, 5: 333-346.

[277] Voulgari A, Pintzas A. Epithelial-mesenchymal transition in cancer metastasis: mechanisms, markers and strategies to overcome drugresistance in the clinic. *Biochimica et Biophysica Acta* 2009, 1796: 75-90.

[278] Naiditch JA, Jie C, Lautz TB, Yu S, Clark S, Voronov D, Chu F, Madonna MB. Mesenchymal change and drug resistance in neuroblastoma. The *Journal of Surgical Research* 2015, 193: 279-288.

[279] Nyce JW. Drug-induced DNA hypermethylation: a potential mediator of acquired drug resistance during cancerchemotherapy. *Mutattion Research* 1997, 386: 153-161.

[280] Baker EK, El-Osta A. The rise of DNA methylation and the importance of chromatin on multidrug resistance in cancer. *Experimental Cell Research* 2003, 290: 177-194.

[281] Wilting RH, Dannenberg JH. Epigenetic mechanisms in tumorigenesis, tumor cell heterogeneity and drug resistance. *Drug Resistance Updatates* 2012, 15: 21-38.

[282] Sui X, Chen R, Wang Z, Huang Z, Kong N, Zhang M, Han W, Lou F, Yang J, Zhang Q, Wang X, He C, Pan H. Autophagy and chemotherapy resistance: a promising therapeutic target for cancer treatment. *Cell Death & Disease* 2013, 4: e838.

[283] Hu YL, Jahangiri A, Delay M, Aghi MK. Tumor cell autophagy as an adaptive response mediating resistance to treatments such as antiangiogenic therapy. *Cancer Research* 2012, 72: 4294-4299.

[284] Abdi J, Chen G, Chang H. Drug resistance in multiple myeloma: latest findings and new concepts on molecular mechanisms. *Oncotarget* 2013, 4: 2186-2207.

[285] Cossa G, Gatti L, Cassinelli G, Lanzi C, Zaffaroni N, Perego P. Modulation of sensitivity to antitumor agents by targeting the MAPK survival pathway. *Current Pharmaceutical Design* 2013, 19: 883-894.

[286] Pritchard AL, Hayward NK. Molecular pathways: mitogen-activated protein kinase pathway mutations and drug resistance. *Clinical Cancer Research* 2013, 19: 2301-2309.

[287] Marciniak SJ, Yun CY, Oyadomari S, Novoa I, Zhang Y, Jungreis R, Nagata K, Harding HP, Ron D. CHOP induces death by promoting protein synthesis and oxidation in the stressed endoplasmic reticulum. *Genes & Development* 2004, 18: 3066-3077.

[288] Park IJ, Kim MJ, Park OJ, Choe W, Kang I, Kim SS, Ha J. Cryptotanshinone induces ER stress-mediated apoptosis in HepG2 and MCF7 cells. *Apoptosis* 2012, 17: 248-257.

[289] Tse AK, Chow KY, Cao HH, Cheng CY, Kwan HY, Yu H, Zhu GY, Wu YC, Fong WF, Yu ZL.

The herbal compound cryptotanshinone restores sensitivity in cancer cells that are resistant to the tumor necrosis factor-related apoptosis-inducing ligand. *The Journal of Biological Chemistry* 2013, 288: 29923-29933.

[290] Polivka JJ, Janku F. Molecular targets for cancer therapy in the PI3K/AKT/mTOR pathway. *Pharmacology & Therapeutics* 2014, 142: 164-175.

[291] GeY, Yang B, Xu X, Dai Q, Chen Z, Cheng R. Cryptotanshinone acts synergistically with imatinib to induce apoptosis of human chronic myeloid leukemia cells. *Leukemia & Lymphoma* 2015, 56: 730-738.

[292] Chen W, Luo Y, Liu L, Zhou H, Xu B, Han X, Shen T, Liu Z, Lu Y, Huang S. Cryptotanshinone inhibits cancer cell proliferation by suppressing Mammalian target of rapamycin-mediated cyclin D1 expression and Rb phosphorylation. *Cancer Prevention Research (Philadelphia)* 2010, 3: 1015-1025.

[293] Ilic N, Utermark T, Widlund HR, Roberts TM. PI3K-targeted therapy can be evaded by gene amplification along the MYC-eukaryotic translation initiation factor 4E (eIF4E) axis. *Proceedings of the National Academy of Science of the United States of America* 2011, 108: E699-708.

[294] Lü JM, Lin PH, Yao Q, Chen C. Chemical and molecular mechanisms of antioxidants: experimental approaches and model systems. *Journal of Cellular and Molecular Medicice* 2010, 14: 840-860.

[295] Fadel O, El Kirat K, Morandat S. The natural antioxidant rosmarinic acid spontaneously penetrates membranes to inhibit lipid peroxidation in situ. *Biochimica et Biophysica Acta* 2011, 1808: 2973-2980.

[296] Zhang Y, Chen X, Yang L, Zu Y, Lu Q. Effects of rosmarinic acid on liver and kidney antioxidant enzymes, lipid peroxidation and tissue ultrastructure in aging mice. *Food & Function* 2015, 6: 927-931.

[297] Ramalho LN, Pasta AA, Terra VA, Augusto M, Sanches SC, Souza-Neto FP, Cecchini R, Gulin F, Ramalho FS. Rosmarinic acid attenuates hepatic ischemia and reperfusion injury in rats. *Food and Chemical Toxicology* 2014, 74: 270-278.

[298] Domitrović R, Potočnjak I, Crnčević-Orlić ZZ, Škoda M. Nephroprotective activities of rosmarinic acid against cisplatin-induced kidney injury in mice. *Food and Chemical Toxicology* 2014, 66: 321-328.

[299] Fox JT, Sakamuru S, Huang R, Teneva N, Simmons SO, Xia M, Tice RR, Austin CP, Myung K. High-throughput genotoxicity assay identifies antioxidants as inducers of DNA damage response and cell death. *Proceedings of the National Academy of Science of the United States of America* 2012, 109: 5423-5428.

[300] Fox JT, Sakamuru S, Huang R, Teneva N, Simmons SO, Xia M, Tice RR, Austin CP, Myung K. Reply to Kojo: Mechanisms of antioxidant-induced DNA damage. *Proceedings of the National Academy of Science of the United States of America* 2012, E2029.

[301] Lu LY, Ou N, Lu QB. Antioxidant induces DNA damage, cell death and mutagenicity in human lung and skin normal cells. *Scientific Reports* 2013, 3: 3169.

[302] Leist M, Single B, Castoldi AF, Kühnle S, Nicotera P. Intracellular adenosine triphosphate (ATP) concentration: a switch in the decision between apoptosis and necrosis. *The Journal of Experimantal Medicine* 1997, 185: 1481-1486.

[303] Burkart V, Wang ZQ, Radons J, Heller B, Herceg Z, Stingl L, Wagner EF, Kolb H. Mice lacking the poly(ADP-ribose) polymerase gene are resistant to pancreatic beta-cell destruc tion and diabetesdevelopment induced by streptozocin. Nature Medicine 1999, 5: 314-319.

[304] Lelli JL Jr, Becks LL, Dabrowska MI, Hinshaw DB. ATP convert necrosis to apoptosis in oxidant-injured endothelial cells. *Free Radical Biology & Medicine* 1998, 25: 694-702.

[305] Hur YG, Yun Y, Won J. Rosmarinic acid induces p56lck-dependent apoptosis in Jurkat and peripheral T cells via mitochondrial pathway independent from Fas/Fas ligand interaction. *Journal of Immunology* 2004, 172: 79-87.

[306] Lin CS, Kuo CL, Wang JP, Cheng JS, Huang ZW, Chen CF. Growth inhibitory and apoptosis inducing effect of Perilla frutescens extract on human hepatoma HepG2 cells. *Journal of Ethnopharmacology* 2007, 112: 557-567.

[307] Margolin N, Raybuck SA, Wilson KP, Chen W, Fox T, Gu Y, Livingston DJ. Substrate and inhibitor specificity of interleukin-1 beta-converting enzyme and related caspases. *Journal of Biological Chemistry* 1997, 272: 7223-7228.

[308] Kim SJ, Zhang Z, Hitomi E, Lee YC, Mukherjee AB. Endoplasmic reticulum stress-induced caspase-4 activation mediates apoptosis and neurodegeneration in INCL. *Human Molecular Genetics* 2006, 15: 1826-1834.

[309] de Bruin EC, Medema JP. Apoptosis and non-apoptotic deaths in cancer development and treatment response. *Cancer Treatment Reviews* 2008, 34, 737-749.

[310] Tait SW, Ichim G, Green DR. Die another way--non-apoptotic mechanisms of cell death. *Journal of Cell Science* 2014, 127: 2135-2144.

[311] Vitale I, Galluzzi L, Castedo M, Kroemer G. Mitotic catastrophe: a mechanism for avoiding genomic instability. *Nature Reviews Molecular Cell Biology* 2011, 12: 385-392.

[312] Hirt UA, Leist M. Rapid, noninflammatory and PS-dependent phagocytic clearance of necrotic cells. *Cell Death & Differentiation* 2003, 10: 1156-1164.

[313] Brouckaert G, Kalai M, Krysko DV, Saelens X, Vercammen D, Ndlovu MN, Haegeman G, D'Herde K, Vandenabeele P. Phagocytosis of necrotic cells by macrophages is phosphatidylserine dependent and does not induce inflammatory cytokine production. *Molecular Biology of the Cell* 2004, 15: 1089-1100.

[314] Tak PP, Firestein GS. NF-kappaB: a key role in inflammatory diseases. *The Journal of Clinical Investigation* 2001, 107: 7-11.

[315] Mittal M, Siddiqui MR, Tran K, Reddy SP, Malik AB. Reactive oxygen species in inflammation and tissue injury. *Antioxidants & Redox Signaling* 2014, 20: 1126-1167.

[316] Ledoux S, Yang R, Friedlander G, Laouari D. Glucose depletion enhances P-glycoprotein expression in hepatoma cells: role of endoplasmic reticulum stress response. *Cancer Research* 2003, 63: 7284-7290.

[317] Wartenberg M, Ling FC, Muschen M, Klein F, Acker H, Gassmann M, Petrat K, Putz V, Hescheler J, Sauer H. Regulation of the multidrug resistance transporter P-glycoprotein in multicellular tumor spheroids by hypoxia-inducible factor (HIF-1) and reactive oxygen species. *The FASEB Journal* 2003, 17: 503-505.

[318] Hong H, Lu Y, Ji ZN, Liu GQ. Up-regulation of P-glycoprotein expression by glutathione depletion-induced oxidative stress in rat brain microvessel endothelial cells. *Journal of Neurochemistry* 2006, 98: 1465-1473.

[319] Carew JS, Zhou Y, Albitar M, Carew JD, Keating MJ, Huang P. Mitochondrial DNA mutations in primary leukemia cells after chemotherapy: clinical significance and therapeutic implications. *Leukemia* 2003, 17: 1437-1447.

[320] Basu S, Binder RJ, Suto R, Anderson KM, Srivastava PK. Necrotic but not apoptotic cell death releases heat shock proteins, which deliver a partial maturation signal to dendritic cells and activate the NF-kappa B pathway. *International Immunology* 2000, 12: 1539-1546.

[321] Sauter B, Albert ML, Francisco L, Larsson M, Somersan S, Bhardwaj N. Consequences of cell death: exposure to necrotic tumor cells, but not primary tissue cells or apoptotic cells, induces the maturation of immunostimulatory dendritic cells. *The Journal of Experimental Medicine* 2000, 191: 423-434.

[322] Obeid M, Tesniere A, Ghiringhelli F, Fimia GM, Apetoh L, Perfettini JL, Castedo M, Mignot G, Panaretakis T, Casares N, Metivier D, Larochette N, van Endert P, Ciccosanti F, Piacentini M, Zitvogel L, Kroemer G. Calreticulin exposure dictates the immunogenicity of cancer cell death. *Nature Medicine* 2007, 13: 54-61.

[323] Spiridon K, Olga M, Emmanuil P, Maria S. *In vitro* rosmarinic acid accumulation in sweet basil (*Ocimum basillicum* L.). *Biotechnology Letters* 2003, 25: 405–408.

[324] Yesil-Celiktas O, Nartop P, Gurel A, Bedir E, Vardar-Sukan F. Determination of phenolic content and antioxidant activity of extracts obtained from *Rosmarinus officinalis*' calli. *Journal of Plant Physiology* 2007, 164: 1536-1542.

[325] Deus B, Zenk MH. Exploitation of plant cells for the production of natural compounds. *Biotechnology and Bioengineering* 1982, 24: 1965–1974.

[326] Hakkim FL, Shankar CG, Girija S. Chemical composition and antioxidant property of holy basil (*Ocimum sanctum* L.) leaves, stems, and inflorescence and their *in vitro* callus cultures. *Journal of Agricultural and Food Chemistry* 2007, 55: 9109-9117.

[327] Tadhani MB, Patel VH, Rema S. *In vitro* antioxidant activities of *Stevia rebaudiana* leaves and callus. *Journal of Food Composition and Analysis* 2007, 20: 323–329.

[328] Ni XB, Su J. Active constituents of above-ground portion and root of *Salvia miltiorrhiza*. *Chinese Pharmaceutical Journal* 1995, 30: 336-338.

[329] Qi YX, Cao ML, Wang XD, Gao YS, Xia ZL. Determination and comparation of 3 active components in the cultivated *Salvia miltiorrhiza* Bunge and wild *Salvia miltiorrhiza* Bge in Taisha. *Pharmaceutical Biotechnology* 2006, 13: 279-282.

[330] Harborne JB, Williams CA. Advances in flavonoid research since 1992. *Phytochemistry* 2000, 55: 481–504.

[331] Lattanzio V, Lattanzio VMT, Cardinali A. Role of phenolics in the resistance mechanisms of plants against fungal pathogens and insects. In: Imperato F eds. *Phytochemistry: Advances in Research.* Trivandrum, Kerala, India : Research Signpost. 2006: 23-67.

[332] Modarres M, Asili J, Lahouti M, Gangali A, Iranshahy M, Sahebkar A. Simultaneous determination of rosmarinic acid, salvianolic acid B and caffeic acid in *Salvia leriifolia* benth. Root, leaf and callus extracts using a high-performance liquid chromatography with diodearray detection technique. *Journal of Liquid Chromatography & Related Technology* 2014, 37: 1721–1730.

[333] Li J, Liang X, Dong J, Wang G, Liang Z. Localization and identification of phenolic compounds in Salvia miltiorrhiza Bunge roots and leaves. *Journal of Science and Applications: Biomedicine*, 2015, 3: 34-40.

8. Appendix

8.1 Publication

8.1.1 Publication (2014-2016)

Journal paper

1. Seo EJ, **Wu CF**, Khan S, Walker L, Khan I, Efferth T. Inhibition of migration of HepG2 cells by green tea extracts. (In submission)
2. Efferth T, Banerjee M, Paul N, Abdelfatah S, Arend J, Elhassan G, Hamdoun S, Hamm R, Hong C, Kadioglu O, Naß J, Ochwangi D, Ooko E, Ozenver N, Saeed M, Schneider M, Seo EJ, **Wu CF**, Yan G, Zeino M, Zhao Q, Abu-Darwish M, Andersch K, Alexie G, Bessarab D, Bhakta-Guha D, Bolzani V, Dapat E, Donenko F, Efferth M, Greten H, Gunatilaka L, Hussein A, Karadeniz A, Khalid H, Kuete V, Lee IS, Liu L, Midiwo J, Mora R, Nakagawa H, Ngassapa O, Noysang C, Omosa L, Roland FH, Shahat A, Saab A, Saeed E, Shan L, Titinchi S. Biopiracy of natural products and good bioprospecting practice. *Phytomedicine* 2016, 23(2): 166-173.
3. **Wu CF**, Seo EJ, Klauck SM, Efferth T. Cryptotanshinone deregulates unfolded protein response and eukaryotic initiation factor signaling in acute lymphoblastic cells. *Phytomedicine* 2016, 23(2): 174-180.
4. **Wu CF**, Bohnert S, Thines E, Efferth T. Cytotoxicity of the root extract of Salvia miltiorrhiza against multidrug-resistance cancer cells. *Am. J. Chin. Med.* (in press)
5. **Wu CF**, Karioti A, Rohr D, Bilia AR, Efferth T. Production of rosmarinic acid and salvianolic acid B from callus culture of Salvia miltiorrhiza with cytotoxicity towards acute lymphoblastic leukemia cells. *Food Chem.* 2016, 201: 292-297.
6. **Wu CF**, Klauck SM, Efferth T. Cytotoxicity of cryptotanshinone towards acute lymphoblastic leukemia cells. *Arch. Toxicol.* DOI: 10.1007/s00204-015-1616-4
7. **Wu CF**, Hong C, Klauck SM, Efferth T. Molecular mechanisms of rosmarinic acid in acute lymphoblastic leukemia cells. *J. Ethanolpharmacol.* 2015, 176:55-68
8. **Wu CF**, Efferth T. Miltirone Induces G2/M Cell Cycle Arrest and Apoptosis in CCRF-CEM Acute Lymphoblastic Leukemia Cells. *J. Nat. Prod*. 2015, 78(6):1339-1347.
9. Dörsam B, **Wu CF**, Efferth T, Kaina B, Fahrer J. The eucalyptus oil ingredient 1,8-cineol induces oxidative DNA damage. *Arch. Toxicol.* 2015, 89(5):797-805.
10. Hamm R, Chen YR, Seo EJ, Zeino M, **Wu CF**, Müller R, Yang NS, Efferth T. Induction of cholesterol biosynthesis by archazolid B in T24 bladder cancer cells. *Biochem. Pharmacol.* 2014, 91(1):18-30.

Conference paper

1. **Wu CF**, Efferth T. Miltirone induced apoptosis in acute lymphoblastic leukemia cells via ROS production and mitochondrial dysfunction. Gesellschaft Deutscher Naturforscher und Ärzte GDNÄ 2014, Conference at the University of Mainz, Germany, Sep 2014.
2. **Wu CF**, Efferth T. Therapeutical potential of cryptotanshinone on acute lymphoblastic leukemia cells. GDNÄ 2014, Conference at the University of Mainz, Germany, Sep 2014.
3. **Wu CF**, Efferth T. Rosmarinic acid inhibited cellular movement and proliferation on acute lymphoblastic leukemia cells. GDNÄ 2014, Conference at the University of Mainz, Germany, Sep 2014.
4. Dörsam B, **Wu CF**, Efferth T, Kaina B, Fahrer J. Eucalyptol induces oxidative DNA damage in epithelial cells. Opentox 2013 Conference at the University of Mainz, Germany, Sep 2013.

Book chapter

Seo EJ, **Wu CF**, Greten HJ, Efferth T. Epidermal Growth Factor Receptors and Downstream Signalling Pathways as Cancer Treatment Targets for Medicinal Plants. Chapter 16, Ethnopharmacology, in press.

8.1.2 Publication (before 2014)

Journal paper

1. **Wu CF**, Lin YL, Huang YT. Hepatitis C virus core protein stimulates fibrogenesis in hepatic stellate cells involving the obese receptor. *J. Cell. Biochem.* 2013, 114(3):541-50
2. Lin YL, **Wu CF**, Huang, YT. Effects of Rhubarb on migration of rat hepatic stellate cells *J. Gastroenterol. Hepatol.* 2009, 24(3):453-61
3. Lin YL, **Wu CF**, Huang, YT. Phenols from the roots of *Rheum palmatum* attenuates chemotaxis in rat hepatic stellate cells *Planta Med*. 2008, 74(10):1246-52.
4. Hsu YC, Chiu YT, Cheng CC, **Wu CF**, Lin YL, Huang, YT. 2005. Antifibrotic effects of tetrandrine on hepatic stellate cells and rats with liver fibrosis. *J. Gastroenterol. Hepatol*., 2007, 22(1): 99-111

5. Hsu YC, Chiu YT, Lee CY, **Wu CF**, Huang, YT. Antifibrotic effects of tetrandrine on bile duct ligated rats. *Can. J. Physiol. Pharmacol*. 2006, 84: 967-976.

Conference paper

Wu CF, Lin YL, Huang YT. Hepatitis C virus core protein induces oxidative stress and hepatic fibrogenesis. Asian Pacific association for the study of the liver 2010 (APASL 2010) Abstract PP-522, Beijing, China, Mar 2010.

Master thesis

Bioassays of Herbs in Attenuating Migration of Rat Hepatic Stellate Cell Line HSC-T6. **Wu, Ching-Fen** 2006/6

8.2 Curriculum Vitae

8.3 Permission to publish

Permissions to publish have been granted by the following copyright holders:

Figure 1:
https://s100.copyright.com/CustomerAdmin/PLF.jsp?ref=1991a4bd-4566-4ee8-a12d-847c0aa4b411

Figure 2:
Fig. 1A. Fionn E. O'Brien et al. Human P-glycoprotein differentially affects antidepressant drug transport: relevance to blood–brain barrier permeability. International Journal of Neuropsychopharmacology (2013) 16 (10): 2259-2272. Use of the OUP Material is restricted to: Inclusion in the forthcoming Ph.D. dissertation/thesis titled "Molecular mechanisms and Pharmacogenomics of constituents of Salvia miltiorrhiza for anticancer therapy" by Ching-Fen Wu to be submitted in print and in PDF format to the institute of Pharmacy and Biochemistry, Germany in April 2016 and uploaded to the university's research repository, URL (NB: the © line must appear on the same page as the OUP material). Territory: Germany. Language: English.

Figure 3:
https://s100.copyright.com/CustomerAdmin/PLF.jsp?ref=f568a2fc-fbcb-465a-b240-1e1000f5dcc4

Figure 4:
https://s100.copyright.com/CustomerAdmin/PLF.jsp?ref=4e4b79d1-6215-4dfa-9054-20a4dcb44577

Figure 6:
https://s100.copyright.com/CustomerAdmin/PLF.jsp?ref=5f98109e-9040-48e7-8fae-da4b4cbc143a

Figure 7:
https://s100.copyright.com/CustomerAdmin/PLF.jsp?ref=3c4ff6c2-0738-48a5-a172-c2c68037ce6b

Figure 8:
https://s100.copyright.com/CustomerAdmin/PLF.jsp?ref=e096f107-1196-42fe-bb3e-72c23e8b95cf

Figure 9:
https://s100.copyright.com/CustomerAdmin/PLF.jsp?ref=56e15312-5a9e-452d-841d-968f5765fab9